



UNIVERSIDADE DA BEIRA INTERIOR

Ciências

Understanding the interaction between pDNA and different chromatographic supports

Gregory Silva Dutra

Dissertação para obtenção do Grau de Mestre em

Bioquímica

(2º ciclo de estudos)

Orientador: Prof. Doutor Ana Cristina Mendes Dias Cabral

Co-orientador: Prof. Doutor Fani Sousa

Covilhã, outubro de 2016

Só por hoje...

Acknowledgments

First of all, I would like to thank Professor Cristina Dias-Cabral for her guidance, supervision, support and encouragement. Her enthusiastic and contagious passion in this investigation project was essential in this work accomplishment.

A special thanks to my co-supervisor Professor Fani Sousa. Her prompt availability and help were also a key for the project to come forward.

I would also like to acknowledge the research center CICS-UBI and lab colleagues, especially from my work group. Patrícia, Filipa, Cláudia, Sara, John, Gonçalo, Francisco and João thanks for the best working environment. This is also yours.

A very special tanks to John for his friendship and lessons. You already change someone in the world.

To my friends, especially from Desertuna, thank you for being part of my life.

To my little brother that have the capability to cheer me up even in my worst days.

Now and always to mom and dad.

Resumo Alargado

A terapia gênica e as vacinas de DNA são terapias recentes que aproveitam o potencial do DNA plasmídeo (pDNA) como uma molécula terapêutica para o tratamento e cura de muitas doenças. Na última década, as empresas farmacêuticas deram muita atenção a ambas as técnicas devido à sua simplicidade, versatilidade e segurança.

O uso do pDNA como uma molécula com um propósito farmacêutico requer a sua produção em grande escala, com um alto grau de pureza e homogeneidade. Estes parâmetros são fundamentais para garantir uma boa resposta e a segurança do paciente.

São utilizados vários processos na purificação de plasmídeos, tanto na eliminação de impurezas como restos celulares, proteínas, DNA genómico, etc., como para separar as diferentes isoformas em que um plasmídeo se pode encontrar (linear, circular aberto ou superenrolado). As propriedades únicas do pDNA fazem com que a sua purificação seja a parte mais complicada de todo o processo de fabrico.

A cromatografia de troca aniónica e de interação hidrofóbica são as técnicas utilizadas com mais sucesso na purificação de plasmídeos. Contudo, o mecanismo de separação de plasmídeos por estas técnicas não é totalmente compreendido. É difícil prever o comportamento das moléculas durante a separação, e ainda, os métodos usados na escala laboratorial são economicamente e ambientalmente incompatíveis com a escala industrial. Assim sendo, uma melhor compreensão dos mecanismos subjacentes à cromatografia terá um elevado interesse prático.

A análise dos eventos termodinâmicos dos processos de adsorção através da Microcalorimetria de Fluxo (FMC) tem vindo a provar a sua boa utilidade na obtenção de uma melhor compreensão das forças motrizes, dos mecanismos e das cinéticas envolvidas no processo de adsorção de biomoléculas em diferentes sistemas cromatográficos. Por isso, neste trabalho, através da utilização da microcalorimetria de fluxo, pretende-se compreender e comparar o mecanismo de adsorção de um plasmídeo na sua forma linear (*ln pDNA*) a um suporte cromatográfico de troca aniónica (*Q-sepharose Fast Flow*) e a um suporte cromatográfico de interação hidrofóbica (*Phenyl-sepharose 6 Fast Flow*), e ainda a adsorção de um plasmídeo na sua forma linear e superenrolada (*sc pDNA*) a um suporte cromatográfico de troca aniónica (*Q-sepharose Fast Flow*). Os resultados serão analisados dando ênfase às diferenças entre cada sistema. Para além da microcalorimetria de fluxo, foram também realizados estudos da capacidade de ligação em modo estático (*static binding capacity*) para obter uma melhor compreensão do mecanismo de adsorção.

Os resultados obtidos nos estudos de capacidade de ligação revelaram que o processo de adsorção do plasmídeo na forma linear segue uma isotérmica de Langmuir até uma certa

concentração de plasmídeo em equilíbrio. Em todos os casos testados, a capacidade de ligação do suporte aumenta com o aumento da concentração de plasmídeo em equilíbrio até se atingir um patamar em que a saturação do suporte cromatográfico é alcançada. O suporte de troca iônica revelou ter uma capacidade de ligação maior para o ln pDNA do que o suporte de interação hidrofóbica, como esperado. Não foi possível fazer os mesmos testes com o sc pDNA dado a sua instabilidade nas condições em que os testes são realizados. Não obstante, conseguiu-se de forma teórica chegar a uma previsão da capacidade máxima de ligação do sc pDNA ao suporte de troca aniônica que revelou ser inferior à capacidade teórica atingida na adsorção de ln pDNA.

Os estudos realizados utilizando a microcalorimetria de fluxo foram efetuados na zona linear das isotérmicas. Dois modos diferentes de injeção foram utilizados através da introdução de um pulso de amostra na célula do microcalorímetro ou através da alimentação contínua de amostra à célula. Estes modos de injeção foram conseguidos usando *loops* de diferentes volumes.

Considerando os resultados do FMC obtidos com a adsorção do ln pDNA à Phenyl Sepharose, todos os termogramas são compostos por um pico endotérmico seguido de um ou dois picos exotérmicos, dependendo do modo de injeção, e um último pico endotérmico. Os termogramas foram deconvolvidos e as áreas e o *timing* dos picos considerados na comparação com o processo de adsorção do ln pDNA a Q-Sepharose. O primeiro pico endotérmico relaciona-se com o processo de desolvatação. O primeiro pico exotérmico está associado à interação entre o ln pDNA e o suporte. Visto que este apresenta valores energéticos similares aos da interação do ln pDNA com a Q-Sepharose, verificou-se que a Phenyl Sepharose também interage electrostaticamente com o DNA plasmídeo através de interações anião- π . Utilizando a alimentação contínua da coluna (loop de 430 μ L), encontraram-se diferenças não só na magnitude e no *timing* de cada sinal, como também no perfil do termograma. A presença de diferentes picos num termograma indica a existência de diferentes eventos durante o processo de adsorção. O segundo pico exotérmico, encontrado apenas utilizando o modo de alimentação contínua, está relacionado com adsorção secundária. Este processo também acontece na adsorção do ln pDNA à Q-Sepharose. Considerou-se que o último pico endotérmico estivesse relacionado com a reorganização das moléculas de água e iões na interface do ln pDNA com a solução. Acredita-se que este processo seja causado pela alta concentração de sulfato de amónio na solução.

As experiencias realizadas no FMC com sc pDNA e Q-Sepharose resultaram em termogramas compostos por um pico endotérmico seguido de um exotérmico. O pico endotérmico obtido com o *loop* de 430 μ L foi deconvolvidos, posteriormente, em dois sinais endotérmicos. Tal como no caso anterior, as intensidades, áreas e o *timing* dos sinais foram considerados na comparação com a adsorção do ln pDNA à Q-Sepharose. Acredita-se que o primeiro sinal endotérmico esteja relacionado com processo de desolvatação, tal como na adsorção do ln pDNA. Contudo,

verificou-se que o processo é mais energético no caso do sc pDNA dado que este tem uma maior densidade de carga que é conferida pela isoforma superenrola, conduzindo a um maior gasto energético na desolvatação. Ao utilizar o *loop* de 430 μL conseguiu-se promover uma sobrecarga no volume de amostra que passa na coluna. Este método resultou no aparecimento de um segundo sinal endotérmico. Este sinal relaciona-se com as repulsões entre as moléculas de sc pDNA livres na solução. Por último, a área e o *timing* do pico exotérmico leva-nos a acreditar que este está relacionado com a reorientação da molécula e com adsorção secundária.

As entalpias de adsorção revelaram que o processo global de adsorção é exotérmico (perto de zero) na adsorção do ln pDNA à Phenyl Sepharose. Alguns estudos mostram que os processos cromatográficos que envolvem interações hidrofóbicas são fortemente influenciados pela variação da entropia, e são muitas vezes considerados maioritariamente endotérmicos. Neste caso particular, não temos um processo só com interações hidrofóbicas o que explica a divergência dos resultados. Na adsorção do sc pDNA à Q-Sepharose, o processo global é conduzido entropicamente visto que este é endotérmico para todos os casos estudados, este resultado é similar aos obtidos anteriormente com o estudo da adsorção pela análise de van 't Hoff [24].

Palavras-chave

Microcalorimetria de Fluxo; Adsorção; DNA plasmídeo linear e superenrolado; Cromatografia de troca aniónica; cromatografia de interação hidrofóbica.

Abstract

Gene Therapy and DNA vaccines are recent therapies that take advantage of the potential of plasmid DNA as a therapeutic molecule for the treatment and cure of several diseases. In the last decade both techniques have received a great deal of attention by pharmaceutical companies due to their simplicity, versatility and safe profile. Hence, the usage of pDNA as biopharmaceutical molecule requires its production at the gram scale, with a high purity and homogeneity level as a vital parameter to ensure a good response and the patient safety.

Anion-exchange chromatography and hydrophobic interaction chromatography have been successfully used in pDNA purification. Nevertheless, the mechanism of pDNA separation for both purification techniques is still not completely understood. A better understanding of the driving forces and mechanisms underlying both purification processes are of great interest to help optimize chromatographic systems.

Flow Microcalorimetry (FMC) has proven its ability to provide an improved understanding of the driving forces, mechanisms and kinetics involved in the interaction process during biomolecules adsorption onto several chromatographic systems]. Thus, using Flow Microcalorimetry as a central technique, this study aims to understand and compare the interaction between different pDNA isoforms (pVAX1-LacZ) and the anion-exchange support (Q-sepharose Fast Flow) or the hydrophobic support (Phenyl Sepharose 6 Fast Flow), considering only the isotherm linear conditions, showing the role of nonspecific effects on the adsorptive process.

The results obtained in the binding capacity studies revealed that the ln pDNA adsorption process follows a Langmuir isotherm up to a specific ln pDNA equilibrium concentration. In all cases, the binding capacity increases with the plasmid concentration in equilibrium until it reaches a level at which saturation of the chromatographic medium is achieved. The anion-exchange support was found to have a higher binding capacity for ln pDNA adsorption than the hydrophobic interaction support, as expected. FMC results revealed that for both processes the endothermic heat major contributor was suggested to be the desolvation and changes in the solvation shell processes while exothermic heats were related to the interaction (electrostatic attraction) between pDNA and support and also to the secondary adsorption of already adsorbed pDNA molecules. The enthalpies of adsorption showed that the overall adsorption process is mainly enthalpically driven for the adsorption of ln pDNA onto Phenyl Sepharose and entropically driven for the sc pDNA-Q-sepharose system.

Keywords

Flow Microcalorimetry; Adsorption; Supercoiled and linear plasmid DNA; Anion-exchange chromatography; Hydrophobic Interaction chromatography.

Table of Contents

1. Introduction.....	1
1.1. Plasmid DNA (pDNA).....	1
1.1.1 Gene Therapy and DNA Vaccines: pDNA as biopharmaceutical molecule	1
1.1.2. Structure and Proprieties	3
1.1.3 Plasmid conformational forms	5
1.2. Biotechnological plasmid DNA production.....	7
1.2.2. Upstream Processing	8
1.2.3. Downstream Processing	9
1.3. Liquid Chromatography technique for pDNA purification	13
1.3.1. Physical proprieties of different stationary phases.	15
1.3.2. Anion-Exchange Chromatography principles for pDNA purification	17
1.3.3. Hydrophobic Interaction Chromatography principles for pDNA purification	19
1.4. Adsorption process and equilibrium	21
1.4.1. Langmuir Model and static binding capacity.....	22
1.5. Thermodynamic study of biomolecules adsorption	25
1.5.1. Flow Microcalorimetry	25
1.6. Goal of Study	29
2. Materials and methods.....	31
2.1. Materials	31
2.2. Apparatus and Software	31
2.3. Plasmid DNA Production	31
2.3.1. Fermentation.....	31
2.3.2. Recovery	32
2.3.3. Plasmid DNA quantification.....	33
2.3.4. Plasmid Isoform Separation.....	33
2.3.5. Agarose Gel Electrophoresis	33
2.4. Plasmid DNA Purification	33

2.4.1.	sc pDNA purification with Toyopearl GigaCap Q 650-M.....	33
2.4.2.	sc pDNA purification with CIM DEAE	34
2.4.3.	Sample Concentration and buffer change.....	34
2.4.4.	Sample Characterization	34
2.5.	Flow Microcalorimetry (FMC)	35
3.	Results and Discussion	37
3.1.	Plasmid production	37
3.2.	sc pDNA Purification	38
3.2.2.	Toyoperl GigaCap Q 650-M.....	38
3.2.3.	CIM DEAE	40
3.3.	Static Binding Capacity	41
3.4.	Flow Microcalorimetry	43
3.4.1.	ln pDNA adsorption onto Phenyl-Sepharose.....	44
3.4.2.	sc pDNA adsorption onto Q-Sepharose.....	53
4.	Conclusion and Future work	61
5.	References	63
6.	Appendix	69

Figures

Figure 1.1.1 - Indications addressed by plasmid-based gene therapy clinical trials. Adapted image from The Journal of Gene Medicine [59]	1
Figure 1.1.2 - Vectors used in gene therapy clinical trials. Adapted image from The Journal of Gene Medicine [59]	2
Figure 1.1.3 - DNA nucleotide chemical structure	3
Figure 1.1.4 - DNA different nucleotide bases.....	4
Figure 1.1.5 - DNA chain.....	4
Figure 1.1.6 - Linear, open circular and supercoiled plasmid DNA, respectively.	5
Figure 1.1.7 - Schematic model a negatively supercoiled plasmid [19,30]. The DNA double helix is represented by the thick line. The superhelix axis is the dashed curve crossing the nodes and bisecting the area enclosed by the two DNA double strands between adjacent nodes. The superhelix radius is the distance between the superhelix axis and the DNA double strands.....	6
Figure 1.2.1 - Schematic process steps for the development of plasmid DNA.	7
Figure 1.3.1 - LC molecule-stationary phase base interaction illustration. Respectively SEC, HIC, IEX and AC [31].....	14
Figure 1.3.2 - Structure illustration of the different types of stationary phase's composition. A) Gels (e.g. agarose, cellulose...) B) Rigid porous media (e.g. Silica, alumina...) C) Composite media (e.g. Silica/dextran, agarose/dextran...) D) Monoliths (e.g. Polyacrylamide) [22].	15
Figure 1.3.3 - Different ligand architecture in the stationary phase pore; A) without spacer - Because they are connected directly on the surface wall, the interaction may be limited once many of them are accessible. B) with spacers - the spacers where designed to attend the accessibility problem, however, some controversial discussions throughout the literature whether it will be a source of non-specific interactions. C) Polymeric modification (Graft) - grafted ligands shows a more promising alternative for attend the accessibility drawback and have already showed a higher binding capacity [23].	16
Figure 1.3.4 - Anion-exchange separation principles. Adapted from GE Healthcare handbook.	17
Figure 1.3.5 - Typical AEC chromatogram. (D) - Denaturated pDNA (OC) - open circular isoform (SC) supercoiled isoform. [60]	19

Figure 1.3.6 - A) Highly ordered water shells surround the hydrophobic surfaces of ligands and proteins. Hydrophobic substances are forced to merge to minimize the total area of such shells. Salts enhance the hydrophobic effect. B) The equilibrium of the hydrophobic interaction is controlled predominantly by the salt concentration [31].	19
Figure 1.3.7 - Solubilizing properties of water molecules and its ability to interact with dipoles and form hydrogen bonds [31]	20
Figure 1.4.1 - Langmuir adsorption isotherm with the limiting behavior for low and high C values. M is the initial slope and 1/K is the liquid phase concentration in equilibrium with one-half of q_m [22].	24
Figure 1.5.1 - Flow microcalorimeter representative scheme.....	26
Figure 1.5.2 - Typical FMC thermogram for linear pDNA adsorption on Q-Sepharose.	27
Figure 3.1.1 - Electrophoresis results of pDNA in different conformations. A - pDNA after recovery and clarification with Qiagen Kit. B - pDNA after 1 day at room temperature after A. C - pDNA after 2 day at room temperature after A. D - (a) pDNA after 3 day at room temperature after A and (b) pDNA after Hind II digestion. 1 - Open circular (oc) pDNA. 2 - linear (ln) pDNA. 3 - supercoiled (sc) pDNA. 4 - molecular weight marker (adapted from [1]).	37
Figure 3.1.2 - Typical chromatogram obtained by injection of the plasmid sample recovered from the the Qiagen Kit, onto the CIMac™ DEAE column.	38
Figure 3.2.1 - Chromatographic profile of the plasmid isoform separation from a clarified pDNA sample (sc + oc) in the Toyoperl GigaCap Q 650-M column. The Elution method was based in the separation method suggested by Prazeres et al.[18].....	39
Figure 3.2.2 -Tipycal chromatographic profiles of the plasmid isoform separation from a clarified pDNA sample (sc + oc) in the Toyoperl GigaCap Q 650-M column. Different colors mean different injection concentrations.	40
Figure 3.2.3 - Chromatographic profile of the plasmid isoform separation from a clarified pDNA sample (sc + oc) in the with the CIM® DEAE-0.34 Disk.....	41
Figure 3.4.1 - Thermograms of ln pDNA adsorption onto Phenyl-sepharose using the 230 μ L loop. Black 124.97 μ g pDNA/g Phenyl Sepharose; Red 171.75 μ g pDNA/g Phenyl Sepharose; Blue 413.18 μ g pDNA/g Phenyl Sepharose. Vertical dashed line represents the time where the pDNA solution plug is replaced with pDNA-free mobile phase around 1650 seconds.	44
Figure 3.4.2 - Thermograms of ln pDNA adsorption onto Phenyl sepharose using the 430 μ L loop. Black 117.67 μ g pDNA/g Phenyl Sepharose; Green 363.42 μ g pDNA/g Phenyl Sepharose; Orange	

614.70 μg pDNA/g Phenyl-Sepharose. Vertical dashed line represents the time where the pDNA solution plug is replaced with pDNA-free mobile phase around 2100 seconds. 44

Figure 3.4.3 - PEAKFIT de-convolution of 230 μL loop thermograms for loading concentrations of A - 124.97 μg pDNA/g Phenyl Sepharose; B 171.85 μg pDNA/g Penyl Sepharose; C - 413.18 μg pDNA/g Phenyl Sepharose. Curves shown are for experimental data. Total peak fit (black line (-)) and peaks resulting from deconvolution (blue and red lines (...)) Vertical dashed line represents the time where the pDNA solution plug is replaced with pDNA-free mobile phase around 1650 seconds. 46

Figure 3.4.4 - PEAKFIT de-convolution of 430 μL loop thermograms for loading concentrations of A - 117.45 μg pDNA/g Phenyl Sepharose; B - 362.91 μg pDNA/g Penyl Sepharose; C - 613.82 μg pDNA/g Phenyl Sepharose. Curves shown are for experimental data. Total peak fit (black line (-)) and peaks resulting from deconvolution (blue and red lines (...)). Vertical dashed line represents the time where the pDNA solution plug is replaced with pDNA-free mobile phase (Grey - 230 μL loop and Black - 430 μL loop). 47

Figure 3.4.5 - Endothermic heats of ln pDNA adsorption onto (●) Phenyl Sepharose (◆) Q-Sepharose [1]. 49

Figure 3.4.6 - Exothermic heats of ln pDNA adsorption onto (●) Phenyl Sepharose (◆) Q-Sepharose [1]. 50

Figure 3.4.7 - Comparison between the ln-pDNA-Q-Sepharose first endothermic peak energy (◆) and ln-pDNA-Phenyl Sepharose second endothermic peak (●). 51

Figure 3.4.8 - Net heats (sum of all energetic contributions) of ln pDNA adsorption onto (●) Phenyl Sepharose (◆) Q-Sepharose [1]. 52

Figure 3.4.9 - Thermograms of sc pDNA adsorption onto Q-sepharose using the 30 μL loop. Black 13.24 μg pDNA/g Q-Sepharose; Red 52.97 μg pDNA/g Q-Sepharose; Blue (-) 102.85 μg pDNA/g Q-Sepharose. Vertical dashed line represents the time where the pDNA solution plug is replaced with pDNA-free mobile phase around 1150 seconds. 53

Figure 3.4.10 - Thermograms of sc pDNA adsorption onto Q-sepharose using the 430 μL loop. Black 117.26 μg pDNA/g Q-Sepharose; Blue 1172.60 μg pDNA/g Q-Sepharose. Vertical dashed line represents the time where the pDNA solution plug is replaced with pDNA-free mobile phase around 2100 seconds. 53

Figure 3.4.11 - PEAKFIT de-convolution of thermograms for loading concentrations of A - 13.24 μg pDNA/g Q-Sepharose; B -13.24 μg pDNA/g Q-Sepharose; C - 102.85 μg pDNA/g Q-Sepharose. Curves shown are for experimental data. Total peak fit (black line (-)) and peaks resulting from

deconvolution (blue and red lines (...))Vertical dashed line represents the time where the pDNA solution plug is replaced with pDNA-free mobile phase around 1150 seconds. 55

Figure 3.4.12 - Endothermic heats of sc pDNA adsorption (●) and ln pDNA adsorption (◆) onto Q-Sepharose[1]. 57

Figure 3.4.13 - PEAKFIT de-convolution of thermograms for loading concentrations of A - 117.86 μg pDNA/g Q-Sepharose and B - 1172.60 μg pDNA/g Q-Sepharose. Curves shown are for experimental data. Total peak fit (black line (-)) and peaks resulting from deconvolution (blue and red lines (...))Vertical dashed line represents the time where the pDNA solution plug is replaced with pDNA-free mobile phase around 2100 seconds. 57

Figure 3.4.14 - Endothermic heats of sc pDNA adsorption onto (●) and ln pDNA adsorption (◆)onto Q-Sepharose [1]..... 59

Figure 3.4.15 - Net heats (sum of all energetic contributions) of sc pDNA adsorption onto (●) and ln pDNA adsorption (◆)onto Q-Sepharose [1]. 60

Figure 3.4.16 - Thermograms of ln pDNA adsorption onto Q-Sepharose, at pH 8. Injection loop: 30 μL . (a) Black (-) 12.6 μg ln pDNA/g Q-Sepharose; red (- -) 53.4 μg ln pDNA/g Q-Sepharose; blue (-.-) 111.2 μg ln pDNA/g Q-Sepharose; (b)-(d) PEAKFIT deconvolution of thermograms for loading concentrations of (b) 12.6 μg ln pDNA/g Q-Sepharose, (c) 53.4 μg ln pDNA/g Q-Sepharose and (d) 111.2 μg ln pDNA/g Q-Sepharose. Curves shown are for experimental data (red line (-)); total peak fit (black line (-)) and peaks resulting from deconvolution (blue line (...)). Vertical dashed line represents the time where the pDNA-containing plug of solution is replaced with pDNA-free mobile phase. 70

Figure 3.4.17 - Thermograms of ln pDNA adsorption onto FF Q-Sepharose. Injection loop: 429 μL . PEAKFIT de-convolution of thermogram for loading concentrations of 1359.6 μg ln pDNA/g Q-Sepharose. Vertical dashed line represents the time where the pDNA-containing plug of solution is replaced with pDNA-free mobile phase. 71

Tables

Table 1.2.1 - Agencies guidelines for application of pharmaceutical grade of sc pDNA.	11
Table 1.3.1 - Branches of modern Liquid Chromatography summary.	13
Table 2.3.1 - Recovery of pDNA using QIAGEN® Plasmid Maxi Kit.	32
Table 3.4.1 - Heat of adsorption for ln pDNA adsorption onto Phenyl-sepharose using the 230 and 430 μ L loop.	45
Table 3.4.2 - Sum of heat of adsorption for ln pDNA adsorption onto Phenyl-sepharose using the 230 and 430 μ L loop.	45
Table 3.4.3 - Heat of adsorption for sc pDNA adsorption onto Q-sepharose using the 30 and 430 μ L loop.	54
Table 3.4.4 - Classification and properties of the different support media used in Liquid Chromatography.	69
Table 3.4.5 - Heat of adsorption for ln pDNA adsorption on Q-Sepharose at pH 8; flow rate: 1.5 mL/h; adsorbent sample size: 21.89 mg; and temperature: 25°C. Enthalpies were determined from the deconvoluted thermograms.	70

1. Introduction

1.1. Plasmid DNA (pDNA)

1.1.1 Gene Therapy and DNA Vaccines: pDNA as biopharmaceutical molecule

Plasmid DNA (pDNA) is the base for promising DNA vaccines and gene therapies against many infectious resulting from acquired or genetic diseases [3-11]. For approximately two decades, these techniques elicited a great deal of attention and like any other novel therapeutic approach, it has also given rise to excessive short-term expectations [4,12]. The data on Figure 1.1.1 shows the main indications and target diseases where plasmid-based therapies have been applied.

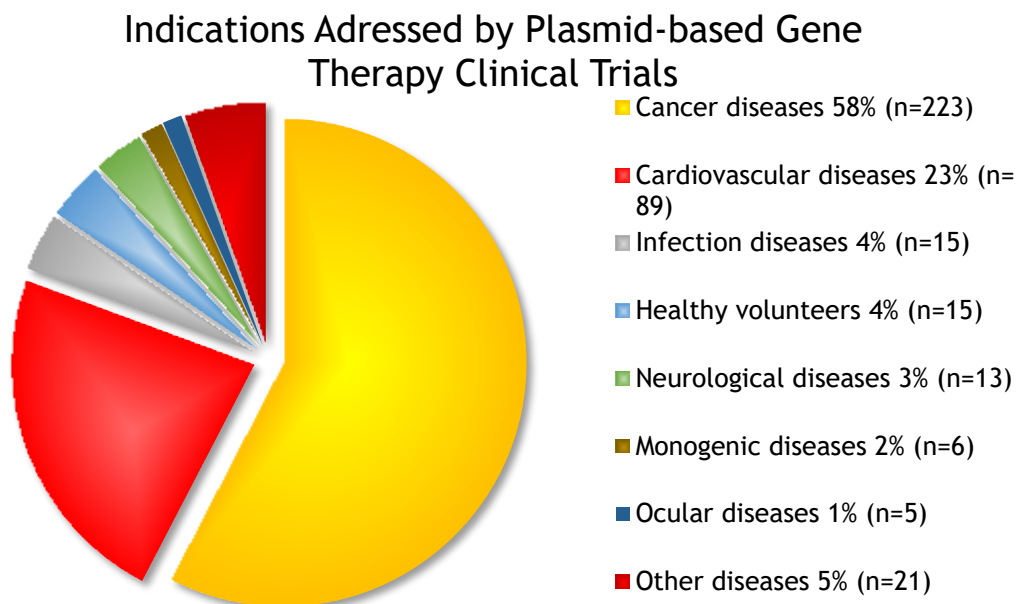


Figure 1.1.1 - Indications addressed by plasmid-based gene therapy clinical trials. Adapted image from The Journal of Gene Medicine [59]

Gene therapy can be defined as a treatment strategy which uses heterologous genetic information, usually in the form of deoxyribonucleic acid (DNA), to compensate or correct a genetic malfunction in order to obtain a therapeutic effect in animal models and human individuals [12]. DNA vaccines are made of small circular genetically engineered pieces of DNA, pDNA, used to generate *in situ* production of antigen that promotes immunological responses against infectious agents [3,10,13]. Naked pDNA vaccines first received attention in the 1990s, since then, a great deal of progress has been made [10].

These therapeutic applications involve essentially three steps: (1) Administration of a gene or a vector containing a gene into the body; (2) Gene delivery from the site of administration to the nucleus of the target cells and (3) gene expression, leading to the production of a therapeutic molecule/antigen[12].

As much significant as the gene that is introduced, the vehicle that will transport it to the target cells also plays a very important role. These vehicles are called vectors, and the main types are viral and non-viral vectors. All viruses attack their hosts and introduce the genetic material into the host cell as a part of their replication cycle [14,15]. Gene therapy based on viral vectors exploit part of this natural process in order to introduce exogenous DNA to the target cells. [15,16]. Following this, a burst of clinical studies came up showing the wide range application for this type of therapy. However, this enthusiastic period didn't last long due to therapy risks, its limitations and the occurrence of deaths during clinical trials [14,15]. Besides some unexceptional results of most clinical studies, other several viral and hosts factors hampered the progress [15]. Nevertheless, the search for a safe gene delivery didn't stop and non-viral vectors began to attract attention as result of their universal application range and, mostly, their high delivery safety level [3,16]. According to the internet Wiley database of gene therapy (www.wiley.com/legacy/wileychi/genmed/clinical/) and as we can see on Figure 1.1.2, 17.4 % of all clinical trials developed until July 2015 used plasmid DNA as non-viral vectors. Thus, gene therapy continues to hold great promise for new therapeutic solutions to as-yet incurable diseases. Also, DNA vaccines are experiencing a resurgence as a result of the success with the prime-boost immunization [3,4,10]. Due to simplicity, versatility, safe profile and low cost storage, pDNA vaccines clinical studies have reappeared. Hence the number of applications of pDNA is still growing [3,10,13], new developments and progress solutions are gradually emerging as a result of the increased demand for the pDNA-based treatments [13].

Vectors use in Gene Therapy Clinical Trials

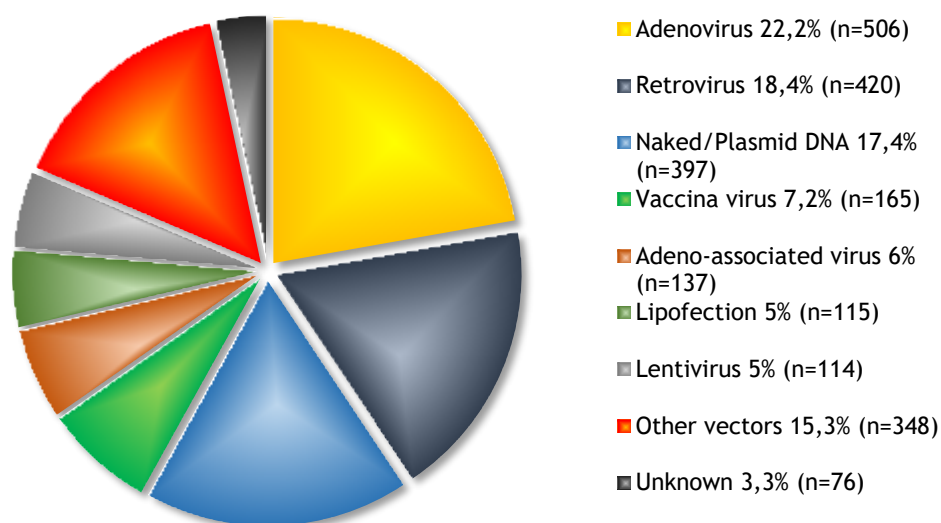


Figure 1.1.2 - Vectors used in gene therapy clinical trials. Adapted image from The Journal of Gene Medicine [59]

To date, three veterinary DNA vaccines are licensed for treatment, the west Nile virus in horses, infectious hematopoietic necrosis virus in salmon and melanoma in dogs [11]. The awareness about the relevance of the pDNA as a therapeutic is growing and causing a substantial demand for this therapeutic molecule. This higher demand of pDNA for different indications combined with the amount of pDNA used per dose, which are much higher compared with the protein-based biotherapeutics, intensifies the need for a large scale of production. In addition, a high purity level and homogeneity is a pivotal parameter to ensure a good therapeutic response and the patient safety. Thus, an efficient purification process is vital as well. Furthermore, the whole production process and storage requires an efficient quality control characterization. Thus, all the manufacturing steps, from production to the final product, are analyzed and controlled by regulatory agencies guidelines like Food and Drug Administration (FDA), European Agency for the Evaluation of Medical Products (EMA) and World Health Organization (WHO). Summarizing, it's needed a well-established and economically affordable process that can be controlled and that ensures a large scale production and highly pure pDNA [3]. The well-publicized potential of gene therapy, together with ongoing clinical trials of DNA vaccines and an increase in the number of the regulatory approvals for veterinary vaccines, makes enormous the market potential for pDNA [3]. Nevertheless, research, laboratory and industrial innovation is still needed to enable the efficient production and control of these high pure quantities [3,10,11].

1.1.2. Structure and Properties

A DNA molecule consists of a linear polymer made of repeated units called nucleotides. These nucleotides are comprised with a phosphate group, a five carbon sugar and a nitrogenous base (Figure 1.1.3). Also, there are two types of nitrogenous bases, purines and pyrimidines. Adenine and Guanine bases belong to purine and Thymine and Cytosine bases belong to pyrimidine type.

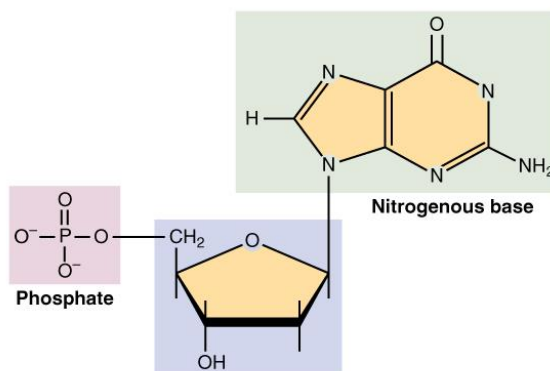


Figure 1.1.3 - DNA nucleotide chemical structure

The unique structure of these nitrogenous bases, as shown in Figure 1.1.4, is responsible for a phenomenon called complementary base pairing, where adenine always pairs with thymine, whereas guanine pairs with cytosine. The linear chain is created by a phosphodiester bond between the sugar of one nucleotide and the phosphate group of the next that creates a sugar phosphate backbone. This backbone structure is negatively charged when the pH > 4 (Figure 1.1.5).

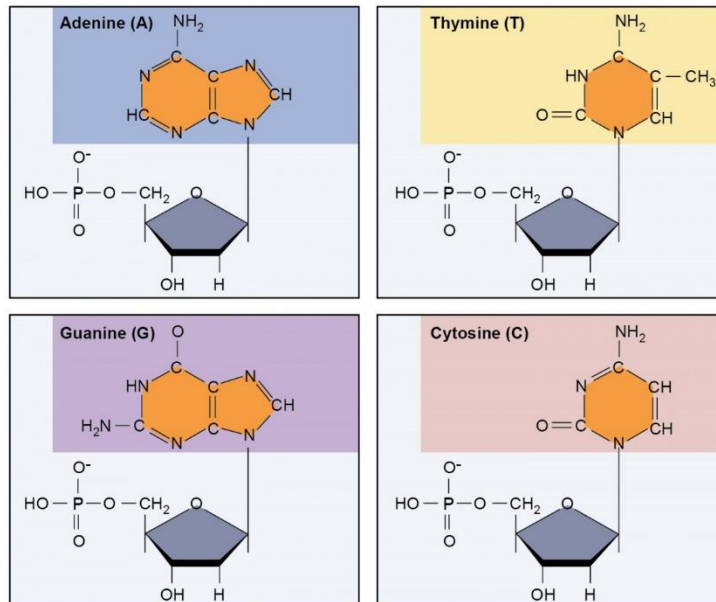


Figure 1.1.4 - DNA different nucleotide bases.

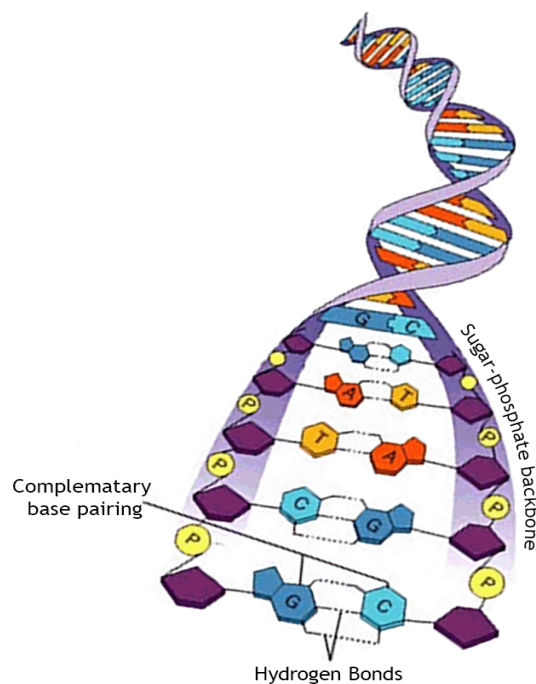


Figure 1.1.5 - DNA chain

The winding of two anti-parallel complementary nucleotides in each DNA strand are connected by hydrogen bonds, along a common axis forming the well-known right-handed double helix structure with highly hydrophobic grooves accessible to solvents and ligand molecules [13].

Plasmids are molecules in which the two ends of the DNA strand are covalently linked, forming a closed loop. Like the chromosomal DNA, it contains genetic information that can benefit the host. In addition, it is physically separated from the chromosomal DNA which makes this molecule a form of gene transmission. Plasmids are considered replicons, which are capable of autonomously replicate inside a suitable host. They can occur naturally in bacteria, but can also be found in some eukaryotic organisms [13,17].

The size of the plasmids can vary from 1 to over 1000 kilo-base pair (kbp) and the number of plasmids inside the same cell can be enormous under some circumstances and may appear in one of many conformations. The conformations can greatly influence the biological activity of plasmids, and this is one of the reasons of the importance of separation studies, that enable the purification of the most active pDNA topology. Thus, different conformational types of pDNA should be regarded in this work [13].

1.1.3 Plasmid conformational forms

The pDNA molecule can mainly exist in three topological conformations namely, linear (ln), open circular (oc) and supercoiled (sc), Figure 1.1.6. The ln pDNA form has been deemed unsatisfactory for clinical purposes due to its perceived risk of recombination, integration into the genomic DNA and more rapid intracellular degradation. The oc pDNA represents a minor risk for clinical application compared with the ln form, but the parameters such as safety, stability and activity are superior in the sc form [13,18].

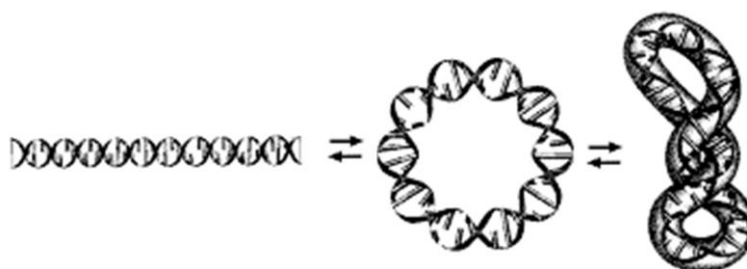


Figure 1.1.6 - Linear, open circular and supercoiled plasmid DNA, respectively.

Supercoiled pDNA is considered as a nanoparticulate material. The length of this molecule may range in order of hundreds of nanometers (nm) whilst having a very small diameter, between 9.9 and 13.4 nm. As we can see in Figure 1.1.6 the supercoiled isoform has a higher order structure due to a coil of the helix axis in space [18].

The number of times that the two strands of DNA helix are intertwined is called linking number, Lk . For an oc pDNA the linking number is Lk_o , which is equal to the number of base pairs (bp) in the molecule divided by the helical repeat (10.6 bp/turn). The negatively charged sc plasmids are characterized by a deficiency in the Lk , in which $Lk < Lk_o$. These supercoiling degree can also be described in terms of a specific linking number difference, or superhelix density, σ , given by: [18,19]

$$\sigma = \frac{(Lk - Lk_o)}{Lk_o} \quad (1)$$

Most supercoiled plasmids molecules isolated from prokaryotes have σ values between -0.05 and -0.07. [18]. At these degree of supercoiling, plasmid molecules have a clearly defined branched shape as shown in Figure 1.1.7.

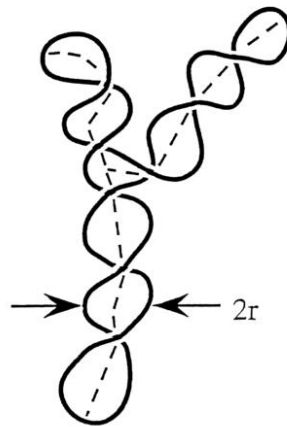


Figure 1.1.7 - Schematic model a negatively supercoiled plasmid [19,30]. The DNA double helix is represented by the thick line. The superhelix axis is the dashed curve crossing the nodes and bisecting the area enclosed by the two DNA double strands between adjacent nodes. The superhelix radius is the distance between the superhelix axis and the DNA double strands.

In addition, Boles et al. [19] found out that for 3.5 and 7.0 kbp molecules, the superhelix axis length is independent of σ and is about 41% of the total DNA length. For the same plasmids, the superhelix radius decreased hyperbolically with the superhelix density, σ , according to the relation [18,19] :

$$\frac{1}{r} = 0.00153 - 0.268\sigma \quad (2)$$

Moreover, it is important to mention that the size of pDNA for vaccine production typically ranges from 3 to 15 kbp, depending on the vector complexity, with the expectation that the size could increase in the future, namely for the production of multivalent vaccines [18,19] .

1.2. Biotechnological plasmid DNA production

As stated before, the potential of gene therapy and DNA vaccines are increasing the interest of using pDNA as a biopharmaceutical molecule. This interest already increased the need of a large scale manufacture and also the improvement of good manufacturing practices (GMP) [3,5].

The pDNA biotechnological production process can be divided into two sequential phases. The upstream processing which comprise the steps that goes from the plasmid production and host development to the cell fermentation. The downstream processing is responsible for the harvest, lysis and purification of the desired molecule. With the scale up to an industrial production, some methods used in laboratory-scale became inadequate and had to be replaced by others more economically reliable and environmentally safer. Figure 1.2.1 shows the general steps in the pDNA production [3,5,13].

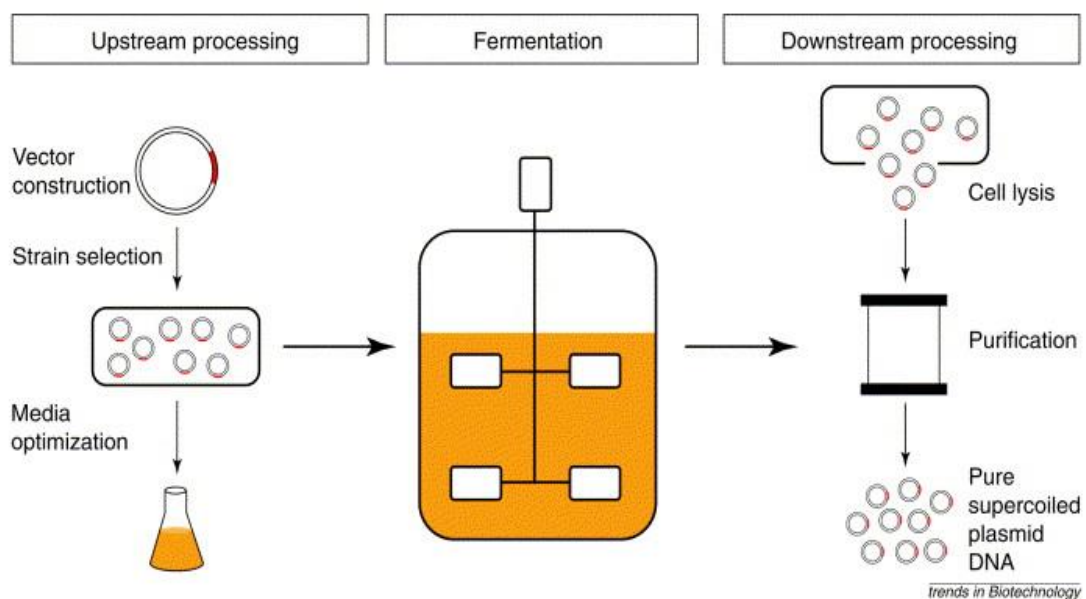


Figure 1.2.1 - Schematic process steps for the development of plasmid DNA.

The final product quality depends on the production system. Thus, it is very important to design and evaluate all the manufacturing steps previous to the scale up in order to achieve the best pDNA productivity and quality. Even with a well stabilized process of manufacturing, it is crucial to control all the steps [5,13].

1.2.2. Upstream Processing

The manufacturing process begins with the isolation of the desired gene and its insertion on the plasmid, a process known as vector construction. Generally, the vector consists of a plasmid backbone that includes very common elements like one replication origin, a stronger promoter, a polyadenylation signal sequence, an antibiotic resistance gene and the encoding therapeutic gene. Next, the host cells to take up the designed vector need to be prepared. All process is well characterized and has been used for years, making the vector construction and cell bank preparation to take about 1-2 weeks. The use of antibiotics assist the strains selection [3,5].

The most commonly used host for pDNA production is the bacterium *Escherichia coli* (*E. coli*) for high cell-density cultivations (HCDC). Several strains have been reported to be effective in the pDNA production and most of them are selected because of its well documented usage in laboratory-scale protocols. For HCDC, the commercial *E. coli* DH5 α strain still have some drawbacks, like the increased aerobic acetate production that causes loss of productivity and waste of carbon source. Even so, this commercial strain has a higher production when compared with the other strains like DH5, DH1, DH10B and JM108 that are used in laboratory-scale as well. In addition, the DH5 α strain cultivations have a higher supercoiled fraction in comparison with the above cited strains. For a plasmid size of 6.1 kbp, the commercial *E. coli* DH5 α have shown to produce 12.73 ± 0.10 mg/L of pDNA with 80% of supercoiled fraction, when cultivated with 100 g/L of glucose to achieve the HCDC in batch mode [5,20].

Nevertheless, the host and strain selection is by far the only factor to have in concern. Other factors as medium composition, growth temperature, and time of fermentation are also very important and have a direct relation on the quality and quantity of the product. At laboratory scale, the production of plasmids seems to be relatively easy and simple once the fermentations are conducted in a batch mode and the quantity needed it's not very high [5]. Plasmids represents around 3% WW⁻¹ of the *E. coli* total extract, and since the open circular and linear ones are considered unsatisfactory by the regulating agencies, the final and desired product will be even smaller [5,13]. Biomass productivity (volumetric yields), plasmid number of copies (specific yields) and quality are key concerns that have to be improved trough the optimization of the biological production system for an economically affordable industrial scale-up. In this process, for an optimal plasmid production both volumetric and specific yields have to be maximized. Thus, high volumetric yields will enable smaller and economical fermentations and high specific yields will increase the plasmid purity leading to an easier and reliable economic separation and purification process [5].

1.2.3. Downstream Processing

Sequentially, after the whole production procedure, the recovery and purification processes are necessary. These include the cell harvest, lysis, separation of the cellular debris, clarification, chromatographic purification and concentration [3,13]. In general, this is the most technically difficult part, since the product of interest are labile requiring mild processing conditions. Specially in this case, pDNA has some concern associated with the conventional purification of biological samples [13]. These major concerns are related substantially with the pDNA structural nature, mainly the conformation. As stated before, only the supercoiled fraction has clinical importance, as it presents higher biological activity. The diversity of biomolecules present in the pDNA containing extracts and the structural and chemical similarities between the pDNA and impurities are also some of the central challenges for the recovery and purification of pDNA [3,13]. Actually, most of the critical contaminants share some similar characteristics like: negative charge (RNA, genomic DNA, and endotoxins), identical size (genomic DNA, endotoxins) and hydrophobicity (endotoxins). Samples with these kind of complexity and similarities usually require the establishment of purification processes with larger number of steps to efficiently separate the different species [5,13]. However, the intensification of the process steps in extraction, isolation and purification induce a considerable structural stress which can result in damage of the supercoiled isoform. Once more, it is crucial to evaluate every step previously in order to avoid product degradation and maximize the product yield [3,13].

Before the lyses, the cell harvest must be performed. This is a process that will decrease the fermentation volume by concentrating the cells 3 to 5 times. Depending on the scale, either centrifugation or filtration are suitable to be used on the cell harvesting. The filtration step needs to minimize shear and permeate control. On the other hand, centrifugation is more cost-effective at large scales but to maintain the throughput necessary, high shear forces are needed; therefore, filtration should be preferred at all scales [5,13].

On the lysis process, the main goal is to disrupt the cell to release the pDNA and eliminate the solid debris. There are chemical, physical and mechanical methods for this step, however for pDNA recovery, alkaline lysis accompanied by the use of detergents such as Triton was developed many years ago and it still is one of the most methods used at laboratory-scale. This is a very well established method, since the detergent solubilizes the cell wall and the alkaline environment denatures the genomic DNA. Generally, after the chemical lysis, a chemical precipitation is performed in order to remove major impurities such as high molecular weight RNA, proteins, endotoxins and genomic DNA and concentrate the sample. It is important to mention that this last step is not a good process for the scale up and other methods should be considered for an industrial scale [3].

At the end of the lysis step the sample remains with some of the impurities and most important, all the plasmid conformational states are present[13],but the initial volume decrease substantially and more vital, the pDNA molecule is maintained in solution which will facilitate the purification process [3,13]. There are a few purifications processes, but liquid chromatography (LC) is the most commonly used technology for biological sample purification, either as processing step or as analytical tool [5,17,18].

In the last few decades, some advances in the biotechnological areas have introduced several technologies for the purification of complex biomolecules [5]. Even so, an evaluation of the global process showed that the downstream operations have a significant relevance, being one of the most important and more expensive steps [5]. Some precipitation and ultrafiltration techniques can be involved in the isolation process, and also aqueous two-phase systems have been applied in the purification steps; however LC is undoubtedly the most used technique [3,5].

Liquid chromatography is central not only to the small-scale purification of plasmids, but also to the industrial large-scale. This technique can be used as a purification step and as an analytical tool used for monitoring process development and product quality control [13,18]. The goal of LC as a separation step consists in the separation of the pDNA from residual impurities and undesirable isoforms through biomolecule capture and flow-through steps [5,18]. The different properties such as the size, the conformation form and hydrophobicity of different nucleic acids have been explored in order to give some insight about the possible interactions that are responsible for their adsorption process. Information is crucial to better understand the chromatographic step, with the final goal of improving future systems [5].

For a therapeutic application of pDNA, the final product has to be in a highly purified and homogenous preparation of sc isoform, to obey the strict guidelines established by the regulatory agencies. Table 1.2.1 shows the prerequisites of pDNA for therapeutic application [3,5,13].

To sum up, the development of a plasmid purification process must first consider the complex origin of the plasmid-containing extract. As stated before, one of the problems on the sc pDNA purification is mainly due to the physiochemical similarities between the target molecule and the contaminants. Unquestionably the central technique used to purify sc pDNA from its other isoforms and related impurities is liquid chromatography.

There are several chromatographic systems used to purify such molecules. These chromatographic systems and their differences will be addressed in the following chapter.

Table 1.2.1 - Agencies guidelines for application of pharmaceutical grade of sc pDNA.

	FDA and EMEA	Units
sc pDNA	>97	%
gDNA	<2	µg/mg pDNA
Proteins	<3	µg/mg pDNA
RNA	<0.2	µg/mg pDNA
Endotoxins	<10	EU/mg pDNA

1.3. Liquid Chromatography technique for pDNA purification

Mikhail Tswett defined chromatography as: “Any liquid or gaseous mixture of the substances is divided into its components during the process of its movement through a layer of sorbent, if there are differences in sorption interaction between the components of the mixture and the sorbent” [21]. Nowadays, LC can be defined as a two-dimensional process that employs a fixed-bed, known as the *stationary phase*, to separate a mixture of components that are carried through the bed by a fluid phase known as the *mobile phase*. When different components are fed into the stationary phase, they are expected to have different types of interaction. The feed components that interact more strongly with the stationary phase are retarded and are eluted later than those that interact more weakly and travel faster. Thus, the nature of interactions of solutes between the two phases depends on the molecular interactions between the feed components, the functional groups present on the surface of the stationary phase and the system conditions provided by the mobile phase. One exception is the size exclusion chromatography, where the stationary phase is steric leading to a separation based only on the size of molecules [22]. Table 1.3.1 provides a brief summary of the various branches of modern LC as they apply to biopolymer separation, defined by the type of stationary phase ligate.

Table 1.3.1 - Branches of modern Liquid Chromatography summary.

Stationary phase interaction type	Mobile phase	Branch	Acronym
None	Aqueous	Size exclusion	SEC
Hydrophobic	Normally an aqueous solution with high kosmotropic salt concentration. Elution by decreasing salt concentration.	Hydrophobic Interaction	HIC
Charged	Normally an aqueous solution with low salt concentration. Elution with increasing salt concentration.	Ion exchange	IEX
Biospecific	Aqueous. Desorption with competitively agents.	Afinity	AC

To the date, these chromatographic branches have already been applied to the pDNA purification with the goal to achieve higher productivities. Figure 1.3.1 illustrates the up mentioned separation principles for purification.

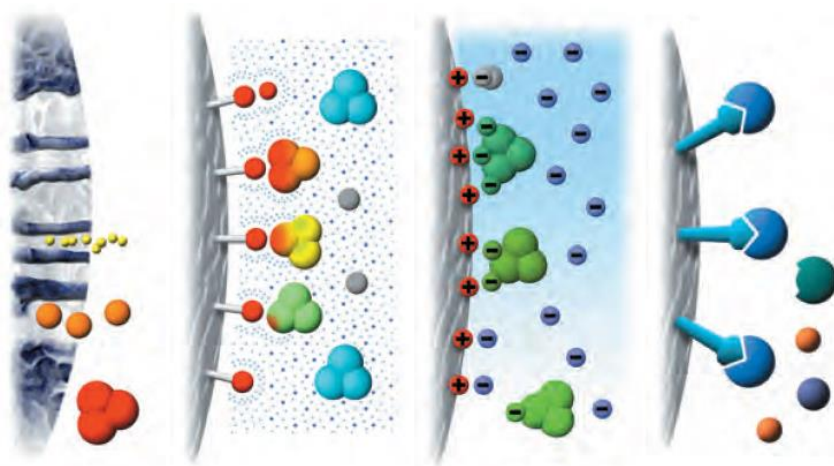


Figure 1.3.1 - LC molecule-stationary phase base interaction illustration. Respectively SEC, HIC, IEX and AC [31].

Size exclusion chromatography (SEC) fractionates the molecules based on molecular size. The molecules do not actually bind to the chromatographic support, which means that the buffer composition does not interfere on the resolution (the degree of separation between two peaks). SEC can be used in the pDNA separation due to the reduction of the plasmid hydrodynamic radius due to the supercoiling, however it's advised to be used as a final polishing technique to separate it from RNA and smaller proteins. [3,13].

Hydrophobic interaction chromatography (HIC) is a well-established bioseparation branch that separates the biomolecules according to differences in their surface hydrophobicity by exploiting the reversible interaction between the molecule and the hydrophobic ligand on the support matrix surface. HIC was introduced as a pDNA purification method due to the fact that single stranded nucleic acid impurities (RNA and desaturated DNA) are more hydrophobic than double stranded DNA [5], thus being applied as a negative chromatography [17].

Ion-exchange chromatography (IEX) principle is based on the electrostatic interactions that occur between biomolecules and stationary phase. Thus, biomolecules are separated according to the differences in their net charges. Plasmid purification by IEX, more specifically anion-exchange chromatography takes advantage from the interaction between the negatively charged DNA backbone created by the phosphate groups and the positively charged ligands on the support surface. [5,13].

Affinity chromatography (AC) has been suggested as an alternative and high selective method that uses natural biological interaction processes such as molecular recognition on the basis of their biological function or chemical structure. In spite of its excellent selectivity, the method

suffers from limitations like slow kinetic and ligand fragility that are associated with low binding capacity [3].

As we have seen through this chapter, the ligands on the stationary phase have a crucial importance on the separation process [23]. Thus, the last decade of research brought also the attention to support matrixes composition [23-25]. At this moment, important information showed that not only the ligand itself but also support matrix composition, physical structure and ligand distribution have some contribution to the separation process [22,24-28].

1.3.1. Physical proprieties of different stationary phases.

The need for high amount of pharmaceutical-grade biomolecules with a therapeutic purpose brought the requirement for high production quantities [5]. Over the last three decades, there have been significant improvements on the upstream processes that have increased the feedstock concentrations. Unfortunately, there hasn't been a concomitant increasing in the downstream processes improvements. As stated above, the downstream processes, more specifically the LC technique, are the most expensive part of the production system. The only way to reduce the costs of such an operation is to increase the overall throughput (i.e, increase the ratio final product per time unit). The most common way to accomplish this is to increase the scale of operation (e.g., increase the number or size of the chromatography columns) or by using continuous methods. Yet, another efficient method is to increase the stationary phase capacity of purification through an optimization of its physical and chemical proprieties [22,23].

Some desirable features for a stationary phase support matrix include low non-specific adsorption, high mechanical strength, high surface functionality for immobilization of ligands, absence of toxic leachable, and stability in solution used for cleaning and sanitation. A variety of materials are available that meet these requirements and form the basis for modern chromatography media, Figure 1.3.2. The Table 3.4.4 (appendix) summarize classification and properties of the different support media used in LC [22]. The majority of supports used to date are based on particles (beads) that are packed into a column forming a homogenous bed. More recently, the continuous stationary phases appeared, and are known as monoliths. The monoliths are produced *in situ* crating a network of pores or channels through which the fluid flows [5,23-25,28].

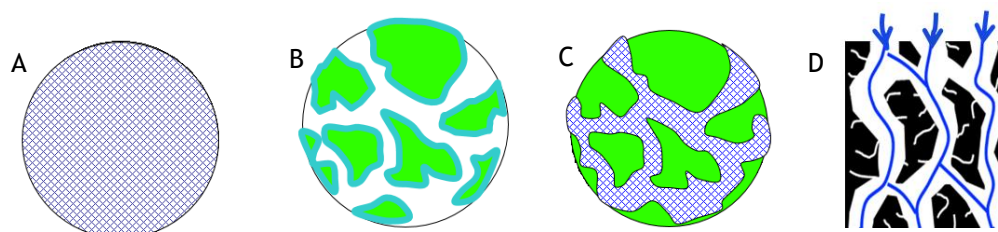


Figure 1.3.2 - Structure illustration of the different types of stationary phase's composition. A) Gels (e.g. agarose, cellulose...) B) Rigid porous media (e.g. Silica, alumina...) C) Composite media (e.g. Silica/dextran, agarose/dextran...) D) Monoliths (e.g. Polyacrylamide) [22].

In order to attain a high productivity a high binding capacity is a crucial parameter. As we have seen in this work, the majority of separation techniques depends on the interaction between the ligand and the molecules. Thus, if the surface of interaction increases, the number sites available for the molecule to interact can also increase leading to a higher capacity [23]. Considering this strategy, both support matrices (beads and monoliths) used in these applications are usually porous [22,23]. The porosity is a form to enhance the surface area available as long as the pore size is sufficient to allow molecule diffusion through the porous network [22]. Some structural illustrations are shown on Figure 1.3.2.

Another important aspect of the construction of stationary phases is the form of how the surface modification is taken to introduce the ligands. The global ligand architecture will affect the binding capacities and sometimes non-specific interactions. These non-specific interactions may unpredictably influence the adsorption process for an individual molecule. Chemical modification is needed in order to functionalize the support matrix. Ligands need to be connected to the base material backbone. There are general possibilities to connect ligands to the pore wall of a resin. Moreover, the final formulation of matrix bound ligands is also a main properties that can influence the binding capacity [23]. A schematic representation is shown on Figure 1.3.3.

The purification of pDNA using conventional chromatographic media (*packed beads*) face some limitations, not only related to the similarities, but also related with the limitations of available stationary phases, mainly because of their low capacity to bind large biomolecules. For instance, it has to be considered that the hydrodynamic radius of a pDNA molecule is larger than the average of a protein and has a very low diffusivity. Hence, the packed columns with soft chromatographic beads are limited by mechanical factors such as bed instability and mass transfer problems [5]. These drawbacks led to the development of monoliths. Chromatographic monoliths represents the 4th generation of stationary phases. Consisting in a single piece of highly porous material and a network of channels through which the mobile phase flows. The particular monolith structure inherently reflects in several key properties such as: very high

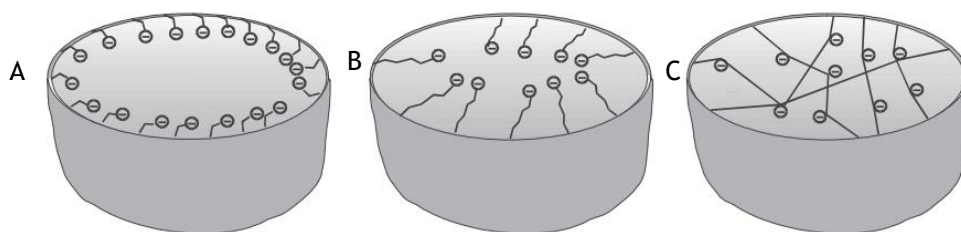


Figure 1.3.3 - Different ligand architecture in the stationary phase pore; A) without spacer - Because they are connected directly on the surface wall, the interaction may be limited once many of them are accessible. B) with spacers - the spacers were designed to attend the accessibility problem, however, some controversial discussions throughout the literature whether it will be a source of non-specific interactions. C) Polymeric modification (Graft) - grafted ligands shows a more promising alternative for attend the accessibility drawback and have already showed a higher binding capacity [23].

porosity, high binding capacity for extremely large molecules and mass transport based on convection [28]. Among the different chromatographic stationary phases methacrylate monoliths seem to be especially attractive due to a short purification time, flow unaffected properties, high dynamic binding capacity and applicability to industrial scale [26,28]. The typical plasmid size found in DNA vaccines ranges from 3 to 15kbp with the future expectation that the size could increase [3]. With the application of monolithic stationary phases, the “small” plasmid purification turned to be easier and separation of plasmids up to 62kbp already began to appear [26-28].

1.3.2. Anion-Exchange Chromatography principles for pDNA purification

An Anion-Exchange chromatographic column consists of a matrix substituted with ionic groups that are positively charged. The first step in a chromatographic procedure is to equilibrate the stationary phase (Figure 1.3.4 A) with a buffer that has adequate pH and ionic strength to bind the negatively charged sc pDNA and not bind positively charged impurities. The bound biomolecules are concentrated in the column while biomolecules with the same charge as the medium pass through the column (flow through), eluting during or just after the sample application (Figure 1.3.4 B). After all the sample has been loaded into the column and non-binding biomolecules eluted (UV signal returns to baseline) conditions are altered by changing the buffer, usually increasing the ionic strength (salt concentration), leading to the elution of the bound biomolecules. These biomolecules start to elute as the ionic strength increases because salt ions start to compete for the medium binding sites (Figure 1.3.4 C). The first biomolecules to be eluted from the column are the ones with the lowest net charge at the

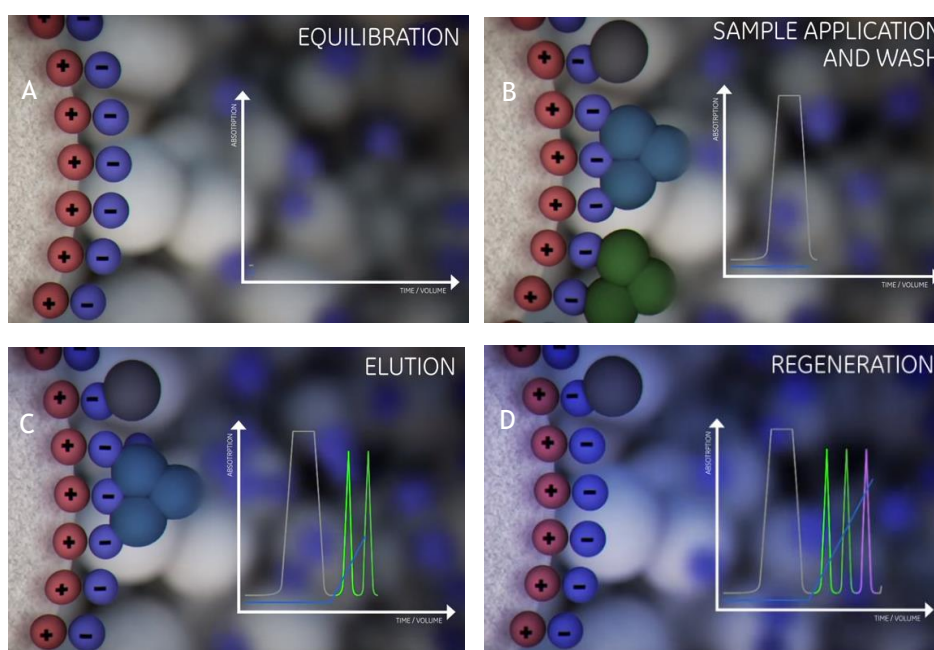


Figure 1.3.4 - Anion-exchange separation principles. Adapted from GE Healthcare handbook.

selected pH, thereafter, the ones with the higher net charge will be most strongly retained and be eluted last. Thus, controlling the changes in ionic strength, different biomolecules can be eluted differentially in a purified and concentrated form [29].

The final step is the regeneration of the column through the use of a very high ionic strength buffer that will remove all the tightly bound biomolecules (Figure 1.3.4 D). Before a next run, the column has to be re-equilibrated using the same initial conditions buffer and the process can work as a cycle [29].

Depending on the source of the feed material, various types of impurities (host cell proteins, nucleic acids, retroviral particles, process additives and lipids) if not removed during the washing, may be trapped in the chromatography medium causing carryover from one cycle to the next. In that case, cleaning-in-place (CIP) of the chromatography column is important for the integrity and safety of the final product. Sodium hydroxide is the gold standard for cleaning and sanitizing chromatography columns [30].

Different molecules exhibit different degrees of interaction with positively charged media according to their overall charge, charge density and surface charge distribution. Hence, the overall interaction between the pDNA and the stationary phase is based in the local attraction generated by the opposite charges. The isoforms will have different retention times in an increasing salt gradient, especially the supercoiled form which have a higher charge density, binds more strongly to the stationary phase eluting after the oc and the ln isoforms [5,13,18]. In addition to the charge density effect, the separation of linear isoforms it's also affected by other parameters such as dispersive forces, hydrogen bonding, dipole-dipole attraction, solvophobic repulsion and AT content which can interfere with the charge density. Nevertheless, the selectivity towards pDNA or impurities (gDNA, RNA and endotoxins) is poor due to the non-specific binding to the anion-exchange stationary phase [5]. Still, when using anion-exchange chromatography to separate pDNA its advised load the sample at a high salt concentration (typically > 0.5 M NaCl) to avoid an unnecessary adsorption of low charge density impurities such as low MW RNA, oligonucleotides and proteins [18]. Under these conditions a significant amount of impurities elute in the flow through and the capacity can be fully exploited for pDNA adsorption. The Figure 1.3.5 shows the typical chromatogram of an anion-exchange chromatography separation process with the different isoforms retention times and elution salt concentration [44].

Some authors suggests that anion-exchange chromatography should be used in series with other purification techniques to guarantee the quality established by the regulatory agencies [5,18]. Notwithstanding, a single step pDNA purification have been further from happening. The combination of ion-exchange and hydrophobic interaction in a single monolith was developed creating the concept of conjoint liquid chromatography. This concept brought the possibility to

achieve a pDNA sample with the level required for human treatment in a single chromatographic step [26].

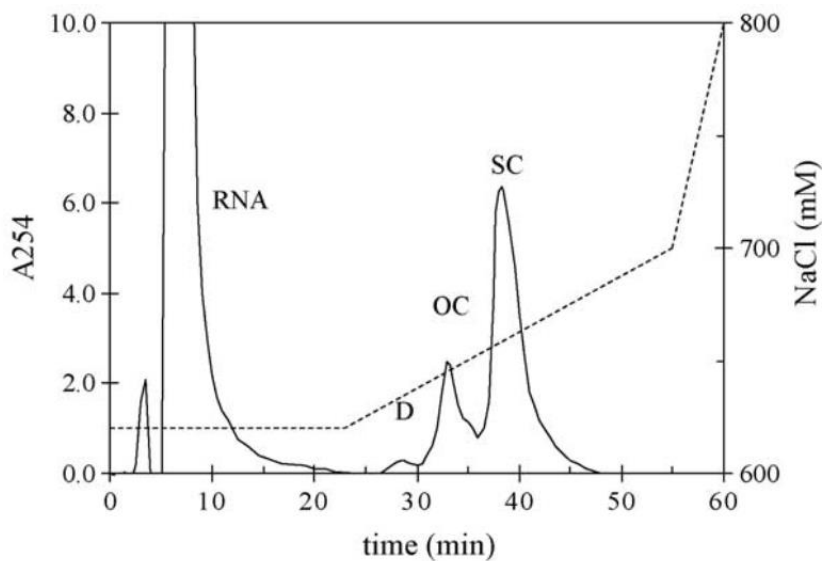


Figure 1.3.5 - Typical AEC chromatogram. (D) - Denaturated pDNA (OC) - open circular isoform (SC) supercoiled isoform. [60]

1.3.3. Hydrophobic Interaction Chromatography principles for pDNA purification

HIC separates molecules according to differences in their hydrophobicity by exploiting a reversible interaction between them and the hydrophobic surface of a HIC medium. Thus, molecules with different degrees of surface hydrophobicity can be separated. In contrast to anion-exchange chromatography, the interaction between the pDNA and the HIC medium is influenced significantly by the presence of kosmotropic salts in the running buffer. In pure water any hydrophobic effect is too weak to cause interaction between ligand and molecules or between the molecules themselves. However, kosmotropic salts enhance hydrophobic effect, and adding salts bring about binding of the target biomolecule to HIC media. High salt

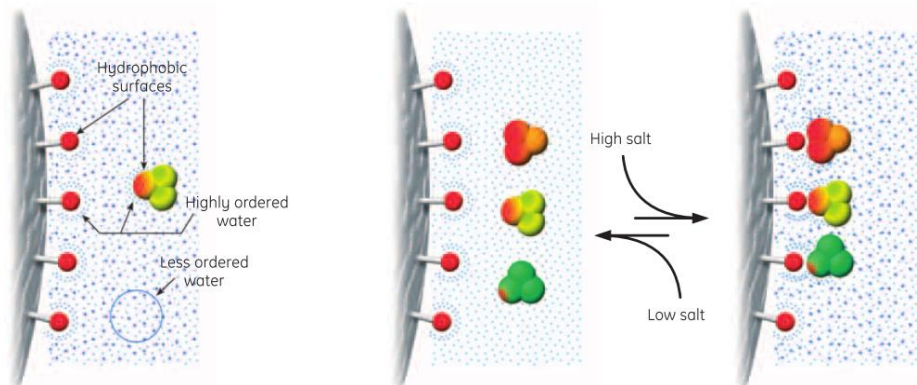


Figure 1.3.6 - A) Highly ordered water shells surround the hydrophobic surfaces of ligands and proteins. Hydrophobic substances are forced to merge to minimize the total area of such shells. Salts enhance the hydrophobic effect. B) The equilibrium of the hydrophobic interaction is controlled predominantly by the salt concentration [31].

concentrations enhances the interaction while lowering the salt concentration weakens the interaction [31]. Figure 1.3.6 shows the main principles in HIC.

Hydrophobic effect depends on the behavior of the water molecules rather than on direct attraction between the hydrophobic molecules. Water is a good solvent for polar substances, but poor solvent for the non-polar ones. In liquid water, the majority of the water molecules occur in clusters due to hydrogen bonding between themselves [31], illustrated on Figure 1.3.7. Although the half-life of water clusters is very short, the net effect is a very strong cohesion among the water molecules. When a hydrophobic substance is immersed in water, the water molecules arrange themselves into a strong shell of highly ordered structure. Here, the possibility to form hydrogen bonds is no longer in balance, but is denominated by the hydrophobic substance immersed because the water molecules cannot “wet” the substance hydrophobic surface. Instead they form a highly ordered shell around the hydrophobic surface due to their inability to form hydrogen bonds in all directions. Minimizing the extent of this shell leads to a decrease in the number of ordered water molecules, that is, a thermodynamically more favorable situation in which entropy increases. So, in order to gain entropy hydrophobic substances are forced to merge to minimize the total area of such shells [31].

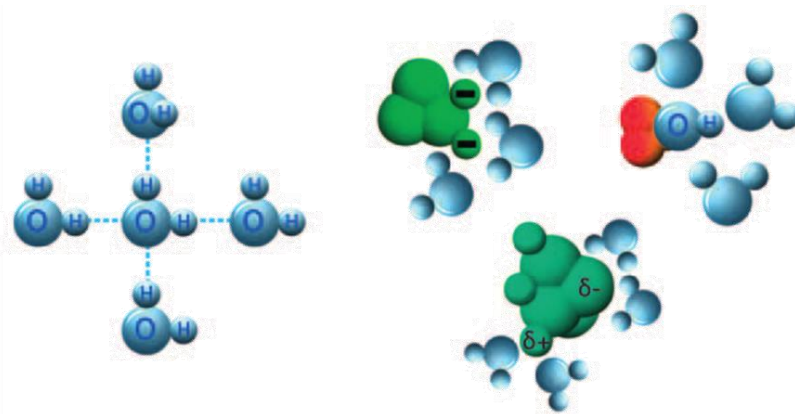


Figure 1.3.7 - Solubilizing properties of water molecules and its ability to interact with dipoles and form hydrogen bonds [31] .

All three pDNA conformations interact with the hydrophobic surface of the HIC medium, but, as the buffer ionic strength (salt concentration) is reduced, the interaction is reversed and the molecule with the lowest degree of hydrophobicity is eluted first. The most hydrophobic elutes last, requiring a greater reduction in salt concentration [31].

The first step on a HIC chromatographic procedure is to equilibrate the medium with the selected buffer with adequate pH and salt concentration to bind the most hydrophobic species. When loading, the sample must have the same salt concentration as the equilibration buffer to ensure the molecules binding. The bound biomolecules are concentrated on the column while

the molecules that don't interact with the media flows through. After all the sample has been loaded into the column and non-binding biomolecules eluted, conditions are altered by decreasing the buffer salt concentration, leading to the elution of the bound biomolecules. The first biomolecules being eluted from the column are the ones with the lowest hydrophobicity at the selected ion strength, thereafter, the ones with the higher hydrophobicity that are strongly retained and be eluted last. Once more, controlling the ionic strength, different biomolecules can be eluted differentially in a purified and concentrated form [31].

The final step is the regeneration of the column through a zero salt concentration buffer that will remove all the tightly bound biomolecules. Before a next run, the column has to be re-equilibrated using the same initial conditions buffer and the process can work as a cycle [31].

HIC has also been used analytically for the monitoring and control of pDNA quality. The sc and oc pDNA isoforms ranging from 4 to 30 kbp were successfully resolved in a TSKgel Butyl-NPR analytical column (Tosoh). Due to the predominantly hydrophilic nature of pDNA, very high salt concentrations (about 3M of ammonium sulfate) is required to bind the sc pDNA onto the resin surface. A reverse salt gradient was used to elute the oc and sc isoforms sequentially. The separation of the isoforms was attributed to the increased exposition of hydrophobic bases as a consequence of the underwinding of the sc form [17].

1.4. Adsorption process and equilibrium

As discussed earlier in this work, the increasing demand for pharmaceutical-grade pDNA is requiring an improvement in the industrial purification systems. These improvements rely on the system optimization, and for that, it is essential to understand the mechanism underlying the adsorption process onto the chromatographic media.

In general, adsorption is defined as the concentration of species at a solid surface. The chromatographic separations may involve many different non-covalent interactions between the molecule and the ligand on the solid support. The interaction with surface can result in two types of forces: dispersion-repulsion forces that are also known as London or van der Waals forces; and electrostatic forces which depends of the molecule net charge. Short-range repulsive forces are dominant very near the surface, but decrease rapidly as the distance from the surface increases, while electrostatic forces are generally longer range. As a result, the concentration of molecules near the surface varies with the distance from it. The process seems quite simple, however, adsorption of macromolecules is usually much more complicated and currently not amenable to a precise theoretical treatment [22].

There are several adsorption complicating factors, and as result of this complexity, empirical or semi-empirical approaches are generally needed to describe the adsorption equilibrium. The

prediction of multicomponent adsorption it's even more challenging. Experimental determinations are almost always necessary. Thus, adsorption equilibria is frequently measured by suspending the particles in a protein solution and allowing the sufficient time for equilibrium to be attained. It is often easier to determine the ultimate binding capacity with a high protein concentration. However, the same can't be applied when working with more labile molecules such as sc pDNA. In addition, determine the binding capacity at low concentration is often difficult since the time needed to achieve the equilibrium can become very long. Chromatographic methods like frontal analysis, isocratic elution and linear gradient elution can be one alternative to determine the adsorption equilibria with molecules like plasmids. In practice, in the context of a biopharmaceutical process development, acquisition of adsorption equilibrium data is often difficult because the amounts of pDNA can be very limited. As a result, care must be taken to ensure that precise data are obtained with minimal waste. Following empirical determinations of adsorption equilibria, the data is generally correlated using suitable adsorption isotherm expressions [22].

1.4.1. Langmuir Model and static binding capacity

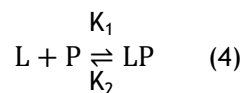
The concentration of adsorbed molecule in the stationary phase at equilibrium with the mobile phase is expressed by the adsorption isotherm. The molecules are adsorbed on a fixed number of located sites, which can accept only one molecule, and are organized as monolayers. [22,32]. So, by definition the binding capacity can be defined as:

$$Q = \frac{\text{Bound molecules}}{\text{Volume of packed resin}} \quad (3)$$

The binding capacity (Q) has to be defined for a specific process, a specific resin and individual type of molecule [23]. The adsorption isotherms are obtained while maintaining constant the mobile phase composition, temperature and pH [22]. A linear relationship between the bounded molecules and free molecules at equilibrium, is expected in the low concentration range, but the relationship becomes non-linear at higher concentrations reaching to a maximum capacity. At high concentrations, the adsorption sites become saturated, leading to a curvature of the isotherm into an asymptote [1,32]. So, the linear limit is dependent on the concentration of accessible binding sites. Conversely, the maximum capacity is generally limited by the accessible area or by the number of binding sites [22].

A model commonly used to describe the protein adsorption equilibrium is the Langmuir isotherms, which was originally developed for adsorption of gases onto metal surfaces [1,22,23,32,33]. Ferreira *et al* (2000) tried to propose a model of adsorption-desorption of plasmid onto an anion-exchange support but given to some drawbacks, the Langmuir model was favored to study the plasmid adsorption mechanism [33]. The Langmuir model states that the molecules are adsorbed on a limited number of sites, which accepts only one molecule. Also, every adsorption site is energetically equivalent and there is no interaction between adsorbed

molecules [32,33]. However, it's important to mention that the Langmuir isotherm model may not be applicable to all biomolecules adsorption mechanisms once it does not consider solute-solute interactions neither steric rearrangements on the solute or the support ligands[1]. Despite that, this model is still being used as a starting point for the adsorption mechanisms studies [22,33]. A simple derivation of the original model [22] assumes a stoichiometric association of an adsorbate molecule, P, with a surface-bound ligand, L, according to the following equation:



where k_1 and k_2 are forward and reverse rate constants for adsorption and desorption, respectively. Accordingly, the adsorption rate is described by the following equation:

$$\frac{d[PL]}{dt} = k_1[P][L] - k_2[PL] \quad (5)$$

which is subject to the following constraint:

$$[L] = [L_0] - [PL] \quad (6)$$

where $[L_0]$ is the total concentration of surface-bound ligands.

At equilibrium,

$$\frac{d[PL]}{dt} = 0 \quad (7)$$

In this case, combining equations 5 and 6 yields:

$$q = \frac{q_m KC}{1 + KC} \quad (8)$$

where $q \propto [PL]$ is the adsorbed concentration, $q_m \propto [L_0]$ the maximum adsorption capacity, $C \propto [P]$ the concentration in solution and $K = k_1/k_2$ is the equilibrium constant for reaction 4. The capacity q is normally expressed per unit volume or mass of stationary phase and can be defined in molar or mass units.

The Figure 1.4.1 illustrates the effects of the parameters q_m and K and the limiting behavior of the isotherm [22]. As $C \rightarrow 0$, the Langmuir isotherm penchants the linear limit:

$$q \approx q_m KC = mC \quad (9)$$

where $m = q_m K$ is the initial slope of the isotherm, which is also called the Henry constant. On the other hand, as $C \rightarrow \infty$, the isotherm approaches the maximum capacity $q \approx q_m$. The term $1/K$ represents the liquid phase concentration at which q is equal to one-half of the maximum capacity, q_m .

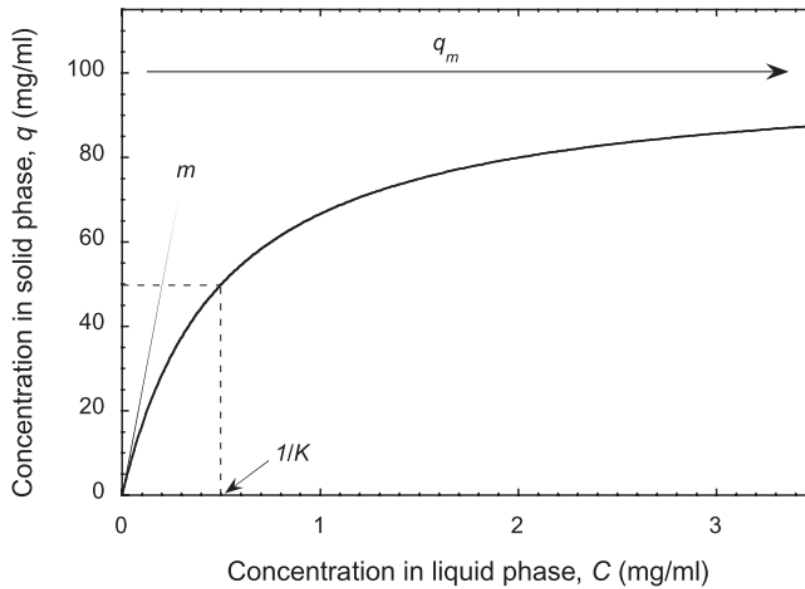


Figure 1.4.1 - Langmuir adsorption isotherm with the limiting behavior for low and high C values. M is the initial slope and $1/K$ is the liquid phase concentration in equilibrium with one-half of q_m [22].

The capacity of chromatographic column to capture molecules is frequently characterized by the dynamic binding capacity (DBC). The DBC is generally related to the equilibrium binding capacity (EBC) also known as static capacity, but is influenced by dispersive factors, approaching the EBC only for conditions where the column has infinite efficiency. The static capacity depends only on thermodynamics and molecule feed concentration and is thus expected to be independent of flow and column length. The relationship between DBC and static capacity is complicated and is dependent on the exact nature of the dispersive mechanisms. However, in a cases where binding is very favorable the DBC can be approximately 75% of the maximum static capacity (q_m) [22].

1.5. Thermodynamic study of biomolecules adsorption

The use of Langmuir isotherms it's a good starting point to explain the adsorption mechanism to IEX and HIC supports. Nevertheless, traditional methods cannot completely characterize complex adsorption mechanisms of biomolecules in liquid chromatography. They are limited once they do not consider non-ideal effects associated with the adsorption of large biomolecules such as large proteins and pDNA. In this way, these complex adsorption mechanisms have been studied by thermodynamic analysis [1,32,34,35]. The biomolecules adsorption and desorption thermodynamic parameters can be accessed by performing batch equilibrium experiments, analyzing data from van't Hoff plots or from microcalorimetric measurements. Notwithstanding, van't Hoff analysis is an indirect method that becomes too complex in the presence of multiple sub processes related with adsorption and batch experiments have a limited resolution. On the other hand, calorimetric methods such as Isothermal Titration Calorimetry (ITM) and Flow Microcalorimetry (FMC) have shown in the past few decades their aptitude to help understand the underlying absorption mechanism of several biomolecules onto different chromatographic media [1,2,32,34-39].

1.5.1. Flow Microcalorimetry

The behavior of biomolecules at liquid-solid interface is the net result of several types of interactions that occur between the different components present in the systems, i.e. the biomolecules, sorbent, solvents and other solutes. The feasibility of a protein or plasmid to be adsorbed is determined by the change in the standard Gibbs free energy, ΔG of the system, which for a reversible process can be written as:

$$\Delta G_{\text{ads}} = \Delta H_{\text{ads}} - T\Delta S_{\text{ads}} \quad (10)$$

where ΔH_{ads} and ΔS_{ads} are the adsorption enthalpy and entropy changes respectively [1,32,35]. During the adsorption and desorption process a small, but measurable, thermal signal is released which can be related to the adsorption mechanism. In this way, adsorption enthalpy measurements through microcalorimetry can provide some useful information that can help to understand the adsorption mechanisms onto a chromatographic support [1,32,34,35].

Microcalorimetric methods allow the measurement of the heat flow caused by interaction during the adsorption process of biomolecules onto chromatographic media. More specifically, FMC allows a dynamic measurement of the heat signals as the signal is measured *online* during the adsorption and desorption process of a biomolecule that flows through a small column packed with the adsorbent. Given to these unique characteristics, FMC is prone to provide an improved understanding of the driving forces, mechanisms and kinetics involved in complete interaction processes [1,2,32,38,39].

As stated above, a flow microcalorimeter has the ability to simulate a packed-bed chromatographic system in a micro-scale (Figure 1.5.1) and results are expected to be representative of the mechanisms that happen in a real chromatographic system. The major advantage of FMC towards a chromatographic system is that the data assessment occurs within the column and not after the column, as in usual chromatography studies [1,32,39].

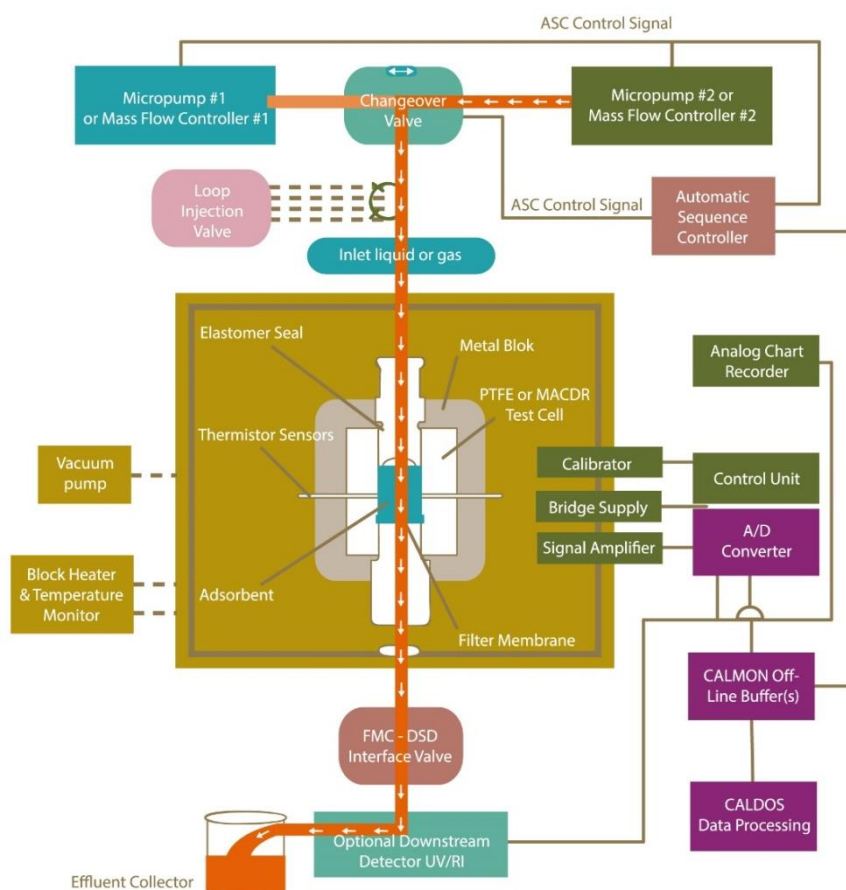


Figure 1.5.1 - Flow microcalorimeter representative scheme.

Interfaced with the microcalorimeter cell (Figure 1.5.1), that has a total volume of 171 μL and where the adsorbent is packed are two highly sensitive thermistors capable of detecting very small energy changes inside the cell within a short thermal response time. The constant system flow rate is controlled by a syringe micropump and the samples injected in the column through a multiport valve system. The injection system has a configurable injection loop that can accommodate different sample volumes. After the cell measurements, the effluent passes through an UV detector which allows the biomolecules output control. At the end, the effluent can be collected and can be analyzed by other techniques.

The FMC thermograms can comprise endothermic and exothermic peaks, which will depend on the absorption or release of energy during the liquid-solid interaction. The endothermic events result in negative peaks on the FMC thermogram as the thermistors register a decrease in the cell energy. Conversely, Exothermic events result in thermogram positive peaks as the

thermistors register an increase in the cell energy [1,32,35]. The Figure 1.5.2 shown a typical FMC thermogram. The first peak has an exothermic profile and is a calibration peak, where a 30 μ W heat impulse were induced during 500 s. Calibration peaks are commonly used to correlate the signal generated (peak area) with the energy impulse. The data obtained in this way provide information on the kinetics of adsorption obtained under the condition of experiment, i.e. flow rate of solution, volume and packing density of adsorbent bed and temperature. Also, it will assist the conversion of energy changes assessed by the thermistors in heats of adsorption [38,40,41]. The following second and third peaks in Figure 1.5.2 represents an endothermic and exothermic event, respectively. The third, has a skewed shape that represents overlapping of second and third events that can be analyzed through peak deconvolution[1,32,37].

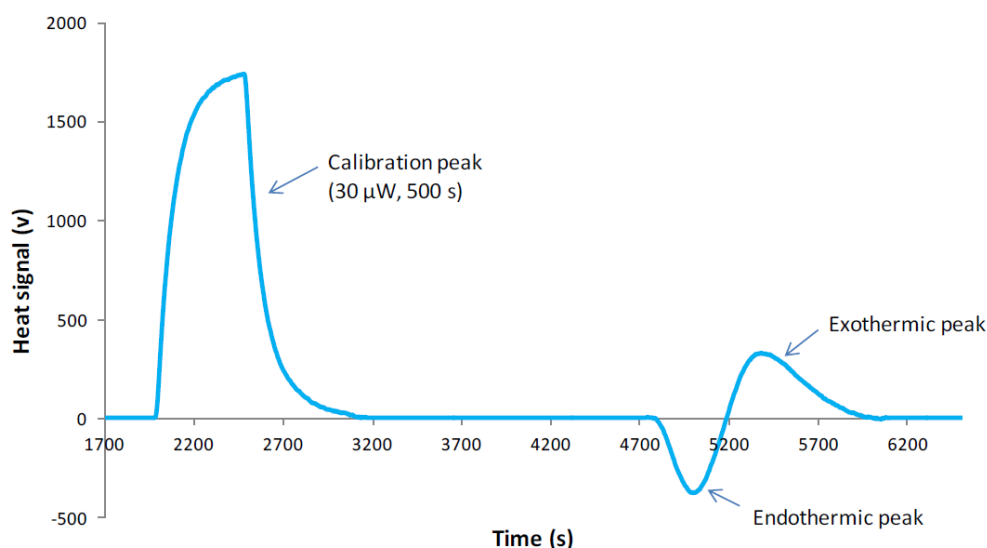


Figure 1.5.2 - Typical FMC thermogram for linear pDNA adsorption on Q-Sepharose.

In ion-exchange chromatography, the main interaction between biomolecules and the chromatographic media during adsorption is thought to be the electrostatic interaction. Therefore, it's expected a release of energy when two surfaces with opposite charges approach each other resulting in an exothermic process. However, the electrostatic interaction is not the only type of interaction during the whole adsorption process. Previous thermodynamic studies in ion-exchange biomolecules adsorption revealed exothermic events related to electrostatic interaction and endothermic events related to several other sources: water and ions release from adsorbent's and biomolecule's surfaces; interaction between the molecule surface hydrophobic groups and adsorbent hydrophilic moieties; repulsive interactions between same charged groups; biomolecule conformational changes and biomolecule reorientation on the adsorbent surface [1,32,35].

On the last decades several studies were performed to understand the protein adsorption mechanisms onto a variety of chromatographic media [2,32,34-36,39-41]. Despite all that,

there's still a lack of data and understanding of the process of plasmid DNA adsorption onto chromatographic media. A batch adsorption of pDNA onto some anion-exchange chromatographic supports study was performed by Ferreira and co-workers (2000). Regardless good contribution, the data obtained does not account for non-ideal effects neither other complex working conditions. Later on 2014, Aguilar *et al.* [1] perform ITC and FMC studies with linear pDNA onto anion-exchange chromatographic media as well. The FMC results showed that the overall adsorption process is exothermic, as expected for an anion-exchange interaction. Also, as the \ln pDNA loading increases the net heat of adsorption became more positive leading to a both endothermic and exothermic enthalpies decrease. As result, each pDNA molecule foot print on the adsorbent surface may decrease in order to accommodate more molecules, thus less water molecules and ions need to be removed in the binding process, leading to a decrease of the endothermic heat signal.

The firsts steps have been made, the next one is to understand the adsorption mechanism of \ln pDNA in other systems and more important the supercoiled isoform of the same pDNA. Despite being the same molecule, the supercoiled isoform has different features such as size and charge density. More important, the sc pDNA is the more biologically active and because of that is most used in therapeutic applications [5,13,26,42].

1.6.Goal of Study

As mentioned earlier, plasmid DNA is the base for two promising therapeutic procedures with an increasing interest. DNA vaccines and gene therapies holds the promise to treat and cure many acquired or genetic diseases [4,6,9,12]. The well-publicized potential of gene therapy and DNA vaccines makes enormous the market potential for pDNA [3]. The use of pDNA to treat diseases requires its production at large scale, with high purity levels and in an economic and environmentally way, complying with the guidelines from the regulatory agencies. Given the pDNA unique characteristics, purification is the most challenging step in the production process. Anion-exchange and hydrophobic interaction chromatography are the techniques of election regarding the pDNA purification [3,5,13,17,18,26-28]. Nevertheless, the mechanism of pDNA separation using anion-exchange or hydrophobic interaction chromatography is still not completely understood. Prediction of separation behavior is generally unreliable and laboratory scale methods do not have an unaffordable outcome at industrial scale. A better understanding of the mechanisms underlying the chromatography of biomolecules may help to optimize the chromatographic methods and consequently assist the design and implementation of scale-up units. Flow Microcalorimetry (FMC) has proven its ability to provide an improved understanding of the driving forces, mechanisms and kinetics involved in the interaction process on biomolecules adsorption onto several chromatographic systems [1,2,32,40,43-45]. Hence, using Flow Microcalorimetry as a central technique, this study aims to understand and compare the interaction of ln pDNA between an anion-exchange and a hydrophobic interaction support, and also the interaction of ln and sc pDNA in an anion-exchange support. Only linear conditions will be addressed emphasizing the adsorptive process differences in each system. Furthermore, static binding capacity will be performed to obtain a better understanding of the adsorption mechanism.

2. Materials and methods

2.1. Materials

E. coli DH5 α strain transformed with the 6.05 kbp plasmid pVAX1-*LacZ* (Invitrogen, Carlsband, CA, USA), bearing kanamycin resistance gene was obtained from CICS - Health Sciences Research Centre, University of Beira Interior (Covilhã, Portugal). Toyopearl GigaCap Q 650-M was kindly offered by Tosoh bioscience (Toquio, Japan). CIM® DEAE-0.34 disk-shaped monolith was kindly offered by Professor Ales Podgornik. Phenyl Sepharose 6 Fast Flow hydrophobic interaction resin and Q-sepharose Fast Flow anion exchanger was obtained from GE Healthcare (Uppsala, Sweden). CIMac™ DEAE-0.1 Analytical Column was obtained by BIA Separations (Ajdovščina, Slovenia). QIAGEN Plasmid Maxi Kit was obtained from Qiagen (Hilden, Germany). Hind III restriction enzyme was obtained from NZYTech (Lisbon, Portugal). All used reagents were of analytical grade, Sigma-Aldrich (Sigma-Aldrich, Madrid, Spain).

2.2. Apparatus and Software

Supercoiled plasmid DNA isoform purification was achieved in ÄKTA Pure system from GE Healthcare (Uppsala, Sweden). Data was collected and analyzed by UNICORN software from GE Healthcare (Uppsala, Sweden).

Plasmid DNA mass was quantified with xMark™ Microplate spectrophotometer from Bio-rad Life Science Research (California, USA).

Thermodynamic studies were performed using a Flow Microcalorimeter FMC 4 Vi from Microscal Ltd (London, UK). Data was collected and analyzed with CALDOS4 software from Microscal Ltd (London, UK). Further analysis was done through peak deconvolution using PEAKFIT software package (version 4.12, Seasolve Software Inc., San Jose, USA).

2.3. Plasmid DNA Production

2.3.1. Fermentation

E. coli DH5 α cells containing pVAX1-*LacZ* plasmid were cultivated overnight on solid agar LB medium (Conda Laboratories, Spain) containing 30 μ g/mL of kanamycin. Cell colonies grown on the solid medium were collected and inoculated on liquid Terrific Broth (TB) medium (12 g/L tryptone, 24 g/L yeast extract, 4 mL/L glycerol, 0.017 M KH₂PO₄, 0.072 M K₂HPO₄) supplemented

with 30 µg/mL of kanamycin, for pre-fermentation. That occurred in 500 mL Erlenmeyers, containing 125 mL of medium, incubated in an orbital shaker at 37 °C, 250 rpm, until OD₆₀₀ ≈ 2.5 was reached. For the fermentation, a fresh batch of liquid TB medium (250 mL in a 1000 mL Erlenmeyer) was inoculated from the pre-fermentation in order to obtain an initial OD₆₀₀ = 0.2. Fermentation was carried out at 37 °C and 250 rpm, until OD₆₀₀ ≥ 6 was reached.

2.3.2. Recovery

The *E. coli* DH5α cells containing pVAX1-*LacZ* plasmid were recovered by centrifugation at 4 °C, 5000 G for approximately 8 min and stored in 50 mL falcon tubes at -20 °C until posterior utilization.

Plasmids (pVAX1-*LacZ*) were recovered from cells using QIAGEN® Plasmid Maxi Kit according to the manufacturer's instructions resumed in Table 2.3.1.

Table 2.3.1 - Recovery of pDNA using QIAGEN® Plasmid Maxi Kit.

Alkaline Lysis	<ul style="list-style-type: none"> Bacterial pellet (250 mL of cells) was re-suspended in 20 mL of 50 mM Tris-HCl, 10 mM EDTA, 100 µg/mL RNase A, pH 8.0 Cell lysis was performed by adding 10 mL of 200 mM NaOH, 1% SDS (w/v) After 5 min of incubation at room temperature, add 10 mL of pre-chilled 3 M potassium acetate, pH 5.5 to precipitate genomic DNA, proteins, and cell debris Centrifuge twice at ≥ 20000 g for 30 min at 4 °C, reserving the supernatant which contains pDNA
pDNA Binding	<ul style="list-style-type: none"> Equilibrate the QIAGEN-tip by applying 10 mL of 750 mM NaCl, 50 mM MOPS pH 7.0, 15% isopropanol (v/v), 0.15% Triton X-100 (v/v) Apply the supernatant from alkaline lysis, allowing the pDNA to bind to the support.
Washing	<ul style="list-style-type: none"> Wash the QIAGEN-tip by applying 60 mL of 1 M NaCl, 50 mM MOPS pH 7.0, 15% isopropanol (v/v), allowing the removal of contaminants that remained bound in the support
Elution	<ul style="list-style-type: none"> Elute the pDNA by applying 15 mL of 1.25 M NaCl, 50 mM Tris-HCl pH 8.5, 15% isopropanol (v/v)
Precipitation	<ul style="list-style-type: none"> Precipitate the pDNA by adding 0.7 volumes of isopropanol to the eluted pDNA Centrifuge at ≥ 15000 g for 30 min at 4 °C and recover the pellet Re-dissolve the pDNA pellet in a suitable volume of buffer (e.g. 1 mL of 10 mM Tris-HCl, pH 8.0)

2.3.3. Plasmid DNA quantification

Plasmid DNA concentrations were assessed by absorbance measurements (UV, 260 nm) with a microplate spectrophotometer. All measurements were performed in triplicates.

2.3.4. Plasmid Isoform Separation

In order to obtain linear plasmid DNA (ln pDNA) an enzymatic digestion was performed. To facilitate the pDNA digestion process, samples were previously left overnight at ambient temperature to allow the conversion of sc pDNA into its oc conformation. Then, linear pDNA conformation was obtained by cleavage of the oc pDNA with the restriction endonuclease Hind III according to manufacturer's instructions (incubation at 37 °C during approximately 2 hours adding the adequate buffers). Hind III enzyme was removed from pDNA samples after the digestion through centrifugation, using 100 kDa membrane concentrators (1400 G at 4 °C). For storage and as a carrier fluid the buffer used was 10 mM Tris-HCl, pH 8.0.

2.3.5. Agarose Gel Electrophoresis

Isolated pDNA was analyzed by horizontal electrophoresis (120 V, 40 min) using 0.8 % agarose gel in TAE buffer (40 mM Tris, 20 mM Acetic Acid, 1 mM EDTA, pH 8.0) and 0.6 µL of GreenSafe as a nucleic acid stain. Gels were pictured in UVITEC Cambridge system (UVITEC Limited, Cambridge, UK).

2.4. Plasmid DNA Purification

Regarding the supercoiled isoform, after the recovery with the QIAGEN® Plasmid Maxi Kit the samples were purified by fast performance liquid chromatography (FPLC).

2.4.1. sc pDNA purification with Toyopearl GigaCap Q 650-M

A XK16 empty chromatographic column (GE Healthcare, Uppsala, Sweden) was packed with 3 mL of Toyopearl GigaCap Q 650-M and experiments were performed in ÄKTA Pure system. Before each assay, the system was equilibrated with at least 5 column volumes of 760 mM NaCl, 10 mM Tris pH 8.0 at a constant flow rate of 3 mL/min. After equilibrating the column with the working buffer, a 500 µL pDNA sample (prepared with the same buffer conditions) was injected onto the column. The elution of bound species was carried out with a 5 column volumes stepwise gradient from 760 mM to 900 mM NaCl. The chromatographic data was collected and analyzed by UNICORN 6.1 software. After each run, the column was washed with 3 column volumes of water followed by 5 column volumes of 0.5 M NaOH, at least 10 column volumes of water, and then equilibrated with the working conditions for the next run.

2.4.2. sc pDNA purification with CIM DEAE

The CIM DEAE 0.34 mL disk was attached into a polypropylene housing (BIA Separations) and experiments were performed in a ÄKTA Pure system. Before sample injection, the system was equilibrated with 30 column volumes of 50 mM Tris-HCl 10 mM EDTA pH 7.2 at a 5 mL/min flow rate. The sample was injected with a 500 µL loop and the binding was favored at the same conditions for approximately 30 column volumes. Next, a 60 column volume stepwise elution from 0 to 660 mM NaCl was performed for the elution of the unwanted material (50 mM Tris-HCl 10 mM EDTA 1.5 M NaCl pH 7.2). After that, the molecule of interest was eluted with a 60 column volume stepwise from 660 mM to 750 mM NaCl. At the end, the column was washed with 1.5 M NaCl for approx. 60 column volumes. The chromatographic data was collected and analyzed by UNICORN 6.1 software.

2.4.3. Sample Concentration and buffer change

At the end of each purification run, the samples were concentrated and buffer changed with the 100 kDa Corning® Spin-X® UF Concentrators. The centrifuge was set at 4 °C and 1300 rpm.

2.4.4. Sample Characterization

The purified sc pDNA samples were characterized with CIMac™ DEAE-0.1 Analytical Column in the ÄKTA Pure system. The system was equilibrated with approximately 25 column volumes of 600 mM NaCl, 200 mM Tris-HCl pH 8 at a constant flow rate of 1 mL/min. The purified sample was injected with a 20 µL loop. After injection, a 90 column volumes linear gradient from 600 mM to 700 mM NaCl was applied. The chromatographic data was collected and analyzed by UNICORN 6.1 software and the supercoiled isoform percentage was determined by peaks relative areas. At the end, the column was washed with approximately 50 column volumes of 1 M NaCl.

2.5.Flow Microcalorimetry (FMC)

Thermodynamic studies were performed in the Flow Microcalorimeter (FMC). FMC column was packed with approximately 171 μ L Q-sepharose Fast Flow and/or Phenyl Sepharose, which after the swelling process filled the 171 μ L of the FMC cell. The swelling process was conducted by passing the equilibration buffer through the cell at a constant flow rate of 1.5 mL/h for at least 12 h. The equilibration buffer was 10 mM Tris-HCl (pH 8.0).

Calibration curve was constructed measuring the heat of 5 different energy impulses generated by a specific outlet (calibrator) in the packed cell: 0.3 mJ (3 μ W for 100 s), 1 mJ (10 μ W for 100 s), 3 mJ (30 μ W for 100 s), 7.5 mJ (30 μ W for 250 s) and 15 mJ (30 μ W for 500 s). All the measurements were performed in triplicates. Considering this range of energy, the relation between the energy impulse and the resulting heat (peak area) was linear for both resins. These experiments also allow to determine the calibration factor of the packed system. This factor will be later used to convert cell temperature changes in heat signals.

To study the adsorption of ln pDNA (pVAX1-*LacZ*) onto Phenyl Sepharose and sc pDNA onto Q-sepharose Fast Flow, first the system was packed as explained above and, after the thermal equilibrium was reached, a sample of pDNA prepared in 10 mM Tris pH 8.0 was loaded into a configurable injection loop (of 30, 229 or 429 μ L) and then injected into the cell through switching a multiport valve, using a constant flow rate of 1.5 mL/h. The adsorption process of the sample into the adsorbent surface causes a temperature change in the cell, which through the calibration factor is converted to a heat signal by the FMC. CALDOS 4 software was used to acquire, store, process and present all the FMC data. In order to know the adsorbed quantity of pDNA a mass balance was calculated subtracting the concentration of the collected effluent to the concentration of the injected sample. Those concentrations were assessed by measuring at 260 nm the absorbance in the UV microplate spectrophotometer. Between injections, it was used 0.5 M NaOH as a washing solution and the system was re-equilibrated with 10 mM Tris pH 8.0 (G.E. Healthcare, 2007).

3. Results and Discussion

3.1. Plasmid production

Completed the *E. coli* DH5 α culture, the cells corresponding to 250 mL of medium were used for pDNA recovery. The use of Qiagen Plasmid Maxi kit[®] yielded approximately a final concentration of 600 $\mu\text{g/mL}$ of 6.05 kbp pVAX1-LacZ plasmid DNA. Subsequently, some pDNA samples were kept at room temperature and, as time passed, it was noticed an increase in the relative amount of open circular and linear pDNA and a parallel decrease in the amount of supercoiled pDNA. In the third day there was only open circular and linear pDNA, after that the samples were digested with the restriction enzyme Hind III to obtain only linear pDNA for the hydrophobic interaction study with Phenyl Sepharose.

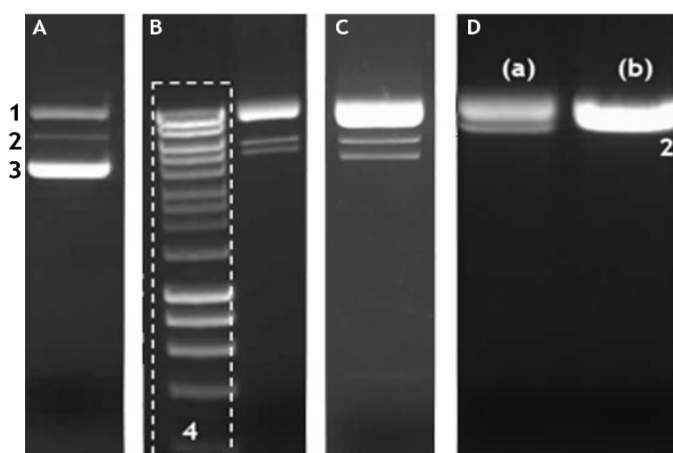


Figure 3.1.1 - Electrophoresis results of pDNA in different conformations. A - pDNA after recovery and clarification with Qiagen Kit. B - pDNA after 1 day at room temperature after A. C - pDNA after 2 day at room temperature after A. D - (a) pDNA after 3 day at room temperature after A and (b) pDNA after Hind II digestion. 1 - Open circular (oc) pDNA. 2 - linear (ln) pDNA. 3 - supercoiled (sc) pDNA. 4 - molecular weight marker (adapted from [1]).

After the recovery and clarification with Qiagen Kit, a sample characterization was performed with the CIMac[™] DEAE-0.1 Analytical Column in order to estimate the sc pDNA ratio (sc pDNA/total pDNA) through the analysis of peaks areas. The Figure 3.1.2 shows a common chromatogram obtained in the sample analysis.

As it can be noticed in the Figure 3.1.1 and Figure 3.1.2, the presence of other isoforms is considerable after sample preparation with the Qiagen Maxi kit[®]. Applying the relationship explained above the sc pDNA ratio was about 0.76. With the goal to study only the sc pDNA-Q-Sepharose interaction, a purification step had to be added in order to increase the ratio.

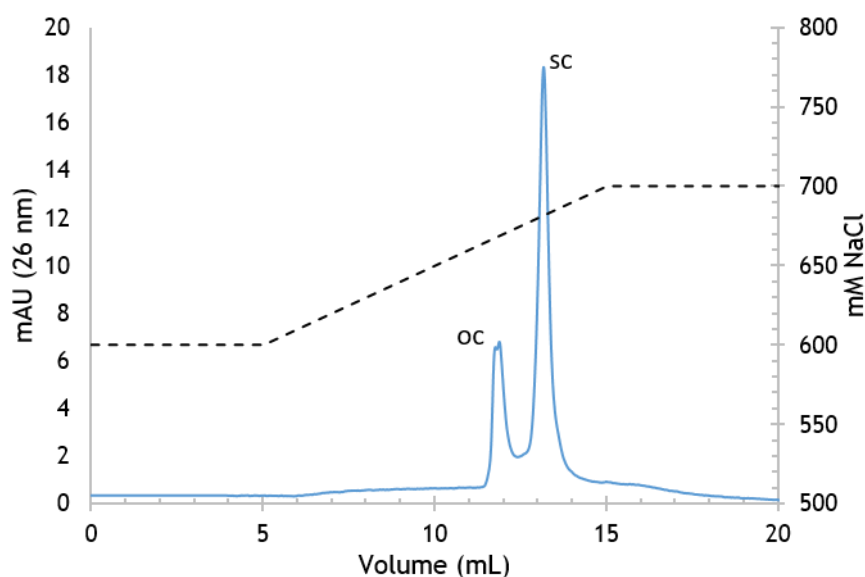


Figure 3.1.2 - Typical chromatogram obtained by injection of the plasmid sample recovered from the the Qiagen Kit, onto the CIMac™ DEAE column.

3.2. sc pDNA Purification

3.2.2. Toyoperl GigaCap Q 650-M

With the goal to obtain the highest ratio of sc pDNA isoform as possible, we used a clarified plasmid DNA sample, composed mainly by sc and oc plasmid isoforms. As a starting point we used the conditions described by Prazeres *et al* shown in Figure 1.3.5 (section 1.3.2). They were able to establish and optimize the separation of plasmid isoforms using Q-Sepharose Fast Flow. In this particular case, we used Toyopearl GigaCap Q-650M which is known to have a high capacity and a high resolution, optimized for the capture and purification of both small and large proteins. These features are related with the stationary-phase matrix. The Acrylic polymers based matrix can hold a higher mechanical strength when compared to other stationary-phases matrices, like Sepharose®, enabling higher flow rates, enhanced chromatographic resolution and reduced elution volume. Even with these good features of the stationary-phase matrix, the reduced pore diameter continues to be principal drawback for the separation of extremely large biomolecules like plasmids leading to low capacities.

Figure 3.2.1 shows the first method applied. As expected, and due to the higher charge density, the supercoiled isoform interacts more strongly with the quaternary amine ligand having a higher retention time. We were able to separate the isoforms, but as we can see the separation resolution is very poor. Thus, in order to enhance the resolution, we performed some scouting experiments and we were able to find the most suitable method for the isoforms separation.

Figure 3.2.2 shows the optimized separation method for the Toyoperl GigaCap Q 650-M resin. A relatively high salt concentration is used to avoid the unnecessary adsorption of undesired species (oc pDNA), so the capacity can be fully exploited for the sc pDNA adsorption [18]. Different plasmid loadings were tested in an attempt to maximize column productivity and as shown in Figure 3.2.2 -Typical chromatographic profiles of the plasmid isoform separation from a clarified pDNA sample (sc + oc) in the Toyoperl GigaCap Q 650-M column. It was verified that the established method was very reproducible. Consistent results were obtained in terms of yield, purity, quality and elution profiles. We obtained a sc pDNA yield average of $26 \pm 5\%$, with a purity average of $91 \pm 3\%$ using a loading average of $22.13 \pm 1.10 \mu\text{g pDNA/ mL gel}$.

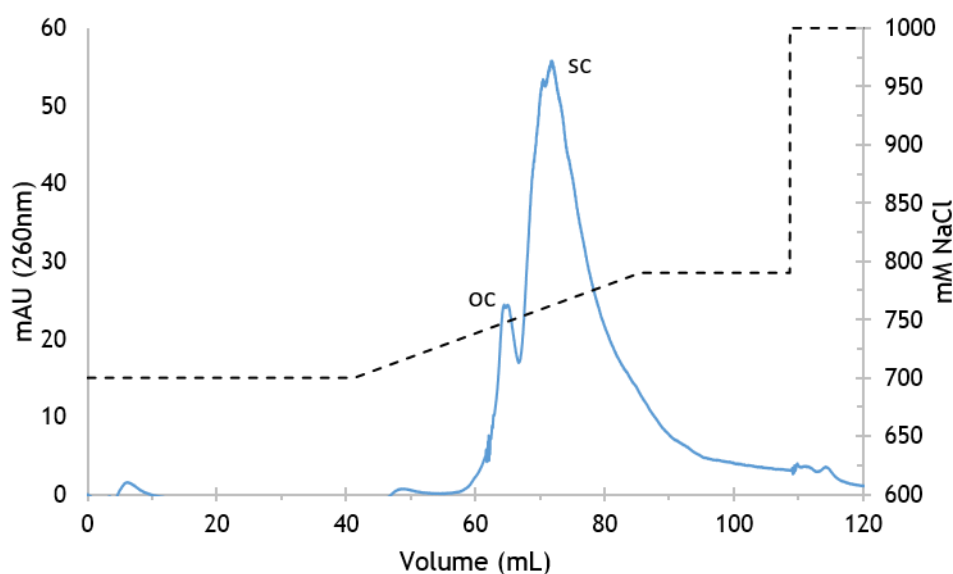


Figure 3.2.1 - Chromatographic profile of the plasmid isoform separation from a clarified pDNA sample (sc + oc) in the Toyoperl GigaCap Q 650-M column. The Elution method was based in the separation method suggested by *Prazeres et al.* [18]

Apparently, we were able to increase the sc pDNA ratio. DNAs are known to bind to anion exchange chromatography stationary phase quite strongly. The pDNA increased binding sites value and the high charge density from the supercoiled isoforms can also favor the selectivity [24,27,28,30,46]. Nevertheless, the very low yield make this process not recommended. *Prazeres et al.* [18] obtained higher yields (approximately 50%) using Q-Sepharose, but the pDNA size, which was 2 times lower, also have to be considered. As mentioned above, Toyoperl GigaCap Q 650-M is a resin designed for small and large proteins and even largest proteins (like BSA) are considered small when compared to plasmids. Hence, the large plasmid adsorption footprint and the reduced resin pore diameter are the principal causes for the resin capacity substantial decrease resulting in the poor yield.

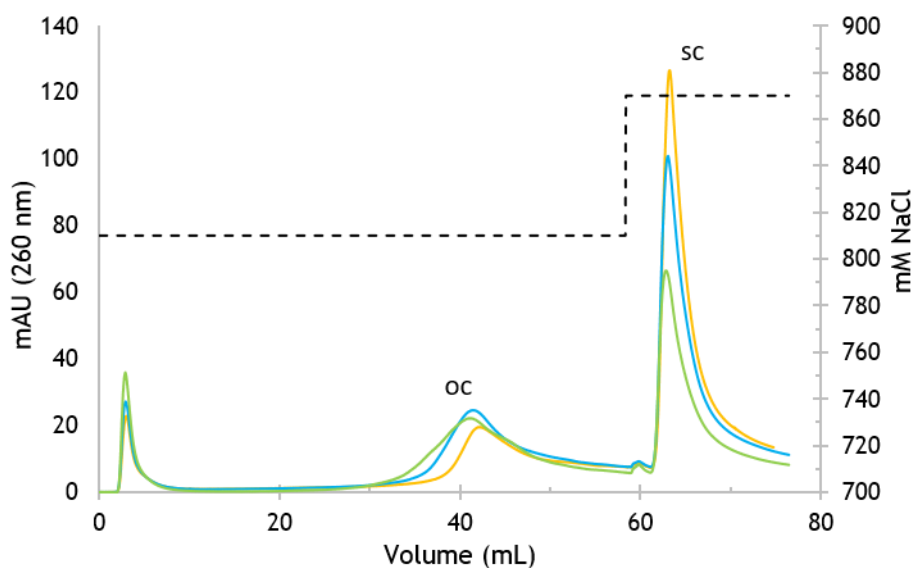


Figure 3.2.2 -Typical chromatographic profiles of the plasmid isoform separation from a clarified pDNA sample (sc + oc) in the Toyoperl GigaCap Q 650-M column. Different colors mean different injection concentrations.

3.2.3. CIM DEAE

With the same purpose, enhance the sc pDNA ratio, and using the same sample characteristics the CIM® DEAE-0.34 Disk was tested. The CIM® DEAE-0.34 is a shallow, disk-shaped monolith suitable for initial screening and method development. DEAE (diethylamine) is a weak type of anion exchange group, fully charged between pH 3-9. The DEAE versatile chemistry has proven to be excellent for any kind of pDNA purification. The poly(methacrylate) matrix forms network channels big enough to fit extremely large biomolecules like plasmid DNA allowing a high-binding capacity. In addition, high productivity can be attained using high flow rates with a considerable small pressure drop. Considering this features the yield problem should be fixed.

The separation was carried out according to the method suggested by BIA Separations for the purification of large plasmids from *E. coli*. After small alterations a good separation with a high resolution was attained as shows the Figure 3.2.3. Applying this method, we obtained yield average of $84 \pm 5\%$, and a purity average of $95 \pm 2\%$ of sc pDNA using a loading average of $558.82 \pm 45.35 \mu\text{g pDNA/ mL gel}$.

Once again our main goal was ensured. As a matter of fact, we obtained higher sc pDNA ratio. Comparing the yield results with the ones obtained with Toyopearl GigaCap Q-650M it can be noticed that with the monolith we have a notorious improvement. These large yield is easily explained by the higher capacity, a consequence of the monolith open structure. Moreover, the monolith convective based transport facilitates the separation of large molecules with low

diffusivities, like polynucleotides. Considering these results, the purification with the monolithic column was our technique of election.

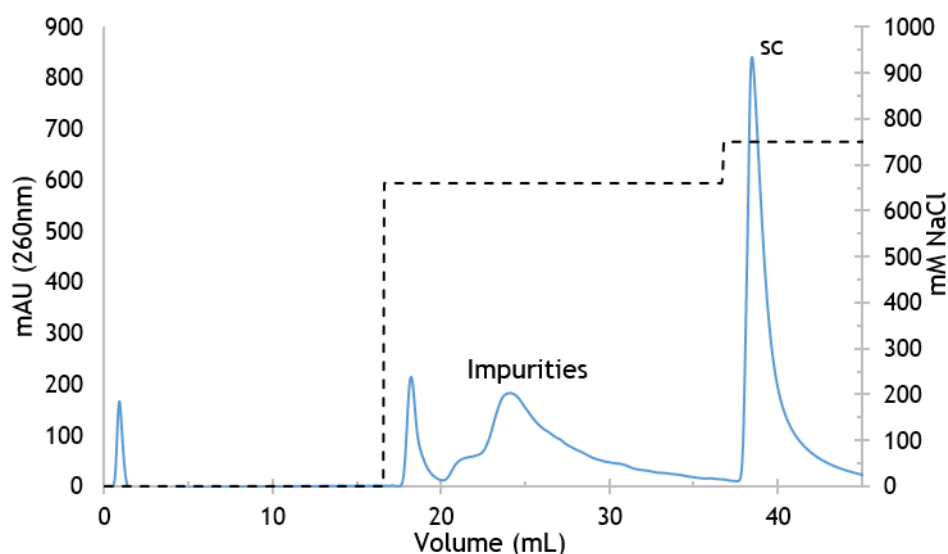


Figure 3.2.3 - Chromatographic profile of the plasmid isoform separation from a clarified pDNA sample (sc + oc) in the with the CIM® DEAE-0.34 Disk.

3.3.Static Binding Capacity

Adsorption behavior under linear and overloaded conditions was studied for ln pDNA adsorption onto a hydrophobic interaction support. As we stated before in section 1.4.1, adsorption equilibria are frequently measured by suspending the resin in biomolecule solution and allowing the sufficient time for equilibrium to be attained. This process cannot be performed with more labile molecules such as sc pDNA. In addition, determine the binding capacity at low concentration is often difficult since the time needed to achieve the equilibrium can become very long.

The adsorption isotherm obtained with Phenyl Sepharose is shown in Figure 3.1.1 along with results for the anion-exchange support Q-Sepharose (data already presented in a previous study [1], included here just for comparison).). In both curves, the surface ln pDNA concentration (qpDNA) increases linearly from zero to a plateau region as the ln pDNA equilibrium liquid concentration (CpDNA) increases. Before, Aguilar et al. [1] showed that the Q-Sepharose Fast Flow isotherm shape fits the Langmuir model. For Phenyl Sepharose, this model is only obeyed for ln pDNA equilibrium concentrations lower than approximately 55 $\mu\text{g.mL}^{-1}$. At higher concentrations, the plateau is followed by a region of rapidly increase in the capacity. Previous authors already discussed this second upturn when proteins were used as adsorbate, and postulated that the increase beyond the plateau was due to re-orientation or conformational alterations of the adsorbed molecules, rather than due to bi-layer formation [43,44]. This

explanation appears to be as well valid for the present case once it is not expected pDNA-on-pDNA adsorption at the studied pH, due to the known biomolecule negative net charge under the considered conditions [30].

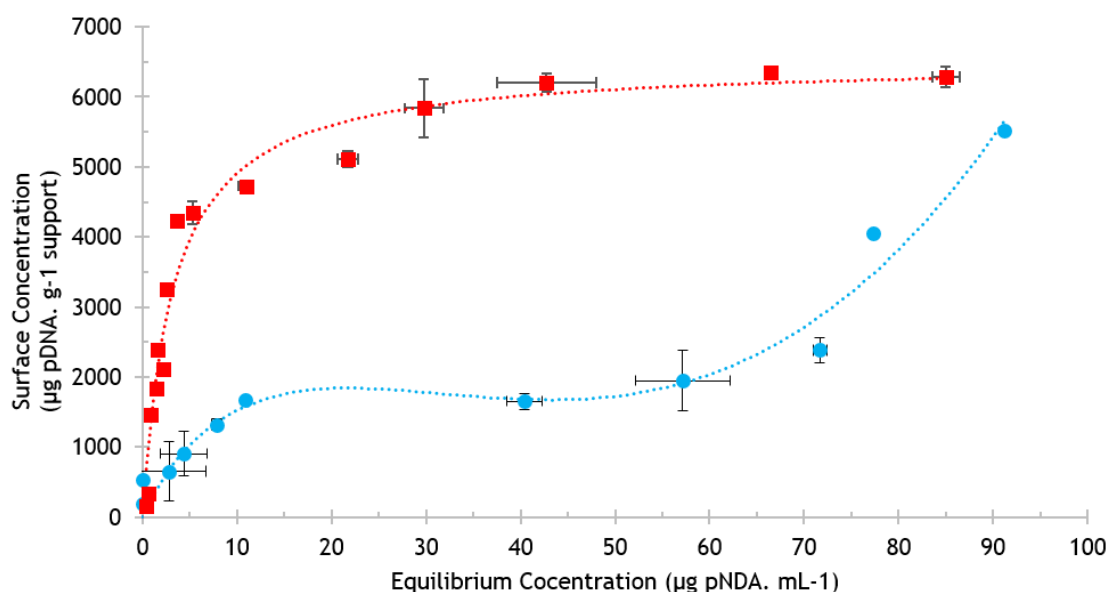


Figure 3.3.1 - Equilibrium binding isotherms for linear plasmid DNA adsorption onto hydrophobic interaction (10 mM Tris HCl with 1.8M (NH₄)₂SO₄ pH 8) and ion exchange (10 mM Tris-HCl pH 8) resins at 25 °C. (●) Phenyl Sepharose 6 Fast Flow, (■) Q-Sepharose Fast Flow [1].

In order to accomplish a more direct comparison between the two isotherms, the Langmuir model was also applied to the Phenyl Sepharose isotherm (equilibrium concentrations lower than 55 µg.mL⁻¹). Fitted parameters, association constant (K_A) and maximum binding capacity (q_{max}), were respectively $0.15 \pm 0.02 \text{ mL.}\mu\text{g}^{-1}$ and $2241 \pm 20.03 \text{ }\mu\text{g.g}^{-1} \text{ gel}$. These results are very different from the ones previously obtained with Q-Sepharose ($K_A = 0.31 \pm 0.02 \text{ mL.}\mu\text{g}^{-1}$ and $q_{max} = 6496 \pm 30.00 \text{ }\mu\text{g.g}^{-1} \text{ gel}$) which show higher affinity and capacity. The observed differences are explained by the support ligand used for the interaction and the structure of the ln pDNA molecule itself. DNA strands have negatively charged edges surrounding a more hydrophobic interior [47] and at the used working pH the biomolecule presents a negative net charge. These two factors may hinder the interaction between the ln pDNA hydrophobic zones and phenyl ligands on the support [47], and may also structure the biomolecule interaction with the ligands due to aromatic π -interactions, explaining the lower affinity and capacity of Phenyl Sepharose.

Regarding the adsorption of sc pDNA onto Q-Sepharose, we were not able to produce an experimental isotherm to apply the Langmuir Model. Nevertheless, we can forecast a maximum binding capacity theoretic value. Using a simple model, like Aguilar *et al.* [1] and Tarmann *et al.* [24], we assumed a simple rod shape for the sc pDNA that assumes an upright orientation

during adsorption. The theoretic maximum adsorption capacity can be obtained from the equation [1]:

$$q_m = \frac{A_m}{N\sigma}$$

where A_m is the support surface area, N is the Avogadro number and σ is the effective area of gel surface covered by a molecule of pDNA. Once Q-sepharose Fast flow can be assumed as nonporous media for pDNA [24], the maximum adsorption capacity has been predicted considering only the support external surface area, which was roughly estimated [22] using support particle diameter (90 μm) and extraparticle porosity (0.38 [48]). We obtained a 0.041 $\text{m}^2 \text{ mL}^{-1}$ for the external area per volume of packed bed. The effective area of gel surface covered by a molecule of pDNA can be estimated considering that the plasmid branched shape, with have 41% of the linear plasmid length [1,19] and a radius of 50 nm. As result, we assumed a rod with the equivalent dimension of 100 nm x 843 nm. The theoretical binding capacity of 248 $\mu\text{g} \cdot \text{g}^{-1}$ gel were calculated. This estimation is much smaller than the value obtained with the linear isoform. This may be explained by the fact that the supercoiled isoform has a higher repulsion between adsorbed molecules or higher footprint.

3.4. Flow Microcalorimetry

FMC experiments were performed in order to have more information about the events and the driving forces present during the interaction of ln pDNA with the Phenyl-Sepharose support and sc pDNA with the Q-Sepharose support. The magnitude and chronology of the thermal events may further elucidate the interaction mechanism, as previously demonstrated for other chromatographic systems [1,2,32,39]. As in Aguilar *et al.* [1] work, in the present study, experiments were run using different loops (30, 230 and 430 μL). Considering the 171 μL of the FMC cell, the use of the 30 μL loop means that the sample is introduced into the column as a pulse because it has 0.2 times the cell volume and the use of the 229 μL loop fulfils the FMC cell, representing 1.3 times of the cell volume. On the other hand, the use of the 429 μL loop we fill the cell 2.5 times, leading to a continuous feed of the biomolecule into the column, resembling the frontal analysis in chromatographic systems [22]. All experiments were performed on the isotherm linear zone.

Aguilar *et al.* [1] work results used for comparison with this present work are available in the appendix.

3.4.1. In pDNA adsorption onto Phenyl Sepharose

Figure 3.4.2 and Figure 3.4.1 illustrate examples of thermograms obtained with the 230 and 430 μL injection loops respectively. In each thermogram, different signals resulted from different loading concentrations. Considering the same loop, it can be noticed that the peak profile is maintained as the injection concentration changes

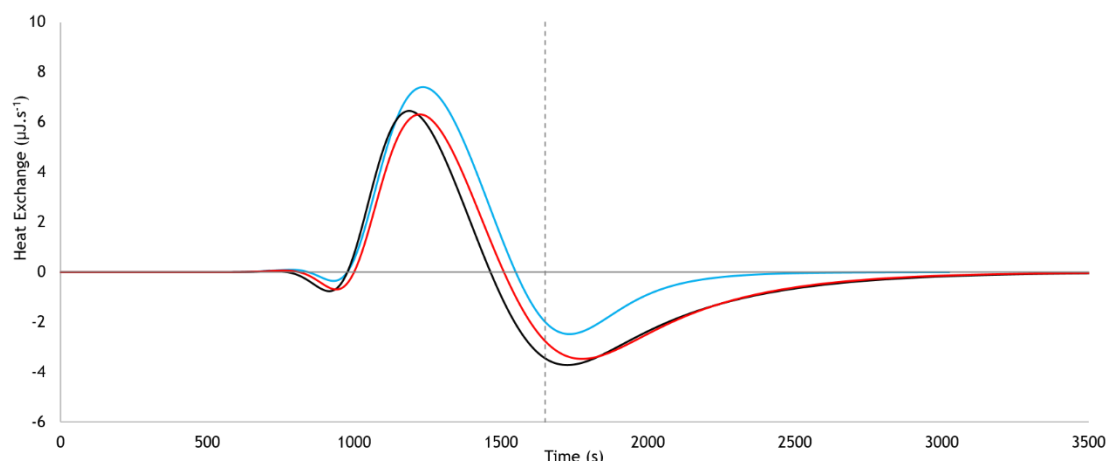


Figure 3.4.1 - Thermograms of ln pDNA adsorption onto Phenyl-sepharose using the 230 μL loop. Black 124.97 μg pDNA/g Phenyl Sepharose; Red 171.75 μg pDNA/g Phenyl Sepharose; Blue 413.18 μg pDNA/g Phenyl Sepharose. Vertical dashed line represents the time where the pDNA solution plug is replaced with pDNA-free mobile phase around 1650 seconds.

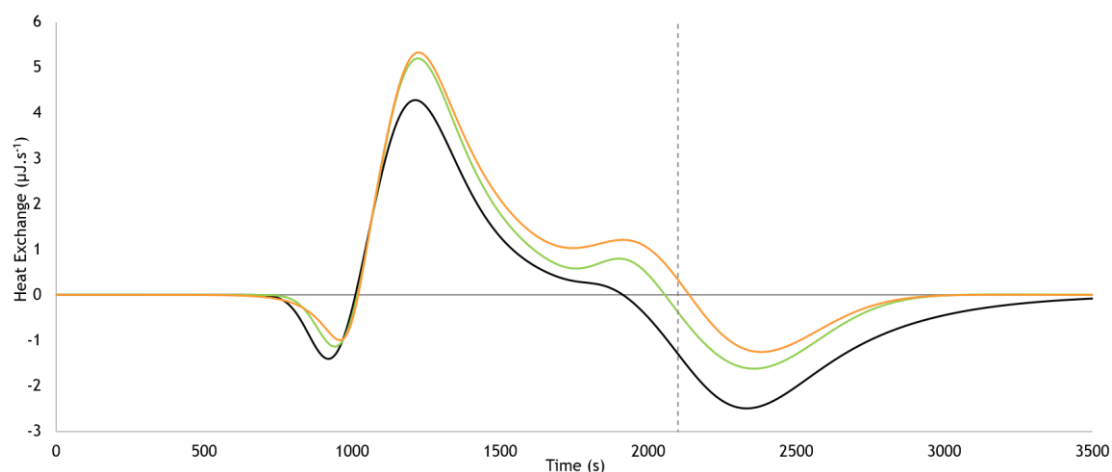


Figure 3.4.2 - Thermograms of ln pDNA adsorption onto Phenyl sepharose using the 430 μL loop. Black 117.67 μg pDNA/g Phenyl Sepharose; Green 363.42 μg pDNA/g Phenyl Sepharose; Orange 614.70 μg pDNA/g Phenyl-Sepharose. Vertical dashed line represents the time where the pDNA solution plug is replaced with pDNA-free mobile phase around 2100 seconds.

All thermograms obtained using Phenyl Sepharose are comprised with an initial small endothermic peak, followed by an exothermic one or two when using 430 μL loop, and ends with an endothermic signal. To note that, for approximately the same surface concentration the second exothermic peak is only visible when the larger loop is used (Figure 3.4.2 and Figure 3.4.1). To be as well highlighted is the presence of the second endothermic signal; this was not present in the thermograms concerning the pDNA absorption onto the Q-Sepharose support [1].

Previous studies have shown that the existence of several peaks at different timings suggests that different events take place separately during the adsorption process [1,2,32,35,40,41]. To compensate for an undesired convolution of the signal and isolate overlapped events, heat signal deconvolution was done for both modes of injection. Each FMC thermogram was deconvoluted, into three or four distinct peaks, depending on the signal, Figure 3.4.3 and Figure 3.4.4. The enthalpy values obtained from the area of the deconvoluted peaks are presented in Table 3.4.1 and Table 3.4.2.

Table 3.4.1 - Heat of adsorption for ln pDNA adsorption onto Phenyl-sepharose using the 230 and 430 μL loop.

Loop (μL)	Loading ($\mu\text{g}\cdot\text{g}^{-1}$)	Endothermic Peaks ($\text{mJ}\cdot\mu\text{g}^{-1}$)		Exothermic Peaks ($\text{mJ}\cdot\mu\text{g}^{-1}$)	
		ΔH^{I}	ΔH^{II}	ΔH^{III}	ΔH^{IV}
230	124.97 ± 0.00	0.70	3.55	-3.60	----
	171.75 ± 0.00	0.47 ± 0.12	1.69 ± 0.04	-2.51 ± 0.16	----
	413.18 ± 0.00	0.15 ± 0.04	0.45 ± 0.07	-0.90 ± 0.11	----
430	117.45 ± 0.16	1.04	2.89	-2.88	-0.71
	362.91 ± 0.52	0.34 ± 0.22	0.76 ± 0.55	-0.94 ± 0.21	-0.25 ± 0.13
	613.82 ± 0.88	0.10 ± 0.05	0.40 ± 0.24	-0.54 ± 0.08	-0.36 ± 0.26

Table 3.4.2 - Sum of heat of adsorption for ln pDNA adsorption onto Phenyl-sepharose using the 230 and 430 μL loop.

Loop (μL)	Loading ($\mu\text{g}\cdot\text{g}^{-1}$)	Endothermic Peaks ($\text{mJ}\cdot\mu\text{g}^{-1}$)	Exothermic Peaks ($\text{mJ}\cdot\mu\text{g}^{-1}$)	Net Heat
		$\Delta H^{\text{I}} + \Delta H^{\text{II}}$	$\Delta H^{\text{III}} + \Delta H^{\text{IV}}$	$\Delta H^{\text{I}} + \Delta H^{\text{II}} + \Delta H^{\text{III}} + \Delta H^{\text{IV}}$
230	124.97 ± 0.00	4.25	-3.60	0.65
	171.75 ± 0.00	2.16 ± 0.21	-2.51 ± 0.16	-0.35 ± 0.05
	413.18 ± 0.00	0.59 ± 0.39	-0.90 ± 0.11	-0.30 ± 0.23
430	117.45 ± 0.16	3.93	-3.59	0.35
	362.91 ± 0.52	1.10 ± 0.28	-1.20 ± 0.34	-0.09 ± 0.01
	613.82 ± 0.88	0.50 ± 0.18	-0.90 ± 0.18	-0.40 ± 0.01

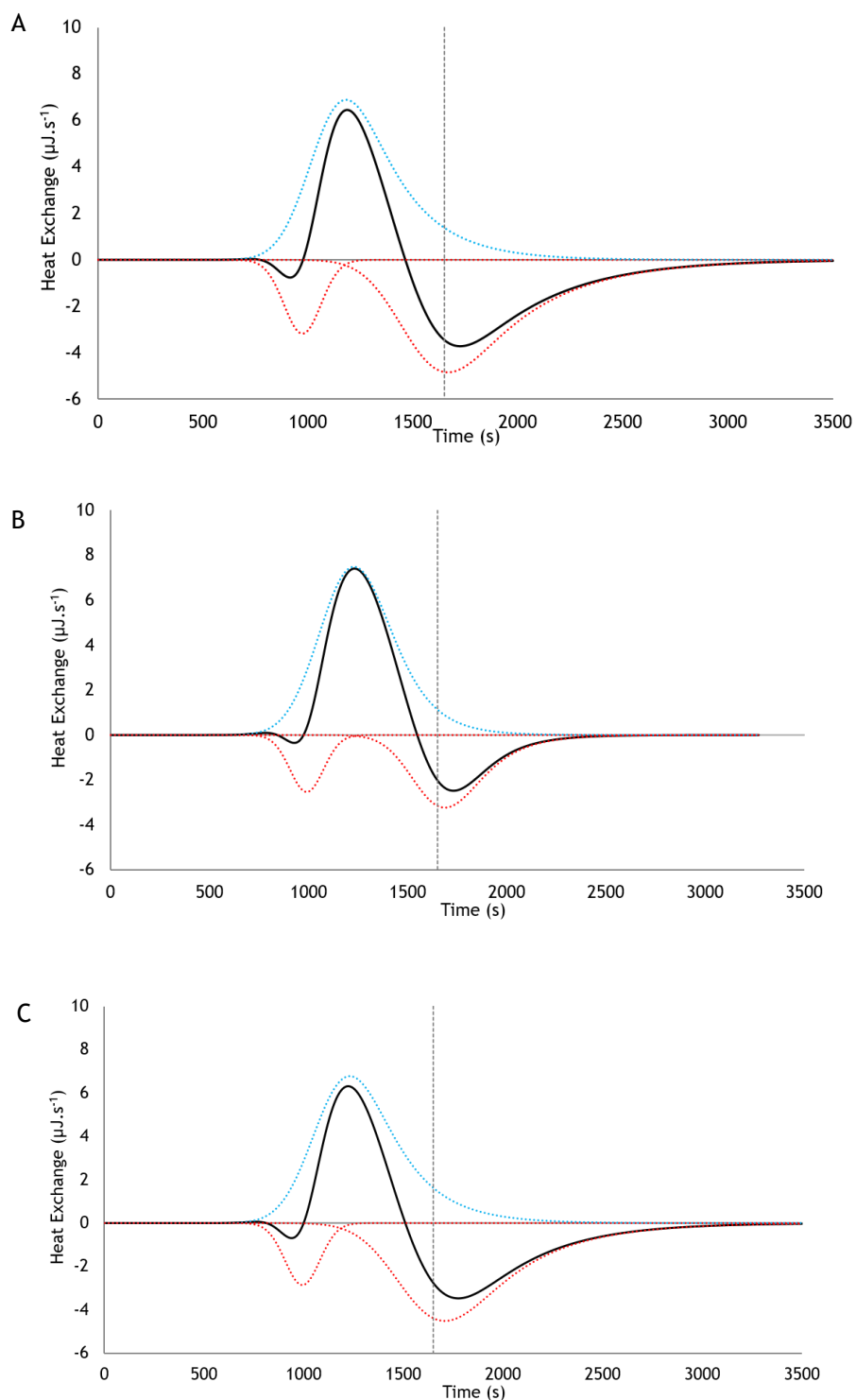


Figure 3.4.3 - PEAKFIT de-convolution of 230 μL loop thermograms for loading concentrations of A - 124.97 μg pDNA/g Phenyl Sepharose; B 171.85 μg pDNA/g Phenyl Sepharose; C - 413.18 μg pDNA/g Phenyl Sepharose. Curves shown are for experimental data. Total peak fit (black line (-)) and peaks resulting from deconvolution (blue and red lines (...)) Vertical dashed line represents the time where the pDNA solution plug is replaced with pDNA-free mobile phase around 1650 seconds.

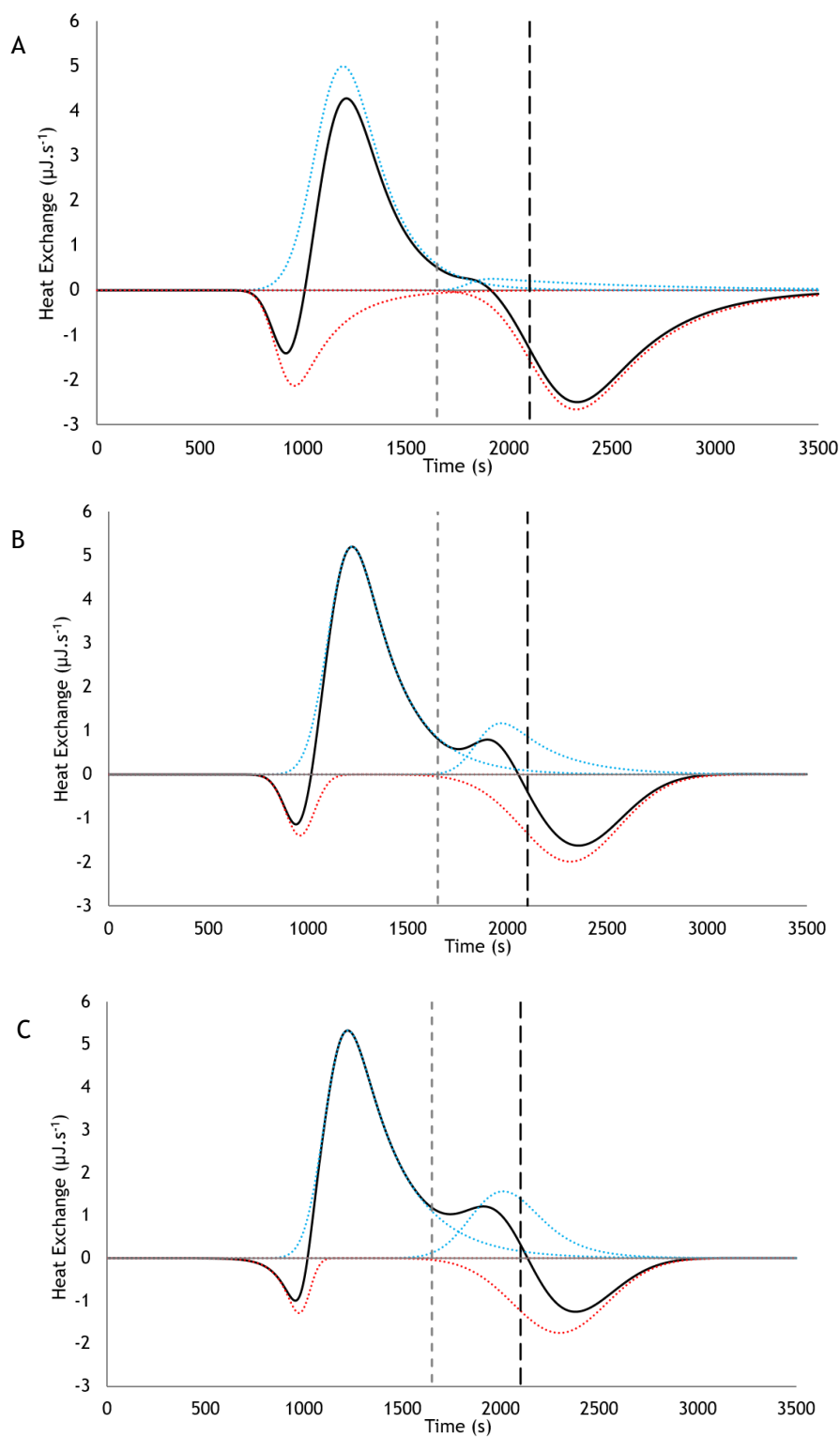


Figure 3.4.4 - PEAKFIT de-convolution of 430 μL loop thermograms for loading concentrations of A - 117.45 $\mu\text{g pDNA/g Phenyl Sepharose}$; B - 362.91 $\mu\text{g pDNA/g Phenyl Sepharose}$; C - 613.82 $\mu\text{g pDNA/g Phenyl Sepharose}$. Curves shown are for experimental data. Total peak fit (black line (-)) and peaks resulting from deconvolution (blue and red lines (...)). Vertical dashed line represents the time where the pDNA solution plug is replaced with pDNA-free mobile phase (Grey - 230 μL loop and Black - 430 μL loop).

For the thermograms analysis, and considering previous studies [1], it is worth doing it in view of the sub processes defined by Chen *et al.* [35,49,50]. According to them, the binding process of biomolecules at a liquid-solid interface can be divided into several sub processes, these include: (1) Dehydration or removal of ions from the biomolecule surface (endothermic process); (2) Dehydration or removal of ions from the sorbent surface (endothermic process); (3) Interactions between the biomolecule and the sorbent (exothermic process); (4) Structural rearrangement of the biomolecule upon adsorption (endothermic process); and (5) Solvation and hydration process of the bound biomolecules and rearrangement of the excluded water molecules or ions in the bulk solution (endothermic process) [35,49]. Previous calorimetric studies have supported the existence of these sub processes. It has been shown that exothermic peaks are mostly a result of attractive biomolecule-sorbent interactions and attractive lateral interactions of already adsorbed biomolecules [1,2,32,35,45]. On the other hand, endothermic peaks have been related to different events, such as water molecules and ions release from the surface of the adsorbent and of the biomolecule [35], repulsive interactions [2,51], conformational changes and molecule reorientation on the surface [2,32,51].

Taking into account the above-described assumptions, the first endothermic event, obtained with both injection modes (Figure 3.4.3 and Figure 3.4.4), can result from one or more of the sub processes (1), (2), (4), (5). At approximately 700 seconds, In pDNA molecules reach the sorbent, but before the adsorption itself, the water molecules and ions have to be partially excluded to decrease the distance between the pDNA and the sorbent [2,35,43]. Given that, we were taken to believe that the first endothermic peak comprises mainly a combination of the sub processes (1) and (2) regarding desolvation. A great contribution from dehydration is expected once we are working with a mobile phase (1.8 M ammonium sulfate) that favors hydrophobic effect. This dehydration endothermic event was already observed by other authors [1,2,32,35,43]. Besides, the first endothermic peak enthalpy decreases with the increase in loading concentration Table 3.4.1. Dias-Cabral and co-workers [43] suggested that the destabilization of organized water molecules around the ligand and the disruption of the water-surface structure by the initial biomolecule adsorption may reduce energetic requirements for the next dehydration process accompanying subsequent biomolecule adsorption. Finally, compared with the anion exchange support (Figure 3.4.5) the first endothermic signal obtained in presence of Phenyl Sepharose is characteristically smaller. This is to be expected, due to the lower energetic requirement for surface (of biomolecule and adsorbent) dehydration. The use of a high concentration of an kosmotropic salt encourage dehydration of the biomolecule and adsorbent surfaces, reducing its energy requirements [2].

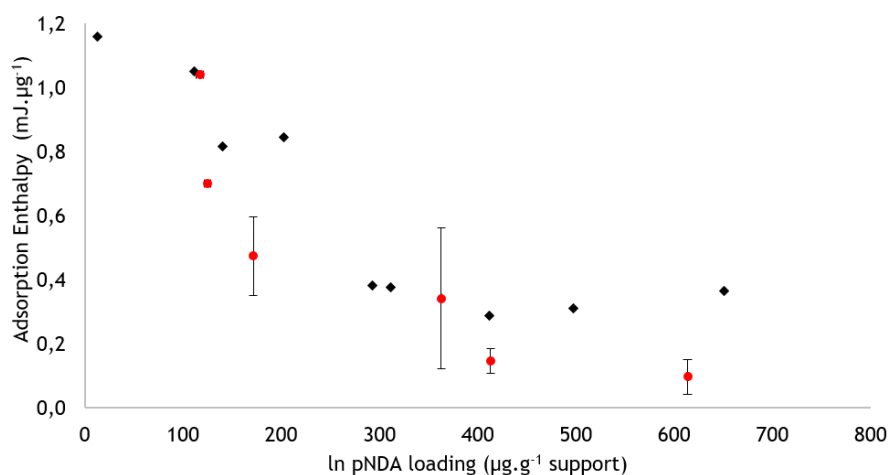


Figure 3.4.5 - Endothermic heats of ln pDNA adsorption onto (●) Phenyl Sepharose (♦) Q-Sepharose [1].

The first exothermic peak (Figure 3.4.3 A) may be related to the heat release caused by the short-range interactions between the ln pDNA and the Phenyl Sepharose ligands (sub process 3). It is important to note that the molecules that already went through the dehydration process start to adsorb whilst the other molecules and sorbent groups are still under the dehydration process. At the beginning, the number of molecules passing through the dehydration process is much higher than the number of molecules interacting with the support leading to the observation of an endothermic peak followed by an exothermic peak. However, according to the deconvolution Figure 3.4.3, the events that cause the first endothermic and exothermic peaks start at the same time. Interestingly, the endothermic peak disappears as the exothermic peak reaches its maximum. This does not mean that the dehydration process stopped, because there are still more molecules entering the FMC cell. Therefore, the energy released from the ln pDNA-solid phase interaction has to be much higher than the energy consumed during the dehydration process. Considering the 430 µL loop injections (Figure 3.4.4), we believe that, the first exothermic peak present is also a result of the interplay between sub processes (1), (2) and (3), but with a greater contribution from biomolecule support interactions.

The short-range attractive interactions that are involved in the exothermic signal, at first sight, are expected to result mainly from van der Waals interactions between the phenyl ligand and ln pDNA hydrophobic zones. In hydrophobic interaction chromatography, the ln pDNA-stationary phase (or support ligand) distance has to be relatively small in order to reduce hydrophobic zones exposure to water [35]. Due to the fact that hydrophobic effect can only be observed owing to the interaction of non-polar patches (hydrophobic zones), the only interactions possible to be established between this zones are the van der Waals ones. In addition, the global adsorption process is expected to be accompanied by large entropy gains that compensate for the enthalpically unfavorable dehydration. Even so, our results are in contradiction with these expectations, overall heat of adsorption is mainly exothermic (Table 3.4.2) and the exothermic enthalpies obtained by the adsorption of ln pDNA onto Q-Sepharose

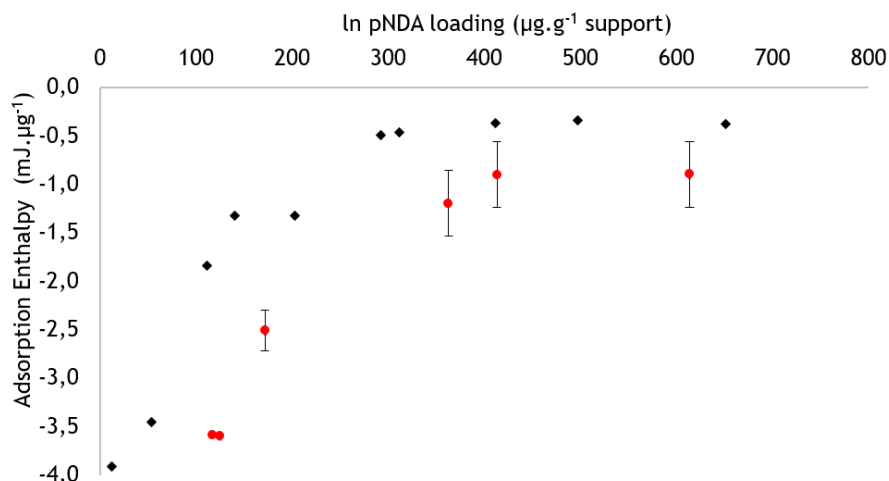


Figure 3.4.6 - Exothermic heats of ln pDNA adsorption onto (●) Phenyl Sepharose (◆) Q-Sepharose [1].

(Figure 3.4.6) are similar to the ones obtained for the present system. Attractive electrostatic forces between the biomolecule and the charged resin Q-Sepharose are anticipated to generate a larger heat release compared to the short range van der Waals interactions observed between Phenyl Sepharose and ln pDNA hydrophobic zones. Thus, other factors seem to be significantly influencing adsorption. More precisely, anion - π interactions may be contributing to the observed exothermic signal [52]. This controversial interaction, intuitively assumed as repulsion, turned from controversial to a well-established noncovalent interaction over the past quarter of a century [52]. A large number of studies revealed that the interactions of anions with π -systems relies mainly on two effects - the electrostatic attraction and the ion-induced polarization [52,53]. Thus, the observed high exothermic heats may be justified by the existence of an attractive electrostatic interaction between pDNA anions and the electron-deficient arenes present in support ligands. This type of interaction is more consistent with the high exothermic enthalpies observed in presence of the Phenyl ligand.

Regarding the 430 μ L loop, the thermograms present a second exothermic peak. This profile also happens in the adsorption of ln pDNA onto Q-Sepharose under the same conditions [1]. Moreover, the peaks have the same timing. We suspect a similar event generate these peaks. Under the continuous injection mode (430 μ L loop) the ln pDNA-support interaction have an extended contact time. Thus, despite the repulsion between the already adsorbed ln pDNA molecules and the ones in the feed solution, this interaction promotes the reorientation and subsequent secondary adsorption of already bound biomolecules. This will create free space for adsorption of ln pDNA in solution. As reported by Aguilar et al. [1], this is further supported, by comparing the thermograms obtained using the 229 μ L and 429 μ L loops. Considering the 429 μ L heat signal and observing it until the 229 μ L loop pDNA plug ends (Figure 3.4.4 A) we can see that the peak profile is similar to the one obtained with the 229 μ L loop (Figure 3.4.3 A). After that, the adsorption enters in the volume overloading and the heat signal magnitude increases due to the up mentioned mechanism.

In all studied cases, the thermogram ended with an endothermic peak (Figure 3.4.3 and Figure 3.4.4). Taking into account the assumptions from Chen et al. [35,49,50] stated above, sub processes (1), (2), (4) and (5) are the ones that may generate those kinds of heat responses. We have already emphasized that sub processes (1) and (2) occur while the sample is entering the cell. At approximately 1650 and 2100 seconds, in the case 230 and 430 μL loops respectively, the buffer containing ln pDNA molecules is replaced by buffer free of sample. After that, we believe that the heat signals are mainly result of sub process (5), nevertheless sub process (4) may also be involved. After the adsorption of all ln pDNA molecules, there is a rearrangement of the excluded water molecules and ions in the adsorbed biomolecules - bulk solution interface. It is important to keep in mind that ammonium sulfate is a kosmotropic salt, a water structuring electrolyte. Furthermore, kosmotropic anions, like SO_4^{2-} , are small and have a high charge density [54]. Remembering that ln pDNA also has a negatively charged surface repulsion between these two entities is expected. Considering this, the distribution of anions and cations on the surface of the adsorbed ln pDNA will be different from the initial state, and will tend to a minimum state energy. Just like any other process that makes changes in biomolecules solvation shell, this process is highly endothermic. Figure 3.4.7 illustrates the comparison between the energy spent on the desolvation process of ln pDNA in the Q-Sepharose system and the energy spent in the ion/water molecules reorganization in the Phenyl Sepharose system (endothermic ending peak). As it can be noticed, the energy spent in rearrangement is even higher. The thermograms untaken by Aguilar *et al.* [1] do not present this final endothermic peak, this further support our hypothesis that the presence of an high concentration of a kosmotropic salt is the main cause for the observed event.

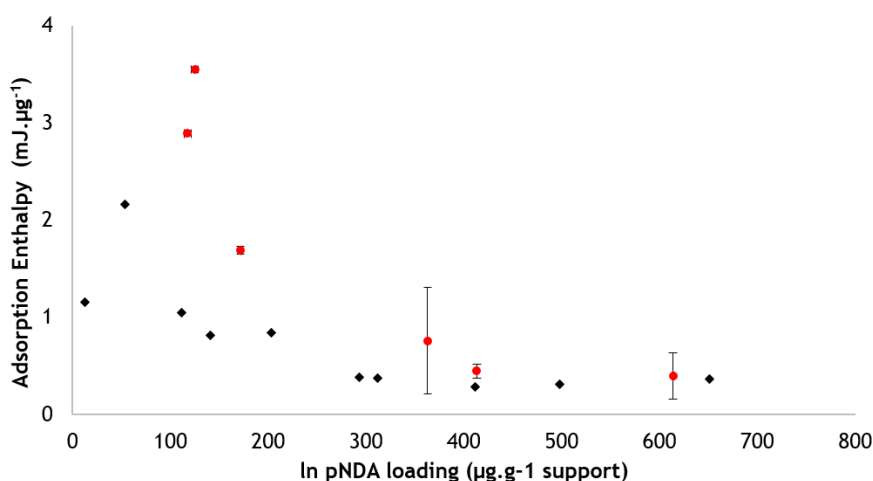


Figure 3.4.7 - Comparison between the ln-pDNA-Q-Sepharose first endothermic peak energy (◆) and ln-pDNA-Phenyl Sepharose second endothermic peak (●).

The adsorption process net heat (sum of all contributions) for both supports is illustrated in Figure 3.4.8. For an interaction to occur the Gibbs free energy ($\Delta G = \Delta H - T\Delta S$) has to be negative [35]. In the case of Q-Sepharose the overall adsorption process is undoubtedly enthalpically driven, once it is exothermic for all the studied conditions [1]. Previous authors have reported that the hydrophobic interaction process is, in most cases, entropically driven [35,43]. Regarding our results with the Phenyl Sepharose resin it is not possible to define a strict conclusion once, as shown in Figure 3.4.8, the process appears to be entropically driven at lower concentrations and enthalpically driven at higher concentrations.

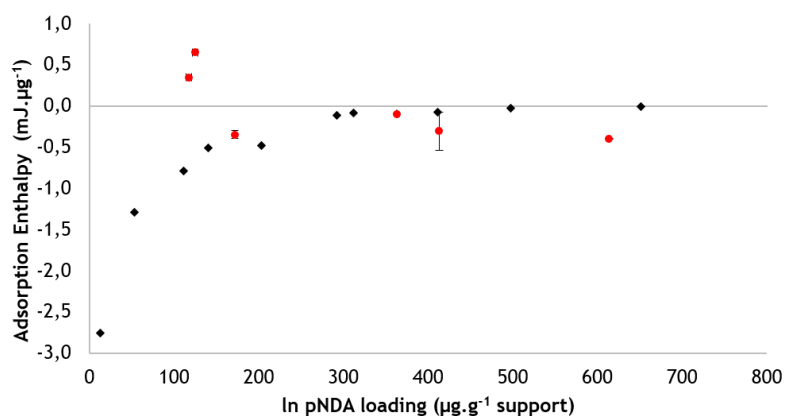


Figure 3.4.8 - Net heats (sum of all energetic contributions) of ln pDNA adsorption onto (●) Phenyl Sepharose (◆) Q-Sepharose [1].

3.4.2. sc pDNA adsorption onto Q-Sepharose

Figure 3.4.9 and Figure 3.4.10 illustrate the thermograms obtained with the 30 and 430 μL respectively. The signals are a result of different loading concentrations that range from 13 to 107 $\mu\text{g}\cdot\text{g}^{-1}$ gel and 117 to 1172 $\mu\text{g}\cdot\text{g}^{-1}$ gel in the 30 μL and 430 μL loop respectively. Once again, we see that the thermogram profile only changes when a different injection loop is used. The profile obtained with the 30 μL loop is very similar to the one generated by the interaction of ln pDNA with Q-Sepharose reported by Aguilar *et al.* [1]. In contrast, the 430 μL loop profile has a great divergence showing that the ln and sc pDNA adsorption onto Q-Sepharose are not so similar after all.

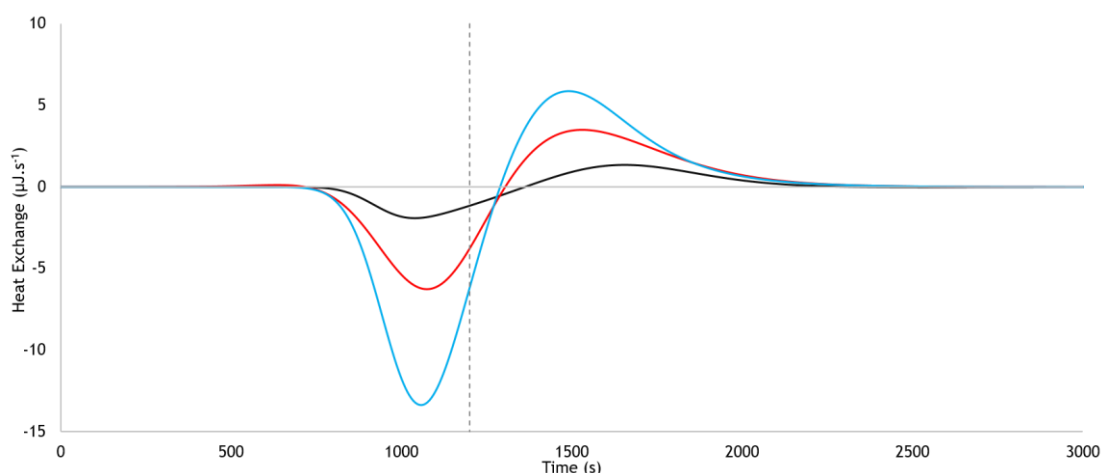


Figure 3.4.9 - Thermograms of sc pDNA adsorption onto Q-Sepharose using the 30 μL loop. Black 13.24 μg pDNA/g Q-Sepharose; Red 52.97 μg pDNA/g Q-Sepharose; Blue (--) 102.85 μg pDNA/g Q-Sepharose. Vertical dashed line represents the time where the pDNA solution plug is replaced with pDNA-free mobile phase around 1150 seconds.

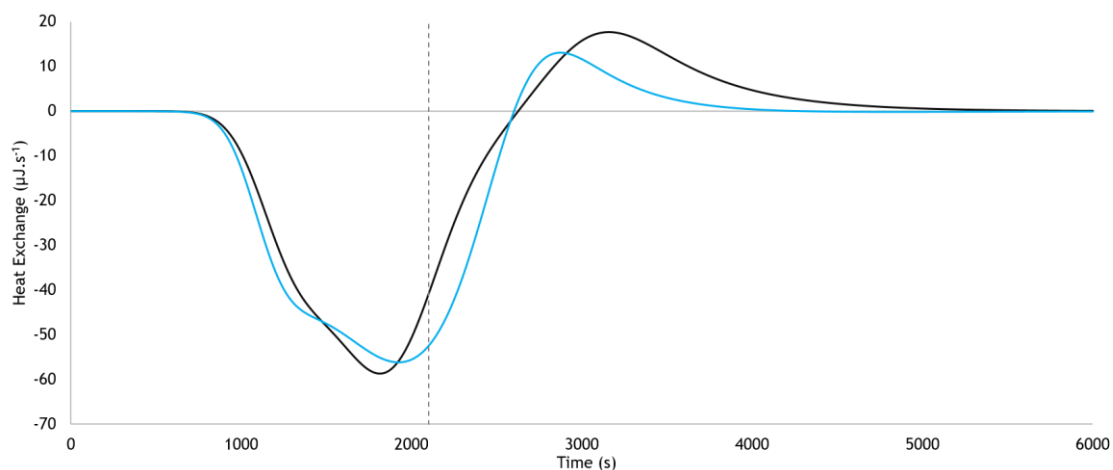


Figure 3.4.10 - Thermograms of sc pDNA adsorption onto Q-Sepharose using the 430 μL loop. Black 117.26 μg pDNA/g Q-Sepharose; Blue 1172.60 μg pDNA/g Q-Sepharose. Vertical dashed line represents the time where the pDNA solution plug is replaced with pDNA-free mobile phase around 2100 seconds.

Comparing the profiles from the thermograms in the Figure 3.4.9 and Figure 3.4.10, besides the thermogram signal increase, it's noticed the appearance of a second endothermic peak in the 430 μL loop thermogram. A profile changing with the injection loop is expected once in presence of a bigger loop we are working in conditions of volume overloading. As we stated earlier, the 430 μL loop fills the cell 2.5 times resulting in a longer contact between the sc pDNA and the support [1,32]. It can be noticed that the new peak overlaps with the first one. Considering these facts, heat signal de-convolution was performed, as earlier stated, in order to identify and isolate overlapped events. The enthalpy values obtained from the area of the deconvoluted peaks are presented in Table 3.4.3.

Table 3.4.3 - Heat of adsorption for sc pDNA adsorption onto Q-sepharose using the 30 and 430 μL loop.

Loop (μL)	Loading ($\mu\text{g}\cdot\text{g}^{-1}$)	Endothermic Peaks ($\text{mJ}\cdot\mu\text{g}^{-1}$)			Exothermic Peaks ($\text{mJ}\cdot\mu\text{g}^{-1}$)		Net Heat $\Delta H^I + \Delta H^{II} + \Delta H^{III}$
		ΔH^I	ΔH^{II}	$\Delta H^I + \Delta H^{II}$	ΔH^{III}		
30	13.24 ± 0.00	3.25 ± 0.17	---	3.25 ± 0.17	-3.49 ± 0.18		0.03 ± 0.01
	52.97 ± 0.00	3.76 ± 0.22	---	3.76 ± 0.22	-3.43 ± 0.05		0.34 ± 0.17
	102.85 ± 3.80	2.73 ± 0.18	---	2.73 ± 0.18	-2.23 ± 0.31		0.51 ± 0.13
430	117.26 ± 0.00	15.43 ± 0.76	10.31 ± 0.56	17.16 ± 1.32	-8.95 ± 0.17		16.80 ± 1.16
	1172.60 ± 0.00	1.42 ± 0.04	2.08 ± 0.07	3.51 ± 0.03	-1.18 ± 0.04		2.32 ± 0.07

Figure 3.4.11 shows the deconvoluted thermograms obtained with the 30 μL loop. These thermograms have a endothermic and exothermic signal that overlap showing that more than one event happens at the same time. All the heat signals begin approximately at 800 seconds, corresponding to the exact moment at which the frontal boundary of the sc pDNA solution reaches the resin in the FMC cell. As previously highlighted (Section 3.4.1) former calorimetric studies showed that endothermic signals are usually generated by the desolvation process [2,32,35,55], biomolecule repulsion, structural rearrangements and hydration and solvation of already bound pDNA molecules [1,32,35,41,50,55]. Conversely, exothermic signals are a result of mostly attractive biomolecule-sorbent interactions [1,2,32,35,45,46,56].

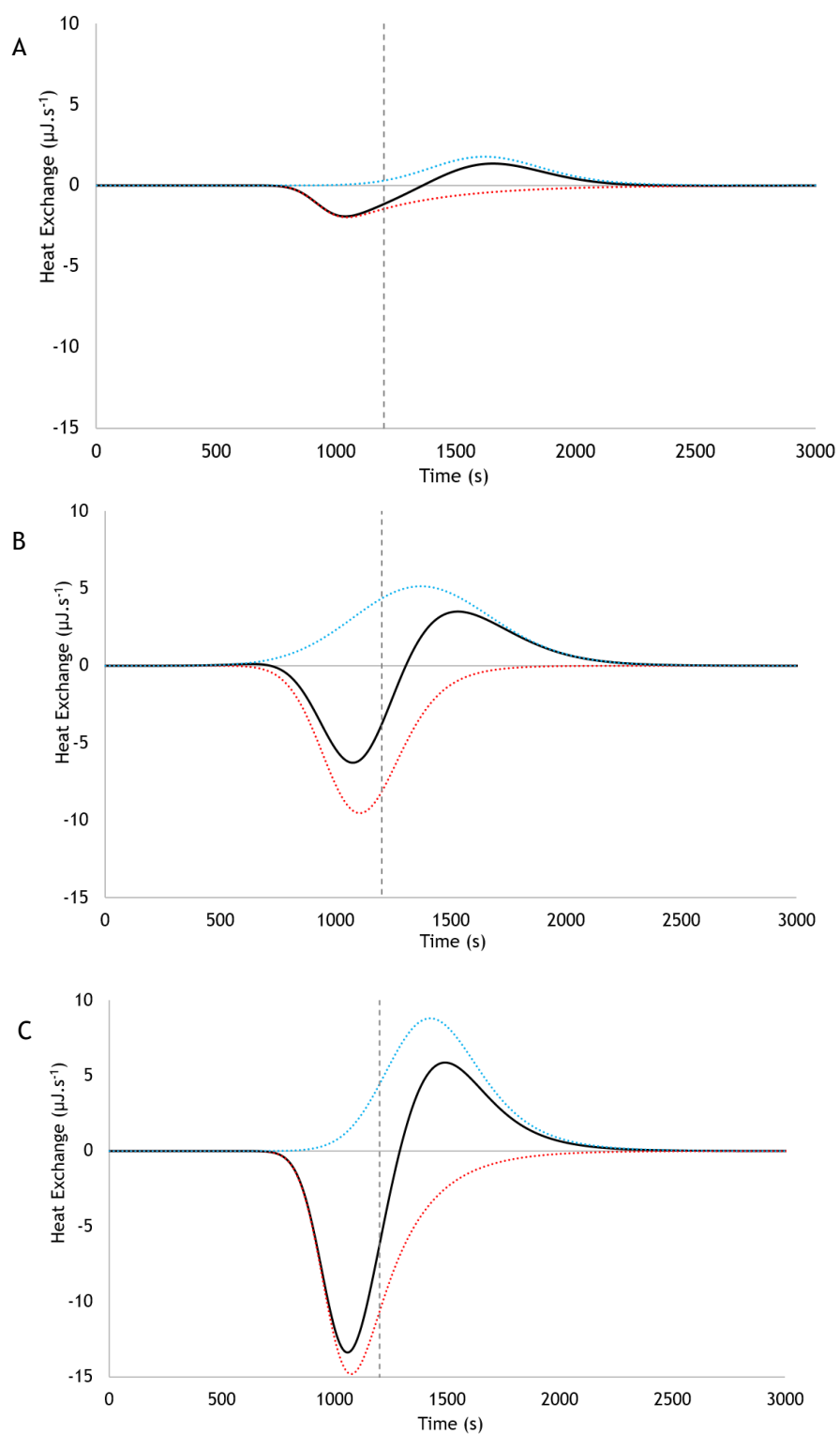


Figure 3.4.11 - *PEAKFIT* de-convolution of thermograms for loading concentrations of A - 13.24 μg pDNA/g Q-Sepharose; B - 13.24 μg pDNA/g Q-Sepharose; C - 102.85 μg pDNA/g Q-Sepharose. Curves shown are for experimental data. Total peak fit (black line (-)) and peaks resulting from deconvolution (blue and red lines (...)) Vertical dashed line represents the time where the pDNA solution plug is replaced with pDNA-free mobile phase around 1150 seconds.

The deconvoluted thermograms were analyzed considering the already mentioned mechanism proposed by Chen *et al.* [35,49,50] that divide the adsorption process into sequential sub processes (Section 3.4.1).

The DNA molecule has a polyelectrolyte nature in solution, which allows its binding to charged ligands, molecular condensation and conformational changes [19,57,58]. DNA molecules are highly-charged in aqueous environment. They need to be charged to avoid precipitation and phase separation at physiological concentrations [19,57,58]. The DNA molecule has an effective charge density of one negative charge every 0.17nm of its length [57,58]. In the present study, where different isoforms of the same plasmid are used, the ln and the sc isoforms have an equal charge number because they are composed of the same number of nucleotides [19]. However, the sc pDNA has a higher charge density once it has the same number of charges confined in less space. These high charge density attracts more water and counter ions which increases the solvation shell. The distribution and disruption of this solvation shell will have important consequences in the thermodynamics of interaction [57,58]. As we can see in the Figure 3.4.11, during the time that the pDNA molecules are entering and flowing through the cell (before the 1200s, pulg end, time where the mobile phase containing sc pDNA molecules is replaced by a pDNA-free mobile phase) the endothermic peak area is much larger than the exothermic one. Taking into account the above stated assumptions, the endothermic heat changes may be mainly caused by subprocesses (1) and (2). Interactions involving a net change in the solvation shell are often strongly driven by entropy alterations attending the release of ions and water molecules [2,35,50,55,57]. Obviously, this process is enthalpically unfavorable, but the release of water molecules contributes to a large entropy gain that compensates the unfavorable condition [1,35]. Aguilar *et al.* [1] reported this same event for the adsorption of ln pDNA onto Q-Sepharose.

Figure 3.4.12 illustrates the comparison between the endothermic enthalpy values for both ln and sc pDNA adsorption onto Q-Sepharose. For the same amount of pDNA it can be seen that enthalpy changes involved in the desolvation process are much higher for the sc pDNA isoform. Since the charge density of sc pDNA is higher when compared to ln pDNA, the amount of energy required for desolvation process will also increase.

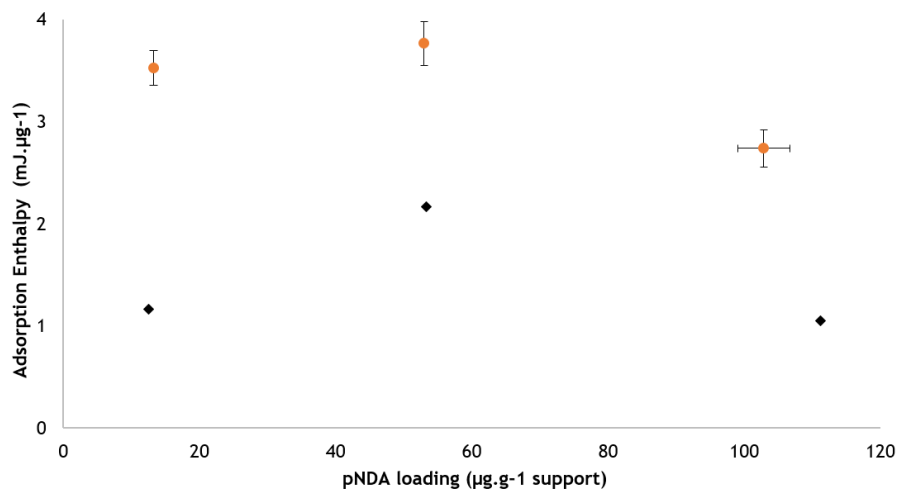


Figure 3.4.12 - Endothermic heats of sc pDNA adsorption (●) and ln pDNA adsorption (◆) onto Q-Sepharose[1].

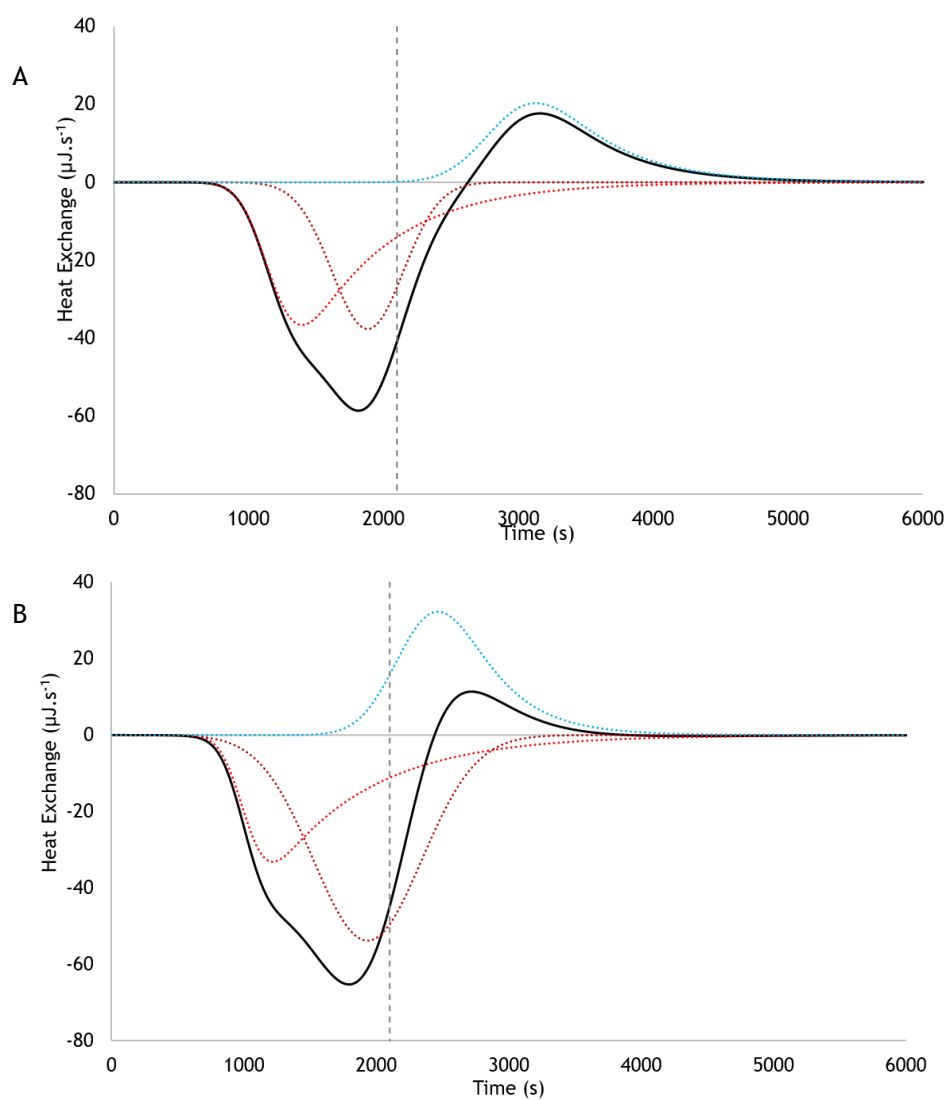


Figure 3.4.13 - PEAKFIT de-convolution of thermograms for loading concentrations of A - 117.86 µg pDNA/g Q-Sepharose and B - 1172.60 µg pDNA/g Q-Sepharose. Curves shown are for experimental data. Total peak fit (black line (-)) and peaks resulting from deconvolution (blue and red lines (...)) Vertical dashed line represents the time where the pDNA solution plug is replaced with pDNA-free mobile phase around 2100 seconds.

Figure 3.4.13 show the deconvoluted thermograms obtained with the 430 μL loop. Changing the injection volume results into different profiles. This happens because the transition from a pulse to a continuous feed of sc pDNA into the cell has influence in the equilibrium already reached by the bound molecules and consequently in the sub processes involved at the adsorption mechanism. This is also supported by Aguilar *et al.* [1]. To analyze the thermograms, the interaction between bound pDNA molecules and free pDNA molecules in the feed solution has been accounted [50].

As in the 30 μL loop, for the 430 μL loop the signal before the plug end (2100s) is mainly endothermic. According to the chronological sequence of sub processes proposed by Chen *et al.* [35,49,50] and the peak timing, the first endothermic event is compatible with the desolvation process. The appearance of a second peak suggests that the heat changes involved in the structural rearrangements upon adsorption, due to the interaction between the bound pDNA molecules and the free pDNA molecules in the feed solution are considerable. For the adsorption of ln pDNA onto Q-Sepharose, Aguilar *et al.* [1] reported that the heat changes involved in the hydration and solvation of already bound pDNA molecules and biomolecule repulsion are considered minimal when compared to the heat changes in desolvation. Nevertheless, under physiological pH conditions molecules with high charge density, like sc pDNA, gives rise to strong repulsion between the same charge neighboring molecules and ions [57,58]. In this particular case, the desolvation process still has a substantial contribution to the endothermic enthalpy changes, but a great part of the enthalpy change is caused by the repulsions between the sc pDNA molecules. In fact, according to the data shown in Table 3.4.3, the energy of the second endothermic event tends to be higher than the energy involved in the desolvation process as the loading increases. This and the fact that the second peak reaches its maximum near the plug end, supports even further our hypothesis, because a system with more free sc pDNA molecules will probably have more repulsion.

Simultaneously to the water molecules and ions release in the desolvation sub process, the interaction of sc pDNA and Q-sepharose occurs through an electrostatic attraction, (Figure 3.4.11 and Figure 3.4.12) (sub process 3) [35,49,50]. This may explain why the exothermic peak overlaps with the endothermic signal in the 30 μL loop thermograms (Figure 3.4.11 B). The electrostatic attractive forces between the sc pDNA molecule and the sorbent are expected to generate larger heats compared to other nonspecific interactions [35]. But, as reported earlier [1], the fact that the maximum of the exothermic peak appears after the sc pDNA plug end (after the mobile phase plug containing pDNA was replaced with pDNA-free mobile phase) indicates the presence of other thermal events, such as secondary adsorption of bound pDNA (biomolecules reorientation) or hydration of the already adsorbed biomolecules, an exothermic process [1,45]. After the primary adsorption of sc pDNA on Q-Sepharose surface, the pDNA molecules may undergo a surface reorientation, shifting to a minimum energetic state, creating new sites on its surface which become available for favorable interactions with the adsorption surface [45].

Comparing the exothermic enthalpies values of sc and ln pDNA adsorption on Q-sepharose obtained using the 30 μL loop, illustrated in Figure 3.4.14, we can see that there are not significant differences between them. Yamamoto and co-workers [46] presented a systematic study of the DNA molecules retention in order to determinate the number of binding sites. They reached the conclusion that once a critical MW (>60000) or length is reached, the number of binding sites is no more directly correlated to the number of charges. Considering this, the similar exothermic enthalpies values of sc and ln pDNA adsorption cannot be correlated with the number of binding sites. In fact, it seems that exists a critical contact area for adsorption [46]. Yamamoto and co-workers [46] postulated that this critical contact area might be related to the molecules structural effects along with thermodynamic aspects during adsorption. In other words, besides the different molecule conformation, the events that occur prior to adsorption are responsible to generate the same critical contact area, resulting in similar exothermic enthalpies values in the sc and ln pDNA adsorption. For the sc pDNA to reach the same critical contact area as ln pDNA, a higher energetic cost is necessary as previously seen.

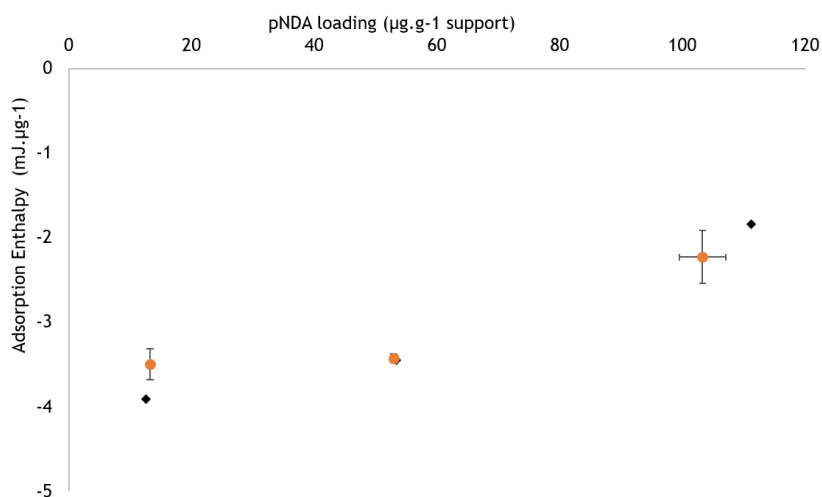


Figure 3.4.14 - Endothermic heats of sc pDNA adsorption onto (●) and ln pDNA adsorption (◆) onto Q-Sepharose [1].

Regarding the 430 μL loop, the thermograms resulted from the adsorption of ln pDNA onto Q-Sepharose revealed the presence of two exothermic peaks, before and after the plug end. Conversely, the adsorption thermograms for the present study presents only one exothermic peak after the plug end (Figure 3.4.13). Here, we hypothesize the energy released by the sc pDNA-Q-sepharose interaction is exceeded by the endothermic heat change involved in the repulsion of free pDNA molecules (second endothermic peak), causing the loss of the exothermic peak that happens before the plug end.

Paying closer attention to the Figure 3.4.11 and Figure 3.4.13, it can be noticed that the exothermic peak maximum has a tendency to get closer to the plug end. In the isotherm linear zone, the increase of the injection concentration leads to the loading increase. But at high injection concentrations, the number of free biomolecules in the bulk solution at the plug end is also high. As we mentioned earlier, the interaction between the adsorbed and free pDNA is

the main cause for the reorientation. Under those circumstances, it is expected that the reorientation starts earlier. This may consist another proof of molecule reorientation.

Figure 3.4.15 illustrates the comparison of ln and sc pDNA adsorption enthalpy net heat changes (sum of all contributions, Table 3.4.3 - Heat of adsorption for sc pDNA adsorption onto Q-sepharose using the 30 and 430 μL loop.). Once in a favorable interaction, the Gibbs free energy ($\Delta G = \Delta H - T\Delta S$) has to be negative. For the sc pDNA-Q-sepharose system, the overall adsorption process is entropically driven since it is endothermic for all the studied conditions. These results are supported by previous reports of adsorption studies, by van Hoff analysis of sc pDNA onto source 30 Q [24]. Aguilar *et al.*[1] reported that, for the ln pDNA-Q-sepharose system, the overall adsorption process is enthalpically driven in accordance with other studies performed with proteins [32,45]. These different behaviors emphasize the importance of characterizing each system independently.

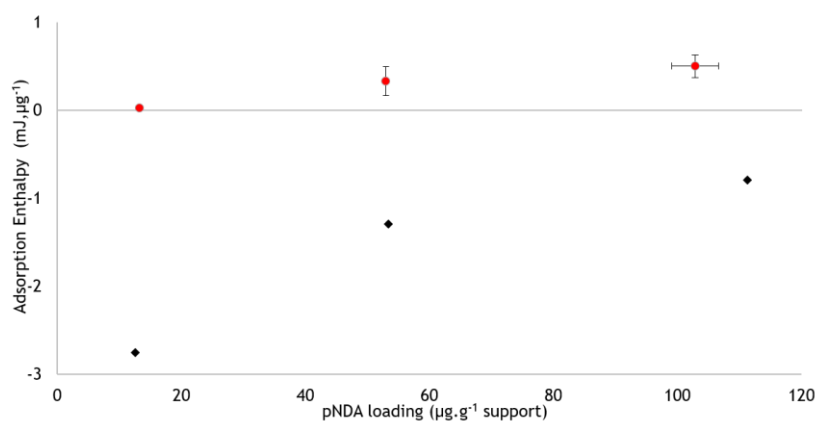


Figure 3.4.15 - Net heats (sum of all energetic contributions) of sc pDNA adsorption onto (●) and ln pDNA adsorption (◆) onto Q-Sepharose [1].

4. Conclusion and Future work

Considering the different thermogram profiles and the energy changes from different sources that are involved in the adsorption process, the flow microcalorimetry technique displayed once more the capability to study the adsorption process, giving a valuable insight on the overall mechanism.

Static binding capacity studies revealed that the mechanism of ln pDNA adsorption onto Phenyl Sepharose also follows a Langmuir-type isotherm profile under a certain equilibrium concentration. However, the association constant and the maximum revealed to be much lower than the adsorption onto Q-sepharose. We were not able to study the sc pDNA adsorption onto Q-sepharose in the same way due to the molecule instability under the test conditions, but theoretical binding capacity calculations were performed for comparison with the ln pDNA case.

Regarding the FMC tests with ln pDNA and Phenyl Sepharose, all obtained thermograms comprised an endothermic peak followed by one or two exothermic peaks, depending on the injection mode, and a final endothermic peak. The thermogram peaks were deconvoluted and the area and timing considered for comparison with the ln pDNA adsorption onto Q-sepharose. The initial endothermic peak was related to the desolvation process. The first exothermic peak was related to the ln pDNA-support interaction. Given the energetic similarity between the ln pDNA interaction between the Phenyl and Q-Sepharose, it was found that Phenyl Sepharose also interacted electrostatically with the pDNA molecule through anion- π interactions. Using the continuous feed (430 μ L loop) differences were found not only in the heat signal magnitude and in the time at which each event took place, but also in the peak profile. The presence of different peaks in a thermogram suggested the existence of different events during the adsorption process. The second exothermic peak, only found in the continuous feed mode, was related to ln pDNA reorientation and secondary adsorption similarly to what happens with the ln pDNA adsorption onto Q-sepharose. The final endothermic peak was found to be related to the reorganization of ions and water molecules in the ln pDNA-bulk solution interface given the presence of a high concentration of ammonium sulfate.

The FMC experiments with sc pDNA and Q-Sepharose resulted in thermograms comprised of an endothermic peak followed by an exothermic one. The endothermic peak obtained with the 430 μ L injection loop was later deconvoluted into two endothermic signals. As in the first case, the peaks intensity, area and timing were considered and compared with the ln pDNA adsorption onto Q-sepharose. The first endothermic signal was found to be related to the desolvation process just like in the ln pDNA adsorption. However, the signal is more energetic in the sc pDNA adsorption due to the high charge density granted by the supercoiled isoform that leads to a higher energetic cost for desolvation. When working with the 430 μ L loop we were able to

promote the column volume overloading which resulted in a second endothermic signal. This signal was related with the repulsions between the free sc pDNA molecules in solution. At last, the exothermic peak timing and area led us to believe that was related to molecule reorientation and secondary adsorption.

The enthalpies of adsorption showed that the overall adsorption process is exothermic, near to zero, for the adsorption of ln pDNA onto Phenyl Sepharose. Some studies reported that liquid chromatographic processes involving hydrophobic interactions are believed to be markedly influenced by the entropy change and are often considered to be mainly endothermic. In this particular case, we do not have a pure hydrophobic interactions system which explains the divergent result. For the sc pDNA-Q-sepharose system, the overall adsorption process is entropically driven since it is endothermic for all the studied cases, these results are supported by previous reports of adsorption studies by van Hoff analysis [24].

For future work, further experiments should be conducted with the same hydrophobic interaction resin in order to understand the influence of arenes and anion- π interaction in the hydrophobic adsorption process. sc pDNA could be used once it is known to have a weak interaction with hydrophobic interaction resins (at low salt concentrations) and a high charge density. Even though, experiments with other hydrophobic interaction resins, like octyl sepharose, should be conducted in order to understand the mechanisms underlying a pure hydrophobic system.

Additionally, chromatographic monoliths represents the 4th generation of stationary phases. They are especially attractive due to a short purification time, flow unaffected properties and high dynamic binding capacity for high molecular weight molecules. It will be interesting to perform the studies using sc pDNA and monoliths to compare the results with ones obtained with particles resins. This will give us information about the stationary phase thermodynamic contributions to the purification process.

5. References

- [1] P. a. Aguilar, A. Twarda, F. Sousa, A.C. Dias-Cabral, Thermodynamic study of the interaction between linear plasmid deoxyribonucleic acid and an anion exchange support under linear and overloaded conditions, *J. Chromatogr. A.* 1372 (2014) 166-173.
- [2] J. Korfhagen, A.C. Dias-Cabral, M.E. Thrash, Nonspecific Effects of Ion Exchange and Hydrophobic Interaction Adsorption Processes, *Sep. Sci. Technol.* 45 (2010) 2039-2050.
- [3] A. Xenopoulos, P. Pattnaik, Production and purification of plasmid DNA vaccines: is there scope for further innovation?, *Expert Rev. Vaccines.* 13 (2014) 1537-1551.
- [4] Kewal K. Jain, *Textbook of Gene Therapy*, Hogrefe & Huber Publishing, 1999.
- [5] F. Sousa, L. Passarinha, J.A. Queiroz, Biomedical application of plasmid DNA in gene therapy: a new challenge for chromatography., *Biotechnol. Genet. Eng. Rev.* 26 (2010) 83-116.
- [6] K. Lundstrom, G. Gun, *New Era in Gene Therapy*, Elsevier Inc., 2015.
- [7] M.A. Liu, DNA vaccines: an historical perspective and view to the future., *Immunol. Rev.* 239 (2011) 62-84.
- [8] W.J. Kelly, Perspectives on plasmid-based gene therapy: challenges for the product and the process., *Biotechnol. Appl. Biochem.* 37 (2003) 219-23.
- [9] D. Fioretti, S. Iurescia, V.M. Fazio, M. Rinaldi, DNA vaccines: developing new strategies against cancer., *J. Biomed. Biotechnol.* 2010 (2010) 174378.
- [10] B. Ferraro, M.P. Morrow, N.A. Hutnick, T.H. Shin, C.E. Lucke, D.B. Weiner, Clinical applications of DNA vaccines: current progress., *Clin. Infect. Dis.* 53 (2011) 296-302.
- [11] Y. Cai, S. Rodriguez, H. Hebel, DNA vaccine manufacture: scale and quality., *Expert Rev. Vaccines.* 8 (2009) 1277-91.
- [12] K.K. Jain, *A Special Report on Gene Therapy*, John Wiley & Sons, 2000.
- [13] A. Ghanem, R. Healey, F.G. Adly, Current trends in separation of plasmid DNA vaccines: a review., *Anal. Chim. Acta.* 760 (2013) 1-15.
- [14] M.B. Appaiahgari, S. Vratil, Adenoviruses as gene/vaccine delivery vectors: promises and pitfalls., *Expert Opin. Biol. Ther.* 15 (2015) 337-51.
- [15] L. Vannucci, M. Lai, F. Chiuppesi, L. Ceccherini-Nelli, M. Pistello, Viral vectors: a look back and ahead on gene transfer technology., *New Microbiol.* 36 (2013) 1-22.
- [16] K. Lundstrom, *Novel Approaches and Strategies for Biologics, Vaccines and Cancer Therapies*, Elsevier, 2015.

- [17] M.M. Diogo, J.A. Queiroz, D.M.F. Prazeres, Chromatography of plasmid DNA, *J. Chromatogr. A.* 1069 (2005) 3-22.
- [18] D.M.F. Prazeres, T. Schluep, C. Cooney, Preparative purification of supercoiled plasmid DNA using anion-exchange chromatography, *J. Chromatogr. A.* 806 (1998) 31-45.
- [19] T.C. Boles, J.H. White, N.R. Cozzarelli, Structure of plectonemically supercoiled DNA., *J. Mol. Biol.* 213 (1990) 931-51.
- [20] G.M. Borja, E. Meza Mora, B. Barrón, G. Gosset, O.T. Ramírez, A.R. Lara, Engineering *Escherichia coli* to increase plasmid DNA production in high cell-density cultivations in batch mode., *Microb. Cell Fact.* 11 (2012) 132.
- [21] S.G. MOKRUSHIN, Definition of Chromatography, *Nature.* 178 (1956) 1244-1245.
- [22] G. Carta, A. Jungbauer, Protein chromatography process development and scale-up, Wiley, 2010.
- [23] E. Müller, Properties and Characterization of High Capacity Resins for Biochromatography, *Chem. Eng. Technol.* 28 (2005) 1295-1305.
- [24] C. Tarmann, A. Jungbauer, Adsorption of plasmid DNA on anion exchange chromatography media, *J. Sep. Sci.* 31 (2008) 2605-2618.
- [25] X. Shi, L. Qiao, G. Xu, Recent development of ionic liquid stationary phases for liquid chromatography., *J. Chromatogr. A.* 1420 (2015) 1-15.
- [26] V. Smrekar, F. Smrekar, A. Strancar, A. Podgornik, Single step plasmid DNA purification using methacrylate monolith bearing combination of ion-exchange and hydrophobic groups., *J. Chromatogr. A.* 1276 (2013) 58-64.
- [27] N.L. Krajnc, F. Smrekar, J. Černe, P. Raspor, M. Modic, D. Krgovič, A. Štrancar, A. Podgornik, Purification of large plasmids with methacrylate monolithic columns, *J. Sep. Sci.* 32 (2009) 2682-2690.
- [28] A. Podgornik, S. Yamamoto, M. Peterka, N.L. Krajnc, Fast separation of large biomolecules using short monolithic columns., *J. Chromatogr. B. Analyt. Technol. Biomed. Life Sci.* 927 (2013) 80-9.
- [29] H. Walton, Ion-exchange chromatography, *Anal. Chem.* (2015) 187.
- [30] D.M.F. Prazeres, T. Schluep, C. Cooney, Preparative purification of supercoiled plasmid DNA using anion-exchange chromatography, *J. Chromatogr. A.* 806 (1998) 31-45.
- [31] GE Healthcare, Hydrophobic Interaction and Reversed Phase Chromatography: Principles and Methods, (2012) 168.
- [32] G.L. Silva, F.S. Marques, M.E. Thrash, A.C. Dias-Cabral, Enthalpy contributions to adsorption of highly charged lysozyme onto a cation-exchanger under linear and overloaded conditions., *J. Chromatogr. A.* 1352 (2014) 46-54.

- [33] G.N. Ferreira, J.M. Cabral, D.M. Prazeres, Studies on the batch adsorption of plasmid DNA onto anion-exchange chromatographic supports., *Biotechnol. Prog.* 16 416-24. <http://www.ncbi.nlm.nih.gov/pubmed/10835244> (accessed February 14, 2016).
- [34] D.S. Gill, D.J. Roush, K.A. Shick, R.C. Willson, Microcalorimetric characterization of the anion-exchange adsorption of recombinant cytochrome b5 and its surface-charge mutants, *J. Chromatogr. A.* 715 (1995) 81-93.
- [35] F. Lin, W. Chen, M.T.W. Hearn, Thermodynamic analysis of the interaction between proteins and solid surfaces : application to liquid chromatography, *J. Mol. Recognit.* 15 (2002) 55-93.
- [36] S.R. Gallant, A. Kundu, S.M. Cramer, Modeling non-linear elution of proteins in ion-exchange chromatography, *J. Chromatogr. A.* 702 (1995) 125-142.
- [37] J.M. Phillips, N.G. Pinto, Calorimetric investigation of the adsorption of nitrogen bases and nucleosides on a hydrophobic interaction sorbent, *J. Chromatogr. A.* 1036 (2004) 79-86.
- [38] M. a. Groszek, Flow Adsorption Microcalorimetry, *Mater. Sci. Forum.* 25-26 (1988) 483-486.
- [39] N.G. Esquibel-King, Maria A.; Dias-Cabral, Ana Cristina; Queiroz, João A.; Pinto, Albumin Under Overloaded Conditions Using Flow Microcalorimetry, *J. Chromatogr. A.* 865 (1999) 111-122.
- [40] M.E. Thrash, N.G. Pinto, Characterization of enthalpic events in overloaded ion-exchange chromatography, *J. Chromatogr. A.* 944 (2002) 61-68.
- [41] M.E. Thrash, N.G. Pinto, Flow microcalorimetric measurements for bovine serum albumin on reversed-phase and anion-exchange supports under overloaded conditions, *J. Chromatogr. A.* 908 (2001) 293-299.
- [42] N.L. Krajnc, F. Smrekar, J. Cerne, P. Raspor, M. Modic, D. Krgovic, A. Strancar, A. Podgornik, Purification of large plasmids with methacrylate monolithic columns., *J. Sep. Sci.* 32 (2009) 2682-90.
- [43] A.C. Dias-Cabral, J.A. Queiroz, N.G. Pinto, Effect of salts and temperature on the adsorption of bovine serum albumin on polypropylene glycol-Sepharose under linear and overloaded chromatographic conditions, *J. Chromatogr. A.* 1018 (2003) 137-153.
- [44] M.A. Esquibel-King, A.C. Dias-Cabral, J.A. Queiroz, N.G. Pinto, Study of hydrophobic interaction adsorption of bovine serum albumin under overloaded conditions using flow microcalorimetry, *J. Chromatogr. A.* 865 (1999) 111-122.
- [45] A. Katiyar, S.W. Thiel, V. V. Gulians, N.G. Pinto, Investigation of the mechanism of protein adsorption on ordered mesoporous silica using flow microcalorimetry, *J. Chromatogr. A.* 1217 (2010) 1583-1588.

- [46] S. Yamamoto, N. Yoshimoto, C. Tarmann, Binding site and elution behavior of DNA and other large biomolecules in monolithic anion-exchange chromatography, *J. Chromatogr. A.* 1216 (2009) 2616-2620.
- [47] C.J. van Oss, Hydrophobicity of biosurfaces - Origin, quantitative determination and interaction energies, *Colloids Surfaces B Biointerfaces.* 5 (1995) 91-110.
- [48] M.C. Flickinger, *Downstream Industrial Biotechnology: Recovery and Purification*, Wiley, 2013.
- [49] W.-Y. Chen, Z.-C. Liu, P.-H. Lin, C.-I. Fang, S. Yamamoto, The hydrophobic interactions of the ion-exchanger resin ligands with proteins at high salt concentrations by adsorption isotherms and isothermal titration calorimetry, *Sep. Purif. Technol.* 54 (2007) 212-219.
- [50] F.-Y.Y. Lin, C.-S.S. Chen, W.-Y.Y. Chen, S. Yamamoto, Microcalorimetric studies of the interaction mechanisms between proteins and Q-Sepharose at pH near the isoelectric point (pI), *J. Chromatogr. A.* 912 (2001) 281-289.
- [51] F.-Y. Lin, W.-Y. Chen, M.T.W. Hearn, Thermodynamic analysis of the interaction between proteins and solid surfaces: application to liquid chromatography., *J. Mol. Recognit.* 15 55-93.
- [52] M. Giese, M. Albrecht, K. Rissanen, Experimental investigation of anion- π interactions - applications and biochemical relevance, *Chem. Commun.* 52 (2016) 1778-1795.
- [53] D.-X. Wang, M.-X. Wang, Anion- π Interactions: Generality, Binding Strength, and Structure, *J. Am. Chem. Soc.* 135 (2013) 892-897.
- [54] M. Chaplin, Kosmotropes and Chaotropes, *Water Struct. Sci.* (2016). http://www1.lsbu.ac.uk/water/kosmotropes_chaotropes.html (accessed October 5, 2016).
- [55] W.-Y. Chen, M.-S. Lin, P.-H. Lin, P.-S. Tasi, Y. Chang, S. Yamamoto, Studies of the interaction mechanism between single strand and double-strand DNA with hydroxyapatite by microcalorimetry and isotherm measurements, *Colloids Surfaces A Physicochem. Eng. Asp.* 295 (2007) 274-283.
- [56] A.M. Lenhoff, Protein adsorption and transport in polymer-functionalized ion-exchangers., *J. Chromatogr. A.* 1218 (2011) 8748-59.
- [57] G.N. Goparaju, Evaluation of cationic peptide-plasmid DNA complexes for gene delivery, 2008.
- [58] D.H. Bloomfield, Victor A.; Crothers, Donald M.; Tinoco, Ignacio, Jr.; contributions from Hearst, John E.; Wemmer, David E.; Kollman, Peter A.; Turner, *Nucleic Acids: Structures, Properties, and Functions*, *J. Chem. Educ.* 78 (2001) 314.

- [59] M.L. Edelstein, Gene Therapy Clinical Trials Worldwide, J. Gene Med. (2015). <http://www.wiley.com//legacy/wileychi/genmed/clinical/> (accessed November 28, 2015).
- [60] G.N.M. Ferreira, J.M.S. Cabral, D.M.F. Prazeres, Studies on the batch adsorption of plasmid DNA onto anion-exchange chromatographic supports, Biotechnol. Prog. 16 (2000) 416-424.

6. Appendix

Table 3.4.4 - Classification and properties of the different support media used in Liquid Chromatography.

Support media class	Matrix material	General features
Natural Polymers	Agarose, Cellulose, Dextran and Chitosan	<p>Low solid densities (90-96% water)</p> <p>Limited mechanical strength</p> <p>Smaller Pores (Gels)</p> <p>Easy functionalization</p> <p>Resistance to CIP</p> <p>Low non-specific binding</p>
Synthetic Polymers	Acrylic polymers, Poly(methacrylate), Poly(styrene-divinyl benzene, Acrylamido and vinyl co-polymers	<p>Higher solid densities (50-80% water)</p> <p>Large pore sizes possible</p> <p>Greater mechanical strength</p> <p>Resistance to CIP</p> <p>Moderate or high non-specific binding</p> <p>Relatively difficult to functionalize</p>
Inorganic Materials	Hydroxyapatite, Silica, Controlled pore glass, Zirconia and TiO ₂ .	<p>Highest solid densities (30-60% water)</p> <p>Larger pore sizes possible</p> <p>Rigidity</p> <p>May not be resistant to CIP</p> <p>Moderate or high non-specific binding</p> <p>Relatively difficult to functionalize</p>

Table 3.4.5 - Heat of adsorption for ln pDNA adsorption on Q-Sepharose at pH 8; flow rate: 1.5 mL/h; adsorbent sample size: 21.89 mg; and temperature: 25°C. Enthalpies were determined from the deconvoluted thermograms.

Loop (μL)	pDNA mass feed (μg)	pDNA loading ($\mu\text{g g}^{-1}$)	Endothermic peak ($\text{mJ } \mu\text{g}^{-1}$)	Exothermic peaks ($\text{mJ } \mu\text{g}^{-1}$)			Net heat of adsorption ($\text{mJ } \mu\text{g}^{-1}$)
			ΔH^{I}	ΔH^{II}	ΔH^{III}	$\Delta H^{\text{II}} + \Delta H^{\text{III}}$	
30	0.27	12.6 ± 1.7	1.16 ± 0.33	-3.91 ± 0.19	0	-3.91 ± 0.19	-2.75 ± 0.38
	1.17	53.40 ± 0.02	2.16 ± 0.37	-3.45 ± 0.55	0	-3.45 ± 0.55	-1.29 ± 0.66
	2.43	111.2 ± 0.1	1.05 ± 0.02	-1.84 ± 0.05	0	-1.84 ± 0.05	-0.79 ± 0.05
	4.44	202.8 ± 0.2	0.85 ± 0.16	-1.33 ± 0.13	0	-1.33 ± 0.13	-0.48 ± 0.20
	9.01	311.5 ± 9.4	0.38 ± 0.02	-0.46 ± 0.02	0	-0.46 ± 0.02	-0.08 ± 0.02
	10.89	497.6 ± 0.1	0.31 ± 0.02	-0.34 ± 0.02	0	-0.34 ± 0.02	-0.03 ± 0.02
229	20.68	820.4 ± 82.9	0.20 ± 0.08	-0.51 ± 0.16	0	-0.51 ± 0.16	-0.32 ± 0.18
	31.72	1222.5 ± 70.8	0.23 ± 0.05	-0.47 ± 0.13	0	-0.47 ± 0.13	-0.23 ± 0.14
429	57.92	1359.6 ± 132.6	0.19 ± 0.05	-0.29 ± 0.11	-0.36 ± 0.06	-0.66 ± 0.12	-0.47 ± 0.13
	87.73	3599.0 ± 111.8	0.05 ± 0.01	-0.32 ± 0.02	-0.08 ± 0.02	-0.40 ± 0.02	-0.36 ± 0.02
	203.78	5489.4 ± 152.7	0.03 ± 0.01	-0.29 ± 0.08	-0.08 ± 0.02	-0.36 ± 0.08	-0.33 ± 0.08

$$\Delta H^{\text{Total}} = \Delta H^{\text{I}} + \Delta H^{\text{II}} + \Delta H^{\text{III}}$$

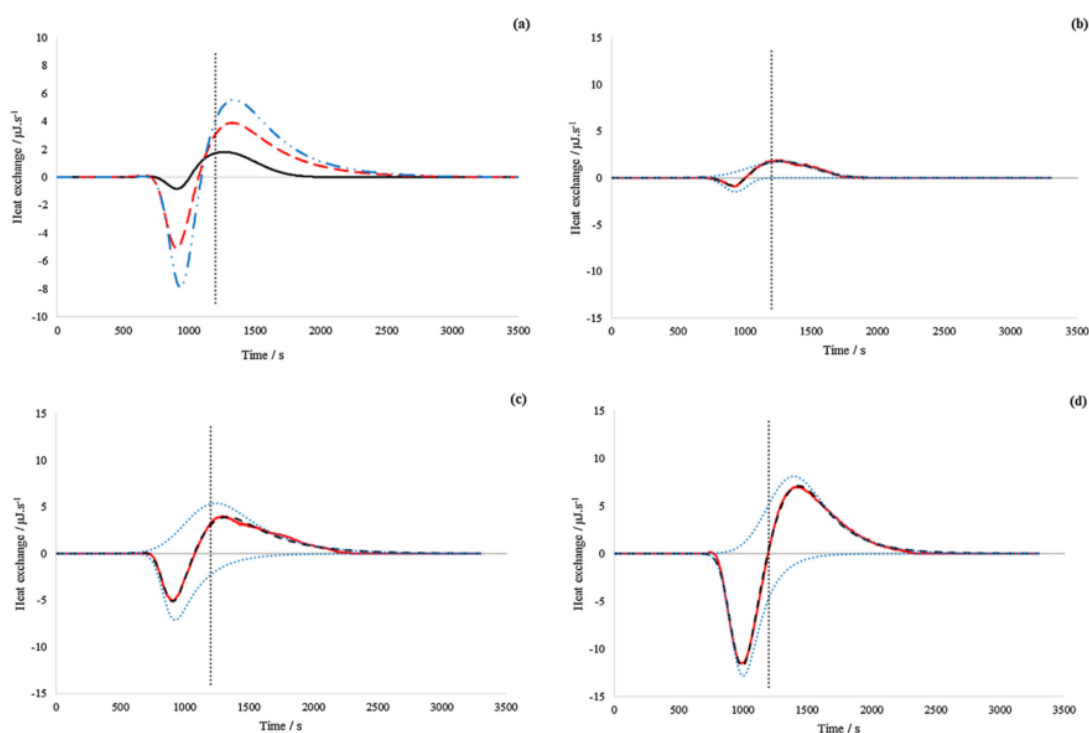


Figure 3.4.16 - Thermograms of ln pDNA adsorption onto Q-Sepharose, at pH 8. Injection loop: 30 μL . (a) Black (-) 12.6 μg ln pDNA/g Q-Sepharose; red (- -) 53.4 μg ln pDNA/g Q-Sepharose; blue (-.-) 111.2 μg ln pDNA/g Q-Sepharose; (b)-(d) PEAKFIT deconvolution of thermograms for loading concentrations of (b) 12.6 μg ln pDNA/g Q-Sepharose, (c) 53.4 μg ln pDNA/g Q-Sepharose and (d) 111.2 μg ln pDNA/g Q-Sepharose. Curves shown are for experimental data (red line (-)); total peak fit (black line (-)) and peaks resulting from deconvolution (blue line (...)). Vertical dashed line represents the time where the pDNA-containing plug of solution is replaced with pDNA-free mobile phase.

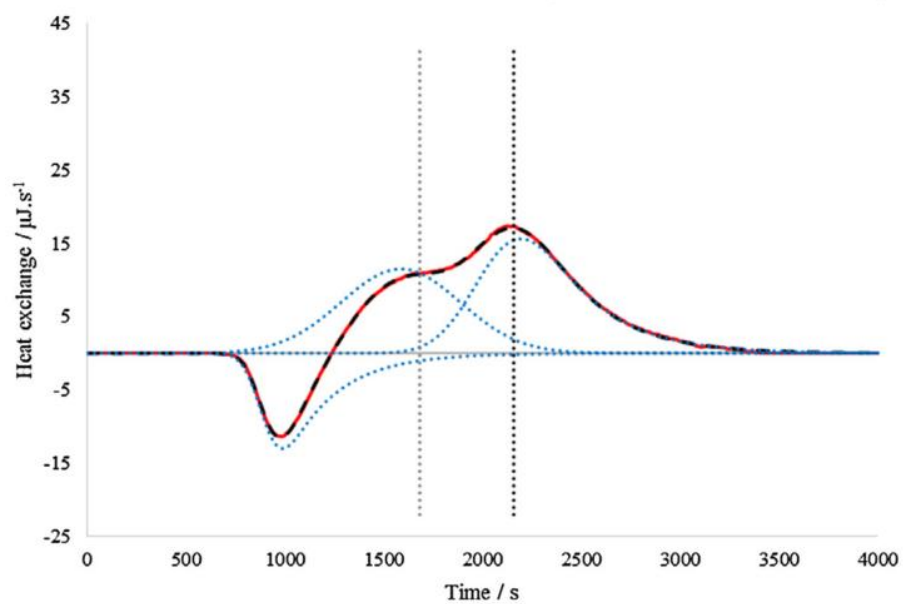


Figure 3.4.17 - Thermograms of ln pDNA adsorption onto FF Q-Sepharose. Injection loop: 429 μL . PEAKFIT de-convolution of thermogram for loading concentrations of 1359.6 μg ln pDNA/g Q-Sepharose. Vertical dashed line represents the time where the pDNA-containing plug of solution is replaced with pDNA-free mobile phase.